5-5-2017

# Ultrasound as a Physical Force for Scaffold-Based Bone Repair

James D. Veronick
*University of Connecticut - Storrs*, james.veronick@uconn.edu

Ultrasound as a Physical Force for Scaffold-Based Bone Repair

James D. Veronick, Ph.D.

University of Connecticut, [2017]

## Abstract

Non-invasive, transcutaneous low intensity pulsed ultrasound (LIPUS) therapy has shown clinical efficacy in bone healing for over the past two decades; however, the exact mechanism of action remains largely unknown. The goal of this work was to find more conclusive evidence as to how LIPUS works in addition to optimizing the currently used clinical therapy. We developed and characterized our own highly tunable ultrasound system as well as a hydrogel scaffold system for tissue mimetics. A series of experiments evaluated the response of our adjustable ultrasound system to: cells alone; hydrogels alone; cell-hydrogel encapsulation; and cell-hydrogel encapsulation implantation into a mouse calvarial model.

By characterizing our tunable ultrasound system with a needle hydrophone, we found that the clinical LIPUS parameter produces a measurable acoustic radiation force previously only recognized in higher intensity ultrasound modalities. Given that bone responds positively to physical forces, we have attempted to relate the documented benefit of LIPUS therapy in bone healing to acoustic radiation forces as a likely candidate for LIPUS efficacy. Through our adjustable LIPUS system and the development of collagen hydrogel scaffolds, we demonstrated that varying LIPUS intensity and duty cycle results in the manifestation of varying physical loads. These loads ultimately lead to the quantifiable deformation of collagen hydrogel scaffolds through the displacement of fluorescent beacons encapsulated within the hydrogels. By application of acoustic radiation force, pre-osteoblast cell-encapsulated hydrogels experienced varied osteogenic

response from the clinical intensity of LIPUS based on their collagen concentration. Also, the exposure of cell-hydrogel constructs to ultrasound resulted in the varied upregulation of certain markers indicative of mechanical stress, based on LIPUS intensity and hydrogel collagen concentration. As fractures are typically immobilized during the fracture healing process, local bone cells receive limited beneficial physical loading. To this end, we used a mouse calvarial defect model to encapsulate donor bone marrow stromal cells (BMSCs) within a collagen hydrogel at the defect site to physically load cells during the fracture healing process in hopes to enhance the currently used clinical LIPUS therapy.

# Ultrasound as a Physical Force for Scaffold-Based Bone Repair

James D. Veronick

B.S., University of Connecticut, [2009]

M.S., University of Connecticut, [2010]

A Dissertation

Submitted in Partial Fulfillment of the

Requirements for the Degree of

Doctor of Philosophy

at the

University of Connecticut

[2017]

APPROVAL PAGE

Doctor of Philosophy Dissertation

Ultrasound as a Physical Force for Scaffold-Based Bone Repair

Presented by

James D. Veronick, M.S.

Major Advisor_____

Yusuf Khan, Ph.D.

Associate Advisor_____

Lakshmi Nair, Ph.D.

Associate Advisor_____

Bryan Huey, Ph.D.

Associate Advisor_____

Wendy Vanden Berg-Foels, Ph.D.

University of Connecticut

[2017]

Dedicated to my family for their unconditional love and support

# ACKNOWLEDGEMENTS

I would like to express my gratitude and indebtedness to those people without whom this work would not have been possible. First and foremost, I owe great thanks to my advisor, mentor, and friend, Dr. Yusuf Khan who provided me with such a great opportunity in the Institute for Regenerative Engineering and exhibited an unwavering level of guidance, support, and patience. Over my years in participating in research work with Dr. Khan, he never ceased to believe in me and my abilities, many times before I could even believe in myself. Dr. Khan has always demonstrated such a level of integrity and dignity, and has continued to be a true role model for myself and many others. He has taught me how to recognize and pursue my goals, yet always remain humble and true to one's values. I am so grateful and fortunate to have had Dr. Khan's guidance and mentorship. I know that many of the qualities he has taught me will be forever instilled in my character and carry themes way beyond the field of research and medicine, such as when presented with any situation, always trying to do the right thing. As President Theodore Roosevelt said, "In any situation, the best thing you can do is the right thing; the next best thing you can do is the wrong thing; the worst thing you can do is nothing." This is one of many creeds I now live by.

As we live in America, we must never cease to forget the freedom we have been provided, and the great cost it has come at through many generations of courageous men and women. As I have never prided myself on being "smart" or "talented" compared to some of my colleagues and former teammates, one thing I have been graciously instilled with through the mentorship of whom I consider to be some of the greatest including Dr. Khan, Hall of Fame Coach Jim Calhoun, my father, and my grandfather, is work ethic and ambition. I have learned to fight through adversity

at an undying level. Simply speaking and as cliché as it sounds, where there is a will, there is a way. These four individuals have brought me to an epiphany, loving and believing in me before I could ever love and believe in myself, and led me to accomplish each and everything I have ever set out to do. Quitting has never been a word in my vocabulary, or an option in my life. As I have always embraced the role of leadership and am recognized as a researcher in medicine, I hope I can pass the message along to others that any goal or dream in America is possible, and that the only thing standing in one's way of reaching it, is themselves. As I used the word 'epiphany' before, I truly believe that once someone realizes the power of hope, work ethic, and ambition, the individual can finally become free. Ever relevant as Ralph Waldo Emerson said, "The mind, once stretched by a new idea, never returns to its original dimensions."

I would also like to extend special thanks to all of my other colleagues and coworkers in the Institute for Regenerative Engineering and at UCONN Health for assisting me with endless experiments, data analysis, and all around support. These colleagues and coworkers along with my whole advisory team (Dr. Yusuf Khan, Dr. Lakshmi Nair, Dr. Bryan Huey, Wendy Vanden Berg-Foels, and Dr. Edward Neth) and family and friends have been ever patient, understanding, and supportive of not only my thesis work, but more importantly battles and adversity I have had to face and overcome in my personal life. When a coworker or individual in a professional setting shows truly genuine compassion and empathy for an individual outside of a place of employment, to me they become family. I am forever indebted to those whom have helped me, and I will always take care of the ones that did. In a world that often is seemingly filled with evil, love is the greatest gift and the only thing that will prevail and last forever. As none of my life would have been possible without my higher power, I must recognize God for providing me with the courage and strength, "I can do all things through Christ who strengthens me" (Philippians 4:13). I will end

here with another creed I try to live by as an imperfect human which can be applied to all aspects in life, the serenity prayer: God grant me the serenity to accept the things I cannot change; courage to change the things I can; and wisdom to know the difference.

## Table of Contents

List of Abbreviations

| | |
|---|---|
| BMP | Bone Morphogenic Protein |
| BMSCs | Bone Marrow Stromal Cells |
| CL | Crosslinked |
| Col1a1 | Collagen Alpha-1 (I) Chain |
| ECM | Extracellular Matrix |
| FGF | Fibroblast Growth Factor |
| GAPDH | Glyceraldehyde 3-phosphate dehydrogenase |
| GFP | Green Fluorescent Protein |
| IPSC | Induced Pluripotent Stem Cells |
| MSC | Mesenchymal Stem Cells |
| OCN | Osteocalcin |
| PDGF | Platelet-Derived Growth Factor |
| PLGA | Poly Lactic Glycolic Acid |
| PLLA | Poly-l-lactide Acid |
| RT-PCR | Reverse Transcription Polymerase Chain Reaction |
| RUNX2 | Runt-related Transcription Factor 2 |
| TE | Tissue Engineering |
| VEGF | Vascular Endothelial Growth Factor |
| Wnt | Wingless-int Proteins |

List of Symbols

| | |
|---|---|
| ~ | approximately |
| % | percentage |
| ° | degree |
| µ | microgram |
| C | Celsius |
| cm | centimeter |
| kDa | kilodaltons |
| g | gram |
| h | hours |
| M | molar |
| nM | nanomolar |
| MPa | mega pascals |
| mg | milligram |
| min | minute |
| ng | nanogram |
| nm | nanometer |
| Pa | pascals |
| s | seconds |

# 1. INTRODUCTION

## 1.1. Clinical Relevance

Annually, orthopedic surgeons perform approximately 2.2 million bone replacement procedures worldwide, of which over 500,000 procedures are performed in the United States, leading to bone being the second most transplanted tissue after blood.[1,2] In the United States alone, bone replacement procedures result in a cost of nearly $2.5 billion per year on the healthcare system.[3] In healthy individuals bone tissue has the ability to regenerate and repair non-critical sized defects.[4,5] However, when patients experience critical sized defects or bone loss due to trauma, tumor resection, developmental deformities, infection, or non-union fractures, bone cannot heal properly on its own resulting in necessary surgical intervention with bone replacements/grafts.[6–9] With the rising age of the population in the United States, particularly considering the baby boomer generation cohort of ~65 million began turning 65 years old in 2011, susceptibility to musculoskeletal ailments increases in part due to age-associated diseases such as osteopenia and osteoporosis contributing to the increased fragility of bone.[10–12] These degenerative conditions commonly lead to increases in bone and joint problems ultimately resulting from weak bone.[13,14] Non-unions or fractures that occur in individuals with degenerative skeletal disease may be further affected and more difficult to treat compared to injuries caused by trauma alone.[15,16]

The healthcare system in the United States will be challenged with treating the needs of the aging population as it relates to bone-related injuries and diseases resulting in bone damage, degeneration, or loss.[12,17] Current treatment options for bone repair and regeneration (i.e. autografts, allografts, and synthetic materials) present significant limitations and risks and

improved treatment methods are necessary. Optimally, a bone graft or bone graft substitute should provide appropriate mechanical support in addition to providing an osteoconductive surface for tissue incorporation and remodeling to eventually be replaced by host tissue. While autografts, which are tissues harvested from the patient, are currently considered the "gold standard" in bone graft procedures as they represent over half of bone substitutes, they are limited by available bone volume capable of being harvested and can result in donor site infection and morbidity.[18,19] Allografts, a secondary option to autografts, are harvested tissues from cadavers and involve risks of immunogenicity and disease transmission.[15,20,21] To avoid donor site morbidity, volume availability, potential immunogenicity, and disease transmission, various bone graft substitutes have been developed although no perfect substitute yet exists that embodies the autograft's ideal qualities.[22]

Current bone graft substitute biomaterials include proteins (i.e. collagen), metals, plastics, and ceramics manufactured into scaffolds in attempts to mimic the natural extracellular environment (ECM) by various methods such as electrospinning, hydrogel formation, microsphere sintering, 3-D printing, thermally-induced phase separation, and particulate leaching to name a few.[23] However, clinical implementation of many biomaterials has yet to be perfected as they often result in the need for additional surgeries do to fatigue, fracture, and toxicity of the material.[15] Therefore, a need for replacement methods is needed to overcome the pitfalls of the current treatments options.

The field of bone tissue engineering has emerged has an alternative and viable option for bone repair and regeneration. Tissue engineering involves the application of biological, chemical and engineering principles towards the development of biological substitutes for the repair, restoration, or regeneration of tissue form and function.[24] Bone tissue engineering

comprises of implementing biomaterial scaffolds which are both biodegradable and porous, with or without the use of bone-forming cells and growth factors, in order to regenerate bone.[25–27] The goal of using a bone graft substitutes is to initiate a healing response from the host defect area resulting in the production of new bone at both the host-graft substitute interface and within its porous body. The choice of the biodegradable scaffold used is critical for the success of bone repair and regeneration as it serves as a temporary and mechanically-stable matrix for cells to infiltrate and proliferate.[25] In addition to the properties of the bone graft substitute itself such as mechanical stability, for optimal incorporation the vascularity of the host bed should contain enough pre-osteogenic or osteogenic cells to infiltrate the scaffold and proliferate.[15] Additionally, scaffold pore structure (i.e. pore size and interconnectedness) plays an essential role in the development process as the nanostructure of the natural ECM acts as a support system capable of allowing nutrient flow and guiding cellular functions such as proliferation, differentiation, adhesion, and migration by way of physical cues.[28–30]

Together, this work focuses on a bone tissue engineering approach using a natural biomaterial protein, collagen I, fabricated into a hydrogel and characterized with and without a remote mechanical stimulus using low intensity pulsed ultrasound (LIPUS) to provide an acoustic radiation force. As bone responds positively to a degree of physical loading described by Wolff's Law,[31] we hypothesize that the clinical effectiveness of LIPUS in fracture treatments in part results from the applied load and deformation from the acoustic radiation force manifested from LIPUS treatment. In addition to developing our own hydrogel scaffold system for tissue mimetics, we developed and characterized our own highly tunable ultrasound system. A series of experiments evaluated the response of our adjustable ultrasound system

to: cells alone; hydrogels alone; cell-hydrogel encapsulation; and cell-hydrogel encapsulation implantation into a mouse calvarial defect model.

### 1.2. Bone Biology

The human body consists of groups of cells with a similar structure which work together for a specific function. These groups of cells are known as "tissues", and the major types in vertebrates include nerve, muscle, blood, lymphoid, epithelial, and connective tissues.[32] The tissues contain a unique assortment of cells that are situated within an extracellular matrix (ECM) composed of macromolecules secreted by cells such as proteins, polymers, and polysaccharides. The ECM is responsible for providing structural support to tissues to facilitate cellular migration, proliferation, and communication. While tissues in the human body differ in and structure and function, they all work together via intracellular and extracellular interactions through various signaling molecules such as hormones, proteins, and biochemicals.[33]

In vertebrates, bone is a metabolically active and highly organized type of connective tissue characterized by its robust and mineralized ECM and functions as a structural support system. The main functions of bone include providing structural support, vital organ protection, mineral metabolism, and a site for hematopoiesis.[33] Bone is a very dense and rigid tissue; however, it is quite dynamic organ that is constantly undergoing a cycle of formation and resorption during the course of one's lifetime known as remodeling. Bone's continual chemical exchange and structural remodeling are both a result of internal mediators and external mechanical demands. Bones are vascularized organs that are made of bone tissue,

bone marrow, and also wrapped in a membrane known as the periosteum, which is a dense and irregular connective tissue.[34] As stated before, bone is a dynamic organ as it must endure the daily stresses of activity where it can undergo tension, compression, torsion and shear forces depending on the location and the individual's activity. Fortunately, bone has evolved to withstand the daily forces acting on it due to its structural integrity and rigidity, but it also exhibits a degree of flexibility which assists in limiting its failure rate.

Bone can exhibit both strength and a degree of flexibility due to the fact that it is a composite material. The main inorganic portion, calcium phosphate (CaP), in the boney tissue provides the rigidity, while the organic portion of bone, primarily type I collagen (Col I) offers the flexibility and elasticity. Based on the age of the patient and the activity level, bones are always adapting to their environment through remodeling so that they can endure the physical stresses without failure. Bone will form a geometrically optimal shape to carry its mechanical loads. Bone responds positively to increases in mechanical stress where bone tissue is added through the process known as apposition, and bone is resorbed where there is a lack of stress. This phenomenon is known as Wolff's Law and can be summarized as "bone is deposited and resorbed in accordance with the stresses placed upon it".[35] There are three main bone cell types responsible for the makeup of bone tissue and the remodeling process. Osteoblasts are responsible for synthesizing new bone and ultimately lead to the formation osteocytes once they become trapped in the matrix that they secrete. Osteoclasts are large multinucleated cells and are responsible for bone resorption. Bone tissue and cell types are furthered described in the following sections.

### 1.2.1. Structure of Bone

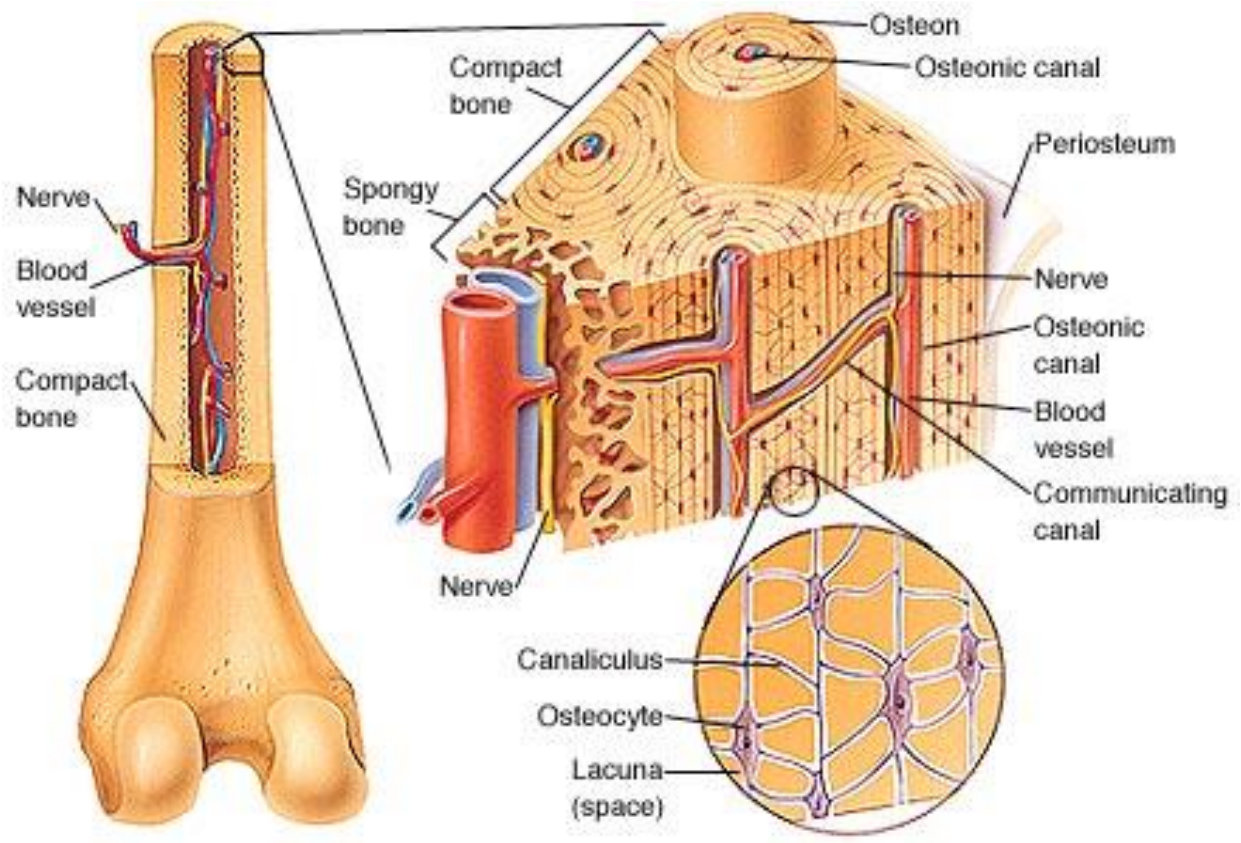


**Figure 1. Diagrams of cortical and trabecular bone tissue in long bones showing the inner structural anatomy.**[34]

As a connective tissue, the structural organization of bone consists of a robust ECM with a sparse distribution of cells. The mass composition of bone contains 8% water, 22% protein, and 70% mineral.[33] The non-mineralized organic and mineralized inorganic portions of bone contain primarily type I collagen (Col I) and calcium phosphate (CaP) respectively. Furthermore the ECM of bone is comprised of 95% Col I, 5% proteoglycans and various noncollagenous proteins.[33] The human body consists of 270 bones at birth which later

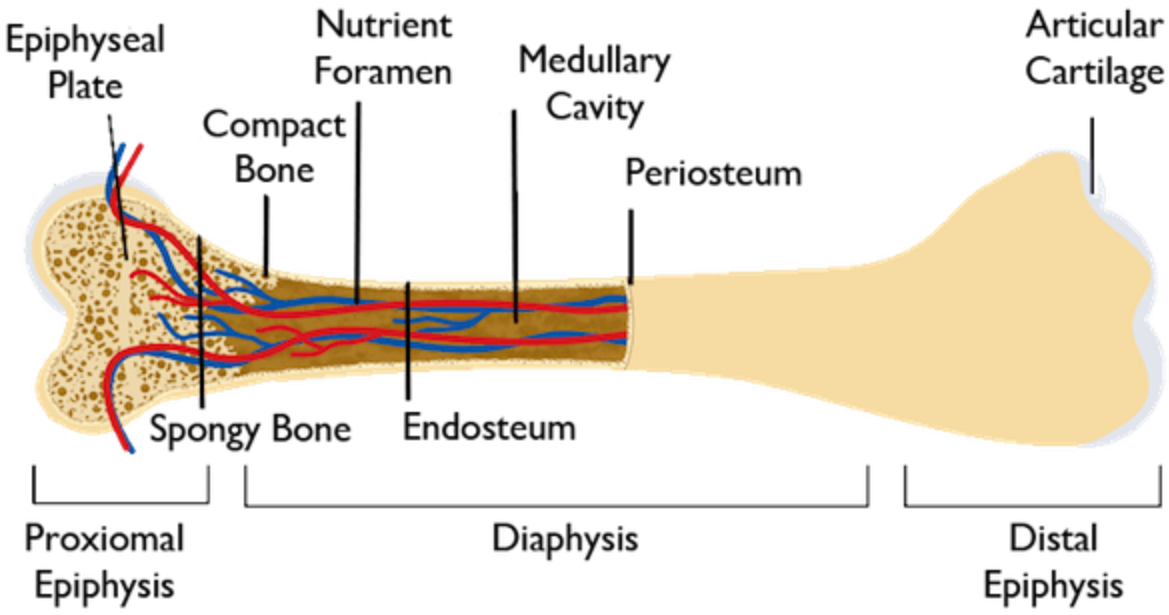


**Figure 2. Diagram of a long bone showing the different macroscopic sections of bone.**[36]

decreases to 206 bones by adulthood as some bones have fused together. Of these, 126 bones comprise the appendicular skeleton and 74 bones make up the axial skeleton.[33] The macroscopic and mechanical properties of the bones in the human skeletal system are principally influenced by particular loading conditions. Bone structures can be classified as long (i.e. femur, tibia, etc.), short (i.e. patella, sesamoid, etc.), flat (i.e. skull, sternum, etc.) and irregular (i.e. vertebrae, sacrum, etc.). Long bones are made of a hollow shaft, or diaphysis, a flared, cone-shaped metaphysis which lies below the growth plates; and rounded epiphyses above the growth plate.[36] The diaphysis contains primarily dense cortical bone; however, the metaphysis and epiphysis contain trabecular meshwork bone surrounded by a relatively thin shell of dense cortical bone. Within the diaphysis is a medullary cavity containing bone marrow.

Bone tissue can be classified as either cortical (compact) bone or trabecular (spongy) bone as can be seen in the illustration in figure 1. Cortical bone is found on the peripheral regions of most bones as it forms the cortex, or outer shell, and is dense and highly mineralized as it exhibits 5-10% porosity, while trabecular bone is commonly found in the end of long bones and is highly porous with 50-90% porosity.[20] Cortical bone is much denser than cancellous bone. With very few pores it is 80-90% mineralized and accounts for 80% of the bone tissue in the body by mass.[33] The high density of cortical bone allows it to be well suited for the mechanical and structural properties of bone as well as to store and release chemical elements such as calcium. Mechanical loading affects the thickness and density of cortical bone; however, other factors are involved. Concentric rings of sheets or "lamellae" of densely packed collagen fibrils account for the cortical bone makeup.

Trabecular, or spongy, bone is found on the interior of bones adjacent to the marrow cavity or within the ends of long bones. Trabecular bone exhibits less than 10% of the compressive strength as well as less than 5% of the compressive modulus of cortical bone.[37] However, trabecular bone exhibits higher surface area than cortical bone and is important for bone functions such as calcium homeostasis as well as acid/base regulation. A fibrous connective tissue sheath surrounds the outer cortical surface of bone known as the periosteum (figure 2). The periosteum contains blood vessels, nerve fibers, and osteoblasts and osteoclasts. Additionally, the periosteum has bone regenerative capabilities as its bone formation continues to be active through the course of one's lifetime. Vasculature and nerves are supplied to bones via the periosteum as well as attachment sites for surrounding tendons and muscles. The periosteum works during fracture healing by promoting the formation of cartilaginous callus, followed by ossification.[38] Another membranous structure known as the

endosteum covers the inner surface of cortical bone, trabecular bone, and the blood vessel canals present in bone known as Volkmann's canals. The endosteum contacts the bone marrow space, trabecular bone, and blood vessel canals and contains blood vessels, osteoblasts, and osteoclasts. The main unit of bone is known as the osteon. Cortical and trabecular bones are composed of osteons.[20] The osteons in cortical bone are called Haversian systems. Lamellae of continuous collagen fibril roughly 50-500 nm arrange in concentric manners around a central Haversian canal to form osteons or Haversian systems in cortical bone.[20] The canals contain blood vessels which supply nutrients throughout the bones. Bone cells and development will be discussed in the following sections.

### 1.2.2. Bone Cells

There are several distinct cell types involved in the formation and remodeling of bone tissue. The types of bone cells and where they can be found within bone tissue are osteoblasts, osteocytes, and osteoclasts as seen in figure 3 and are derived from stem cells.[39] Osteoblasts and osteoclasts are found on the surfaces of bone, while osteocytes permeate the mineralized interior.[40] Osteoblasts are fully differentiated bone cells whose roles include the synthesis of bone matrix on the bone forming surfaces and regulation of matrix mineralization.[40] Osteocytes are terminally differentiated osteoblasts that are encased by the mineralized matrix and help support overall bone structure. Osteoclasts are large, multinucleated cells derived from different cellular precursors (hematopoietic stem cells), and are responsible for the mechanism of bone resorption.[40]

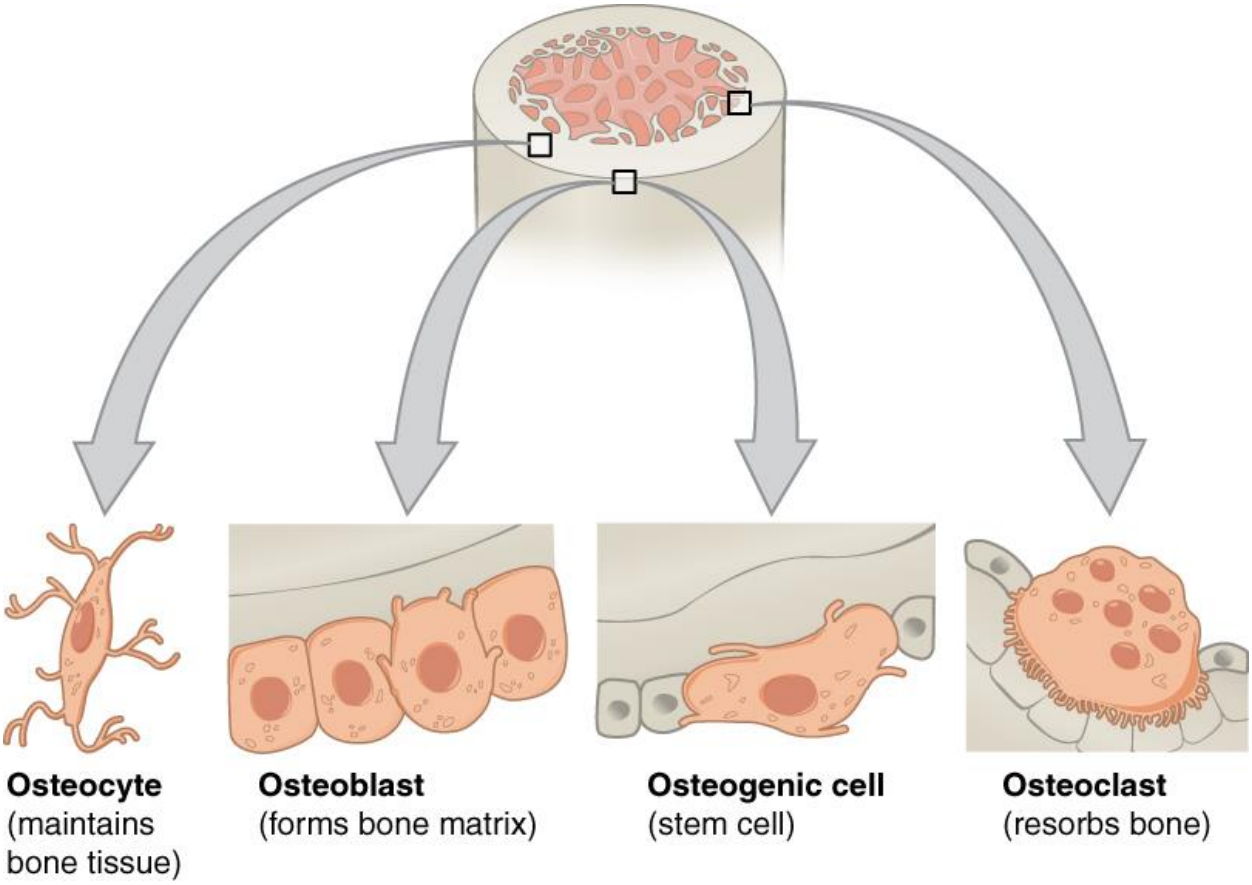


**Figure 3. Diagram of types of bone cells and where they reside.**[39]

Many specialized cell types including nerve, intestinal lining, and bone cells are incapable of renewal by cell division. Rather, these specialized cells are formed from adult stem cells, which have the ability to differentiate into one (unipotent) or many (pluripotent) types of terminally differentiated cells. An embryonic stem cell is one derived from human embryos and is capable of differentiating into any type of cell when supplied the appropriate environmental conditions and stimuli.[32] In contrast, while an adult stem cell is not terminally differentiated, its fate is determined in such that it has undergone an internal chemical change that distinguishes it and its progeny from embryonic stem cells.[32] Embryonic stem cells arise during embryonic development where three germ layers are formed: the ectoderm; the

mesoderm; and the endoderm. As the prefix in the name implies, the mesoderm is the middle germ layer consisting of multipotent mesenchymal stem cells which eventually give rise to the vascular and lymphatic systems as well as all connective tissue.[32] Mesenchymal stem cells are a class of multipotent mesoderm-derived stem cells that can be induced to differentiate into osteoprogenitors that ultimately can become osteoblasts, osteocytes, and bone lining cells. As stated before, hematopoietic stem cells can differentiate into osteoclasts and are also of mesoderm origin, but are multipotent in the sense that they give rise to all formed elements in the blood and immune system.[41]

Osteoblasts are fully differentiated cuboidal cells derived from preosteoblasts or osteoprogenitor cells, which are progenitor cells derived from mesenchymal stem cells located in the bone marrow or the periosteum.[33] A preosteoblast is stimulated to differentiate into an osteoblast via soluble factors including bone morphogenetic proteins (BMPs) and wingless-int proteins (Wnt).[42] The expression of Runt related transcription factors 2 (RUNX2), Distal-less homeobox 5 (Dlx5), and osterix (Osx) are necessary for osteoblast differentiation.[33] Also, RUNX2 is a known as a master gene for osteoblast differentiation due to the fact that RUNX2-null mice lack osteoblasts. As the preosteoblasts have been stimulated to differentiate, they cease proliferation and begin to secrete proteins indicative of osteoblast phenotype. New osteoblasts are located at the surface of developing bone tissue and exhibit a cuboidal morphology. Osteoblasts actively secrete unmineralized osteoid matrix at the location of newly forming bone containing the organic portion of bone ECM primarily composed of collagen type I which makes up approximately 90% of the matrix.[43] The remainder of the osteoid matrix is made of proteoglycans and noncollagenous proteins including osteopontin, osteocalcin, and osteonectin. When the osteoid matrix is being actively produced in addition

to the presence of membrane protein alkaline phosphatase, the osteoblast phenotype is present. Eventually the osteoid matrix around the osteoblast will calcify and roughly 20% of the embedded osteoblasts transition to osteocytes.[44] Any osteoblasts that do not ultimately transition to osteocytes will undergo apoptosis, or cellular death.

As discussed osteocytes are terminally differentiated cells derived from mature osteoblasts that have become embedded within the calcified matrix. As osteocytes account for 90-95% of the total bone cells, they are the most abundant and long-lived cells capable of a lifespan up to 25 years.[33] Osteocytes are derived from mesenchymal stem cells lineage through osteoblast differentiation with four recognizable stages having been proposed: osteoid-osteocyte, pre-osteocyte, young osteocyte, and mature osteocyte.[45] During the transformation from an osteoblast to an osteocyte, the expression of many of the proteins indicative of an osteoblast phenotype including type I collagen, alkaline phosphatase, osteocalcin, and bone sialoprotein, are no longer produced.[33,45] Also, osteocytes produce a network amongst themselves by extending many long processes to adjacent osteocytes known as the lacunar-canalicular network. This network is used for nutrient and waste transfer in addition to communication between the osteocytes via gap junctions.[45] As the osteocyte cell body resides in the lacuna, the osteocyte's processes extend out through the canaliculi to adjacent osteocytes and Haversian canals. These Haversian canals are responsible for supplying vasculature in order to deliver and remove nutrients. A concentric arrangement of lacunar-canalicular network of osteocytes surrounding a Haversian canal is known as an osteon.[33] Importantly, osteocytes have been believed to be the primary mechanosensors in bone. Mechanotranduction, or a mechanism in which cells convert a mechanical stimulus into an electro-chemical activity, is believed to be initiated by fluid flux within the canaliculi resulting

from pressure gradients between lacunae when the bone is loaded.[46] Fluid motion triggers depolarization of the osteocyte process and can propagate to other osteocytes via gap junctions. Mechanotransduction in osteocytes contributes to recruitment of osteoblasts or osteoclasts depending on the particular nature of the loading condition.[46–48]

Osteoclasts are multi-nucleated cells derived from hematopoietic stem cells as opposed to mesenchymal stem cells which give rise to osteoblasts and ultimately osteocytes. Osteoclasts are responsible in bone metabolism for the resorption of bone and exhibit a polarized plasma membrane. Osteoclasts exhibit a polarized plasma membrane which aids in resorbing bone. Two distinct plasma membrane regions are found on the basal surface of the osteoclast: a ruffled portion of the plasma membrane which is the location of where resorption of the bone occurs; and a sealing region that binds the ruffled border to the bone extracellular matrix.[49] A resorption lacuna is the combination of the ruffled and sealing regions of the plasma membrane. An osteoclast initially dissolves the mineralized portion of the bone matrix by secreting hydrochloric acid. Once the mineral content is removed, the protein content of the matrix is degraded by proteolytic enzymes. Contents are transported through the osteoclast in vesicles that are emptied into the extracellular space for use elsewhere.[49–51]

### 1.2.3. Bone Tissue Development

Calcified bone tissue can be formed by two distinct modes of ossification, also known as calcification, classified as either intramembranous ossification[52] (figure 4) or endochondral ossification[39] (figure 5). The type of bone being formed dictates the method of ossification. Flat and irregular shaped bones are formed through intramembranous ossification where long

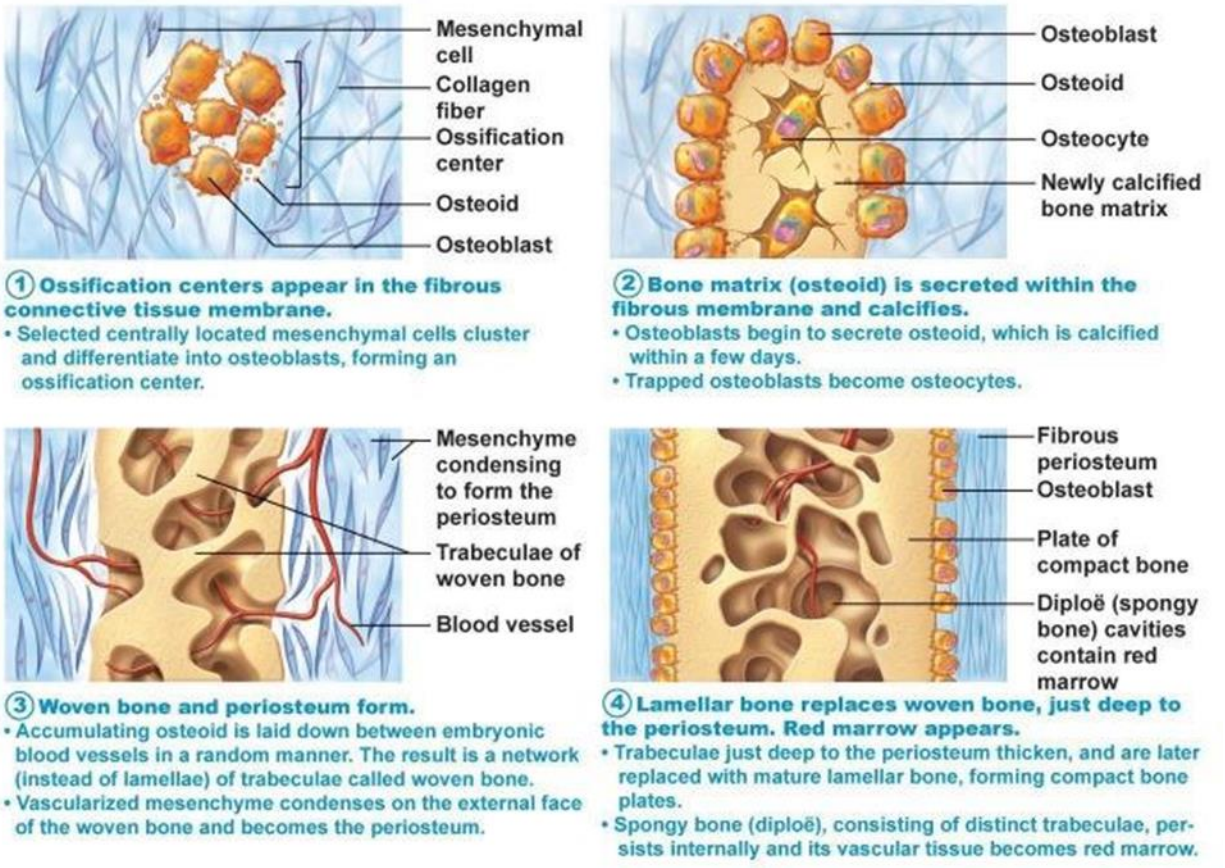


**Figure 4. Diagram showing the stages of intramembranous ossification.**[52]

bones are formed via endochondral ossification.[33,53,54] Intramembranous ossification starts without a pre-existing cartilage model, instead, mesenchymal stem cells form clusters. These stem cells then differentiate to osteoblasts which in turn start to secrete an osteoid matrix which is calcified to form bone spicules. The osteoblasts which become trapped within the bone spicules either terminally differentiate to osteocytes or undergo cell death via apoptosis. Bone spicules radiate outward from the origin of the mesenchymal stem cell cluster. Spicules ultimately join together to create a layer of calcified bone. The periosteum is formed by mesenchymal stem cells apical to the calcifying tissue differentiating. However, the mesenchymal stem cells basal to the calcifying tissue differentiate to osteoblasts which form

subsequent layers of calcified tissue. This resulting bone tissue is classified as woven bone which is formed quickly and characterized by randomly oriented collagen fibrils, yet it is not as mechanically viable as lamellar bone.[33,43,54]

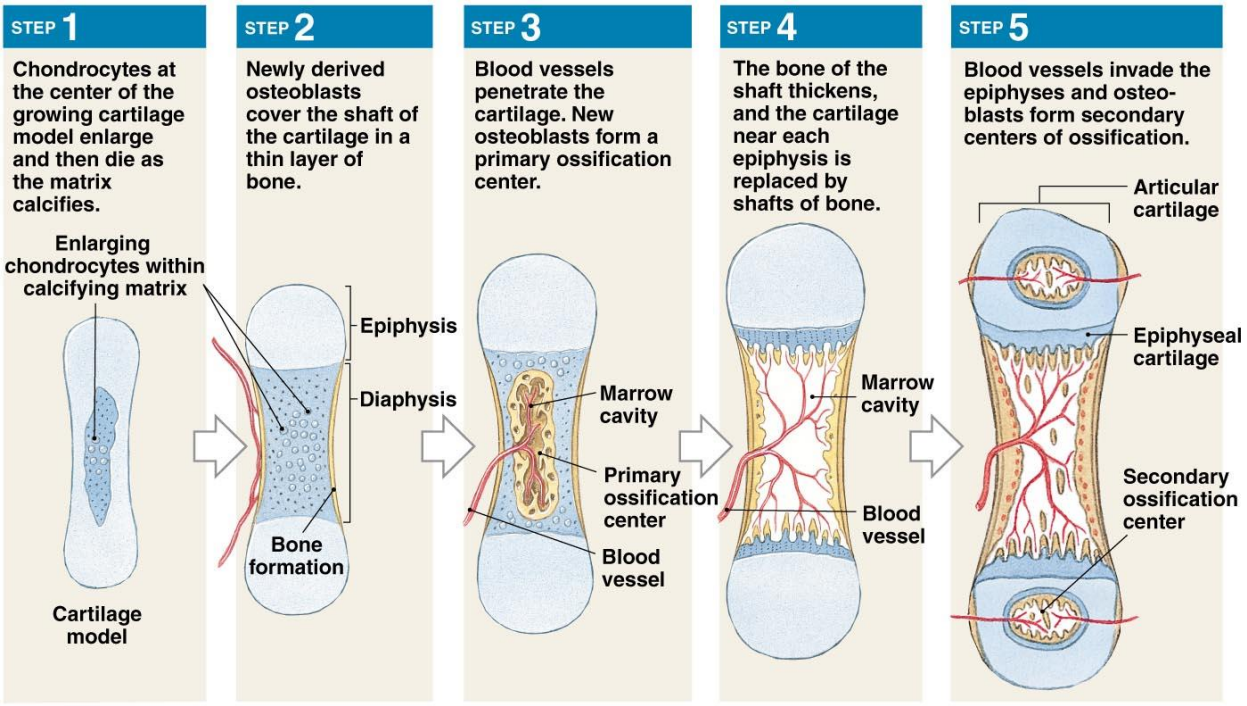


**Figure 5. Diagram showing the stages of endochondral ossification.**[39]

The other type of bone formation known as endochondral ossification occurs in several steps starting with a preexisting cartilage template which begins to be calcified. As this cartilage template becomes calcified, the chondrocytes in the cartilage become hypertrophic and undergo apoptosis.[33,53] Afterwards, mesenchymal stem cells in the membrane surrounding the calcifying cartilage, or periosteum, differentiate into osteoblasts. The osteoblasts secrete an osteoid matrix around the exterior of the cartilage template while a bud of cells originating from the periosteum invades the interior of the partially calcified cartilage template. This periosteal bud leads to vascularization and also innervation of the developing bone as well as

supplying mesenchymal and hematopoietic stem cells into the center of the cartilage template. As previously discussed, the mesenchymal stem cells differentiate to osteoblasts, and the hematopoietic stem cells differentiate to osteoclasts. The osteoblasts and osteoclasts are responsible for remodeling the partially calcified cartilage into woven bone, resulting in ultimately being remodeled to become lamellar bone. Lamellar bone is characterized by collagen fibrils arranged in parallel areas and exhibits greater strength in comparison to woven bone.[33] The bone tissue created from the cells originating from the periosteal bud increases and eventually radiates outward to join the bone tissue created by the osteoblasts on the surface of the cartilage template.[55]

### 1.3. Fracture Healing and Bone Repair

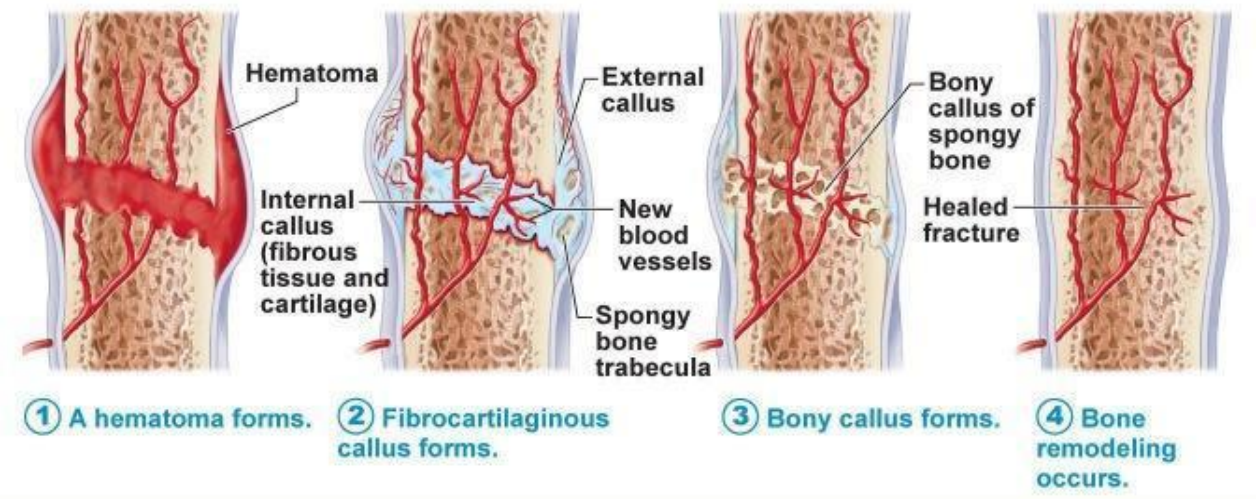


**Figure 6. Diagram showing the stages of the fracture healing process.**[52]

Fractures occur when a force exceeds the mechanical integrity of the bone. Fracture healing is a natural process that can restore the bone to the pre-fracture state function and

mechanical integrity without the formation of scar tissue as seen in figure 6. Broken or fractured bone heals by a mechanism greatly different from the way in which damaged soft tissue is healed. Also, the healing method of bone is indicative of the type of bone damaged (cortical or cancellous). Interestingly, bone is repaired by a process that reiterates many of the events in both intramembranous and endochondral bone formation. Fractured cortical bone is repaired by a callus formation mechanism, in which new bone (callus) composed of fibrous tissue, blood vessels, cartilage, and bone forms in order to bridge the gap between the two fractured bone fragments.[56] Fracture healing occurs in four main stages that temporarily overlap: 1) the early inflammatory stage (hematoma); 2) soft callus formation; 3) hard callus formation; and 4) the remodeling stage.[43,57]

### 1.3.1. Inflammation

The first stage of bone healing is inflammation which is immediately induced by the disruption of the endosteum, periosteum, soft tissue, and blood vessels from the incurred injury. A coagulation cascade is activated as vasoactive mediators and necrotic tissue released resulting in the promotion of blood vessel dilation near the damaged site. The blood that flows from the severed vessels results in the formation of a hematoma at the fracture site containing debris of soft tissue and living and dead bone cells resulting in the recruitment of many signaling molecules involved in the regulation of new bone formation (i.e., ILs, TNF-α, FGFs, BMPs, PDGF, VEGF, etc.).[33,58] Hemostasis is achieved within the hematoma as platelets bind to the fibrillar collagen that forms throughout the site resulting in cell migration, proliferation, and differentiation. New blood vessels are formed from preexisting ones via a process known

as angiogenesis within the hematoma as inflammatory cells, fibroblasts, and preosteoblasts are recruited by growth factors and cytokines released by the inflammatory response.[43] In theory, each population of cells recruited to the fracture site releases a collection of growth factors responsible for additional recruitment of the following cell populations developing a recruitment cascade that sequentially brings the appropriate precursors for new musculoskeletal formation.[58]

### 1.3.2. Soft Callus Formation

The second stage of cortical bone healing is a soft (or primary) callus formation, which includes the formation and organization of fibrous granulation tissue at the site of the fracture which is eventually replaced by mineralized bone in the following stages. During this stage, chondrocytes and fibroblasts produce a semi-rigid soft callus that is able to provide mechanical support for the fracture in addition to serving as a template for the bony callus that will later follow it. The formation of new bone tissue may proceed by either direct or indirect ossification, or intramembranous and endochondral ossification respectively.[59] Generally, the external callus which forms around the periosteum proceeds through intramembranous ossification where pre-existing osteoblasts on the ends of the fracture site proliferate rapidly and directly lay down new bone. In contrast the internal callus undergoes endochondral ossification as fibrocartilage is initially formed and subsequently replaced by mineralized, osteogenic tissue.[58] The growth of the separated cartilaginous regions continues until they unite to generate a big fibrocartilaginous callus which bridges the fracture. Recruited stem cells and fibroblasts from the inflammatory response contribute to the formation of the new

bone, cartilage, fibrous tissue, and blood vessels. Regulation of these cells is controlled by signals from growth factors, hormones, pH, and the mechanical environment.[58]

### 1.3.3. Hard Callus Formation

The third stage of fracture healing is known as hard (or secondary) callus formation, which occurs as hard woven bone replaces the newly synthesized young bone that composes the soft callus. This stage is the most active osteogenic period. High levels of osteoblast activity contribute to the formation of mineralized bone matrix, which arises directly in the peripheral callus. The insecure soft callus is gradually removed followed by revascularization to allow for bridging new hard callus to form. This new bone is known as the hard callus which is characterized typically by irregular and under-remodeled bone tissue; however, it has an increased diameter compared to the original cortex and therefore provides sufficient stability to the defect site. The hard callus formation stage in the fracture healing process, also termed primary bone formation, displays the most rapid osteogenesis which involves: 1) bone cell recruitment and subsequent woven bone formation; 2) chondrocyte apoptosis, osteoclast recruitment, and mineralized cartilage resorption; and 3) continued neo-angiogenesis.[58]

### 1.3.4. Bone Remodeling

After the formation of the woven bone hard callus, the final remodeling stage of fracture healing known as bone remodeling occurs over 12 weeks as the hard callus is gradually remodeled to lamellar bone and the size of the callus is decreased to that of pre-existing bone.

The new bone gradually undergoes a restructuring process that is indicative of the local applied physiological stresses, hence new bone can assume the optimal structure and vasculature to support the mechanical and metabolic needs of the tissue reestablished.[57] This renewal process is achieved by small pockets of old bone being replaced by new bone. In humans, it is estimated that as much as 25% of trabecular bone and 3% of cortical bone is resorbed and replaced each year.[60] Any several humoral or local stimuli of resorption initiate the appearance of osteoclasts and precursors at the remodeling site. The osteoclasts then resorb an amount of bone which produces a small resorption pit known as Howship's lacuna, where they subsequently move on to another site.

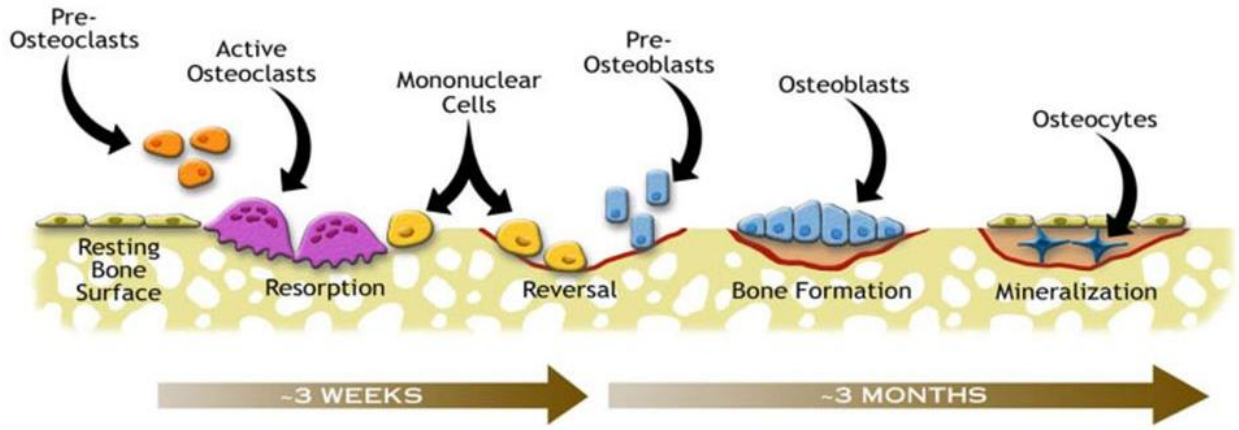


**Figure 7. Diagram showing the process of bone remodeling.**[39]

An active reversal of the resorption phase occurs when a cement line is deposited also known as the reversal phase. A subsequent formative phase occurs as actively synthesizing cuboidal osteoblasts appear and begin to deposit uncalcified matrix known as osteoid which is later mineralized. Resorption and formation always occur successively in the same location as well as in the same order (figure 7). The sequence of resorption and formation described

has been referred to as a basic multicellular unit of bone turnover (BMU).[61] The term coupling refers to when the process of bone resorption is followed by an equal amount of bone formation. The total length of time of the remodeling phase can be from 3 months to several years for full completion.[60]

### 1.3.5. Growth Factors Associated with Bone Healing

Cells receive information from growth factors through the binding of a factor to its receptor which is integrated in the cell's plasma membrane. Each receptor is specific for binding of a particular factor which binds with a high affinity resulting in the stimulation of an intercellular response. Once the factor is bound to the receptor, transmission to the cell may occur in several different ways, depending on the particular factor and its function. Researchers have isolated many of these growth factors for further study and/or incorporation into treatments (i.e. scaffold design, etc.) for bone tissue engineering applications.[58,62–64] Bone healing is a very intricate phenomenon that involves many different steps and factors throughout its process. A summary of commonly studied growth factors associated in the fracture healing process are discussed below for the various bone healing stages.

After a fracture occurs, a blood clot forms at the injury site where platelets release granules to transform the clot into a hematoma. The formation of a hematoma creates an ECM allowing for inflammatory cells such as neutrophils, monocytes, and lymphocytes to have access to the hematoma. Additionally, mesenchymal stem cells (MSC's) are recruited to the site of the fracture within hours of occurring. The recruited cellular response is regulated by secretion of a range of cytokines and growth factors including transforming growth factor-β

(TGF-β), platelet-derived growth factor (PDGF), fibroblast growth factor-2 (FGF-2), vascular endothelial growth factor (VEGF), macrophage colony stimulating factor (MCSF), interleukins-1 and -6 (IL-1 and -6), bone morphogenetic proteins (BMPs), and tumor necrosis factor-α (TNF-α).[64] The factors work in a positive feedback loop to recruit additional inflammatory cells in addition to the migration and invasion of multipotent MSC's.

During the second stage of healing, MSC's are differentiated into chondrocytes resulting in the formation of cartilage. Fibroblast proliferation and chondrocyte proliferation/differentiation occur via a coordinated expression of the following growth factors: TGF-β2 and -β3, PDGF, FGF-1, and insulin-like growth factor (IGF). Cell proliferation and chondrogenesis is also regulated by various factors in the BMP family. The soft callus is subsequently invaded by vascular endothelial cells, angiogenesis, and capillary in-growth via stimulation by pro-angiogenic factors such as BMPs, VEGF, FGF-1 and TGF-β. During the hard callus formation, or primary bone formation, an increase of factors TNF-α, receptor activator of nuclear factor kappa B ligand (RANKL), and macrophage colony-stimulating factor (MCSF) are responsible for mineralized cartilage resorption, the recruitment of MSCs, and induction of apoptosis of hypertrophic chondrocytes. Additionally, various members of the BMP family such as BMP-3, BMP-4, BMP-7, and BMP-8 are upregulated in conjunction with resorption of calcified cartilage and aid in recruiting cells in of the osteoblastic lineage. Upregulation of VEGFs stimulate new blood vessel formation, or neo-angiogenesis. In the final stage of bone healing, the remodeling phase, both osteoblasts and osteoclasts work in combination for the production of secondary bone resulting in the restoration of the bone to its original size, shape, structure, and level of functionality. During this final stage of bone healing, factors IL-1 and IL-6 are upregulated, whereas expression

levels of RANKL, MCSF, and TGF-β gradually decline. In order for the proper bone healing process to occur, the cascade of events occurs by the presence and activation of the appropriate growth factors and cytokines at the specific and appropriate time points. A summary of these growth factors and cytokines for each of the four stages of bone healing can be seen in table 1.[63,64]

| Cytokines/Growth Factor | Bone healing stage | Overall action |
|---|---|---|
| • IL-1, 6<br>• TNFα<br>• PDGFs<br>• GDF-8<br>• RANKL, MCSF<br>• OPG | 1. Inflammation | • Hematoma<br>• Inflammation<br>• MSCs recruitment |
| • VEGFs<br>• TGFβs<br>• BMPs<br>• Angiopoietin<br>• FGF-I<br>• IGF | 2. Soft callus | • Chondrogenesis<br>• Endochondral ossification<br>• Osteoblast/osteoclast precursors recruitment<br>• Vascular ingrowth<br>• New angiogenesis |
| • VEGFs<br>• BMP-2, 7<br>• RANKL, MCSF<br>• Angiopoietin | 3. Hard callus | • Cartilage resorption<br>• Chondrocyte apoptosis<br>• Osteoblast/osteoclast precursors differentiation<br>• Woven bone formation |

| | | |
|---|---|---|
| • IL-1, IL-6<br>• RANKL, MCSF | 4. Remodeling | • Bone remodeling<br>• Marrow establishment<br>• Osteoblast activity |

**Table 1. Growth factors associated with fracture healing.**[63,64]

### 1.3.6. Osteogenic Markers

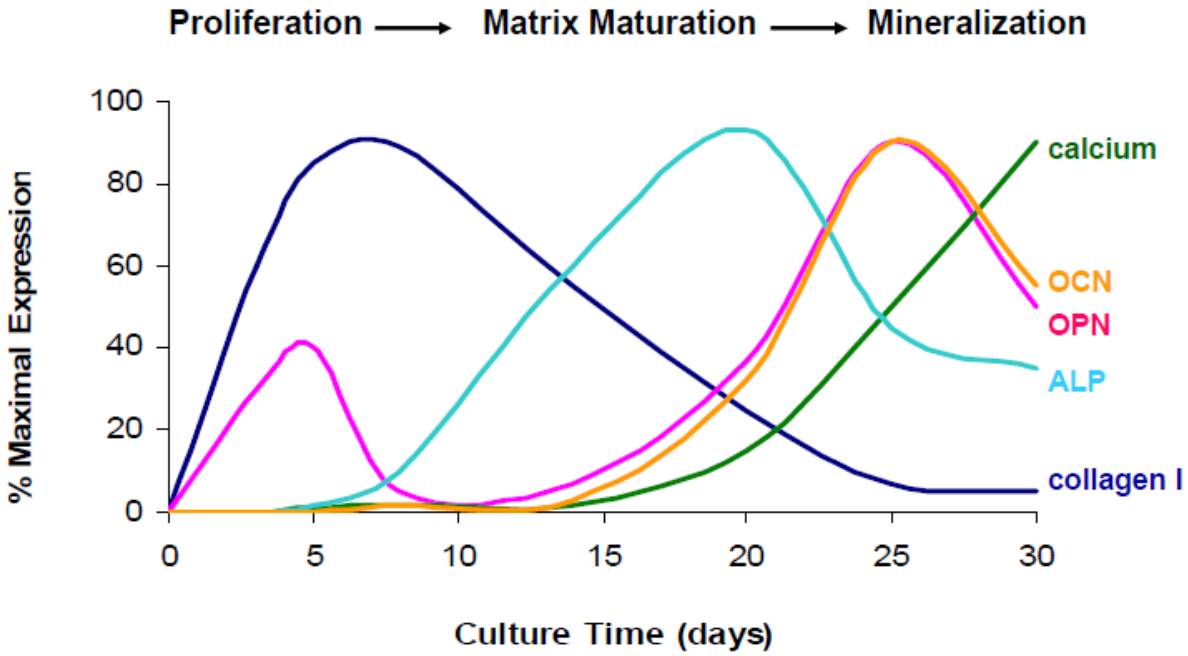


**Figure 8. Expression of osteoblast markers relative to culture time in respect to their contribution to different phases of bone formation.**[65]

Various osteoblast markers are responsible for cell differentiation and matrix mineralization over time as can be seen in figure 8. Expression levels of calcium, osteocalcin (OCN), osteopontin (OPN), alkaline phosphatase (ALP), collagen type I (Col I), and core

binding factor alpha-1 (cbfa1), also known as Runx2, vary over time during osteoblastic differentiation, proliferation, and matrix mineralization.[65] Understanding when differentiating osteoblasts express each specific marker allows for understanding of a cell's approximate stage within osteoblastic development. Mesenchymal stem cells begin culture in a proliferative phase and continue to differentiate into osteoblasts during matrix maturation and mineralization. During this period, the mesenchymal stem cells produce the various proteins and growth factors in a temporal pattern that is indicative upon their functional activity.[33] As the osteoblastic markers expression were of interest to this work particularly relating to ultrasound treatment and mechanical environment, each marker will be discussed further in the following sections.

#### 1.3.6.1. Alkaline phosphatase (ALP)

Alkaline phosphatase (ALP) in bone is a glycoprotein located on the cell membrane of osteoblasts and is known to be the most commonly measured phenotypic osteoblast marker.[66] However, ALP is found in several other non-mineralized tissues including liver, kidney, intestine, and placenta. ALP is an enzyme that hydrolyzes phosphate esters from a number of different types of molecules including proteins and nucleotides, and received its name according to its enhanced activity at high pH levels.[33] ALP has been shown to be important to the process of bone mineralization. Literature has shown evidence of disease states lacking ALP resulting in abnormal or lack of mineralization. Hypophosphatasia, a potentially lethal syndrome that causes abnormal mineralization of the skeleton, results from a missense mutation in the ALP gene.[67] Additionally, ALP-lacking cells hence incapable of

mineralization can be transfected with the gene for ALP in vitro resulting in the acquired ability to mineralize.[68] ALP gene expression generally begins when a cell transitions from the proliferative to the matrix maturation stage, peaks during matrix maturation, and then decreases upon entrance of the osteoblastic mineralization stage. The role of ALP in mineralization can be summarized by the following: 1) ALP hydrolyzes phosphate ester and results in the increase of local phosphate concentrate ultimately promoting bone mineral formation; 2) ALP hydrolyzes pyrophosphate, a calcification inhibitor, into phosphate molecules; 3) ALP transfers phosphate groups from the extracellular fluid and binds calcium to facilitate calcium phosphate precipitation.[69,70]

#### 1.3.6.2. Osteocalcin (OCN)

Osteocalcin (OCN) is a calcium-binding protein that is the most abundant non-collagenous protein in bone tissue. While the exact role of OCN is not completely understood, it is known to have a role in the process of bone mineralization, during which it binds to calcium phosphate in the ECM of osteoblasts.[71,72] It is exclusively produced by osteoblasts and odontoblasts, and its function is dependent on vitamin K.[73] OCN is primarily synthesized during the matrix mineralization stage of osteoblastic development, but may be marginally produced at earlier stages of matrix mineralization.[33] Additionally, it has been suggested that OCN acts as a chemoattractant for osteoblasts, osteoclasts, and blood monocytes.[73] Importantly, most of an organisms OCN is localized within the bone cell matrices; however, when osteoblasts are producing large amounts of OCN during the mineralization phase of

osteoblastic development, some OCN is also emitted into the blood. For this reason, serum levels of OCN are considered to be indicative of new bone formation.

#### 1.3.6.3. Osteopontin (OPN)

Osteopontin (OPN) is a secreted glycoprotein that was originally found in osteoblasts and is produced by a variety of cells including preosteoblasts, osteoblasts, osteocytes, endothelial cells, and macrophages, and its synthesis is stimulated by vitamin D3.[33] OPN has been shown to have a strong affinity for calcified matrix such as bone.[74] When OPN is modified via transglutamation, it binds covalently to collagen type I.[75] In bone, OPN is generally synthesized by osteoblast-lineage cells and incorporated into the extracellular matrix. OPN is synthesized by preosteoblasts late in the proliferation stage, and by osteoblasts throughout the matrix maturation and mineralization stages.[33] While the function of OPN in bone is not completely understood, it is thought to be related to the process of bone resorption due to its proven interactions with osteoclasts[76] and supportive role for their function in mineral resorption.[77] As the molecular conformation of OPN is altered by calcium-binding in a $Ca^{2+}$ concentration-dependent manner, the binding-dependent conformation change has been suggested to expose various binding motifs that resultantly modulate the protein's activity. This modulation ability is thought to directly affect the process of osteoclast-mediated bone resorption.[33]

#### 1.3.6.4. Collagen type I (COLI)

Collagen is the primary protein in a number of animal tissues, including bone, cartilage, tendons, and teeth. Overall, it constitutes approximately 25% of the entire protein content in mammals.[78] Collagen is a long, fibrous protein found in the extracellular matrices of cells that functions as a mechanical support for tissues. The structure of a collagen molecule consists of triple helix subunit that is made up of three polypeptide strands. These strands are each left-handed helices that are wound together into a right-hand coiled coil stabilized by hydrogen bonding; a configuration that gives collagen its characteristic strength.[79,80] Triple helix subunits are wound together in multiples to make collagen fibrils, which can further be assembled into collagen fibers.[33] Various types of covalent cross-linking between triple helices distinguish the 28 different types of collagen that have been identified; however, nearly 90% of the collagen in the body is made up of collagen types I-IV.

Collagen type I (COLI) is the most abundant form of collagen in the human body and constitutes a major component of osteoblast extracellular matrices.[33] As bone tissue is a composite made up of organic (proteins) and inorganic (CaP) components, the unique structure of collagen provides bone tissue with elasticity and helps to prevent fractures under applied stress. Bone tissue contains collagen type I triple helices that are covalently crosslinked and arranged in parallel with 40 nm gaps between the ends of adjacent molecules.[81] In the extracellular space, collagen molecules are attached to cell membranes with the help of a number of different proteins such as fibronectin and integrin.[82] Collagen type I triple helices are composed of two different chains called pro-alpha1(I) and pro-alpha2(I), which are coded for by two different genes, named COL1A1 and COL1A2, respectively.[33] While the chains

are manufactured inside of the cell, they must be processed extracellularly to form the triple helix with the help of enzymes. The majority of collagen type I is produced by late preosteoblasts and osteoblasts during the process of matrix formation.[33]

#### 1.3.6.5. Core binding factor alpha-1 (cbfa1) (RUNX2)

Core binding factor alpha-1 (cbfa1), or Runx2, is a transcription factor thought to be the primary control switch for the production of various osteoblastic marker proteins such as alkaline phosphatase, collagen type I, osteocalcin, and osteopontin.[83] It is the only transcriptional factor that is specifically expressed in osteoblastic lineage cells and is thought to be the earliest specific marker of osteogenesis.[33] Runx2 is part of the Runt family of transcription factors and has been documented to be essential to the differentiation of mesenchymal stem cells into mature osteoblasts.[84,85] While the exact functional role of Runx2 is still not fully understood, growth factors and biochemicals such as transforming growth factor-β (TGF-β), dexamethasone, and bone morphogenetic growth factor-2 (BMP-2) have been shown to increase primary human osteoblastic cbfa1 mRNA levels in vitro.[86] Additionally, another studied showed that mice lacking cbfa1 were completely unable to form bone and contained osteoblasts that lacked osteocalcin and osteopontin, two noncollagenous matrix proteins responsible for matrix maturation and mineralization.[87]

## 1.4. Bone Grafts and Bone Graft Substitutes

While bone is highly vascularized and has the ability to regenerate, beyond a critical point, clinical intervention is required for successful healing. Besides fractures, other large scale defects can result from sources such as trauma or cancer. Additionally, mal-unions, non-unions, or fractures occur at a higher rate in people with degenerative skeletal diseases resulting in more difficulty in treating the injuries as opposed to trauma alone. It comes as no surprise that bone is one of the most commonly transplanted tissues, ranking at second in the world.[22] Critical defects are voids in the bone that are too big to heal by the body's natural process requiring intervention such as bone grafts or bone graft substitutes. Some of the criteria for the ideal bone substitute which is also sought after in bone tissue engineering applications discussed later are osteoconductivity, osteoinductivity, osteogenicity, and immune-compatibility.

### 1.4.1. Autografts

Autografts are currently considered the gold standard for enhanced bone healing as they provide patient-specific tissue and the best chances of successful healing without immuno-rejection or other complications through possessing optimal biocompatibility, biological components, and pore structure. Bone grafts are taken from a healthy site and placed into another site within the same individual. However, autografts have a major limitation as there is only so much tissue that can be harvested from one patient in addition to the need for an additional surgical site which can lead to infection, post-operative pain, and donor site

morbidity. Autologous bone contains osteoblasts and osteoprogenitor cells capable of making new bone, as well as the intact ECM and embedded bioactive proteins/molecules, which makes autologous bone the most suitable choice for bone repair. Importantly, cells typically retain their viability after implantation of the autologous tissue. No adverse immunogenetic responses are associated with autografts as the ability of the graft to be incorporated into host tissue is highly enhanced.[88] Lastly and importantly, there is no risk of disease transmission with autologous tissue.

Autologous bone grafts can be obtained from various bones sources such as iliac crest, tibia, radius, and humerus.[88,89] The iliac crest is the most commonly used donor site due to easy accessibility and the amount of bone available; however, harvesting autologous bone can cause significant donor site morbidity which results in further complications. Donor site morbidity occurs in approximately 20% of all cases.[23,90] When large amounts of bone are needed, the necessary amounts of autograft may not be available from the host. In this case, other bone graft materials must be considered.

### 1.4.2. Allografts

Allografts are the next choice in line for bone graft procedures as they are tissue harvested from one individual and implanted into another individual; however, these run the risk of disease transmission or immune-rejection.[88] Considering the limitations of autografts, allografts are used clinically as a common alternative. Bone allografts can be obtained through regional tissue banks and are used as fragments. Bone allografts are used as fragments, in

powder form and in solid forms and are provided as cortical, cancellous, or cortico-cancellous grafts, similar to autografts.[15]

Allografts are processed as demineralized, fresh, frozen, or freeze-dried forms of bone. There is greater availability of allografts, as they are usually isolated from cadavers.[91] The major advantages of allografts therefore lie in their availability in different shapes and sizes, and avoidance of donor site morbidity. Major disadvantages of allografts include the risk of transferring bacterial and viral diseases, such as human immunodeficiency virus (HIV) and hepatitis viruses. In addition, since they are not autologous, they may induce unwanted immunological responses that could disrupt the bone healing process, and may ultimately lead to rejection of the graft.[91,92]

Allografts from harvested from fresh cadavers undergo very little processing resulting in the preservation of their cellular and organic content. However, fresh bone allografts may present clinical challenges given the higher chance of immune response associated with this type of graft (host cells attacking the transplanted tissue) and the increased risk of disease transmission. Methods for sterilization and storage, such as freeze-drying or treating the grafts with hypotonic solutions (e.g. acetone) or gases (e.g. ethylene oxide), which can remove bacteria and viral particles, result in a decreased risk of disease transmission.[93–95] A drawback of these processes is that they may denature/destroy the proteins within the allograft consequently reducing the osteoinductive capacity.[88,92] As a result, freeze-dried allografts, when compared to autografts, take more time for cellular migration and infiltration. In addition, this method also reduces the biomechanical properties of the graft. Due to these disadvantages of allograft processing, more suitable materials are required for bone grafting.

### 1.4.3. Bone Graft Substitutes

| Class | Description |
|---|---|
| Allograft-based | Allograft bone used alone or in combination with other materials |
| Factor-based | Natural and recombinant growth factors used alone or in combination with other materials |
| Cell-based | Utilize cells to generate new tissue either alone or seeded onto a support matrix |
| Ceramic-based | Includes calcium phosphate, calcium sulfate, and bioactive glasses used alone or in combination |
| Polymer-based | Both degradable and non-degradable polymers used alone and in combination with other materials |

**Table 2. Description of classification system for bone graft substitutes. Many of the currently available bone graft substitutes fall within one or more of the above-described groups.**[92]

Bone grafts and bone graft substitutes can be used alone or in conjunction with other additives to increase successful incorporation. There are several categories of bone graft substitutes encompassing varied materials, material sources, and origin (natural vs. synthetic). A bone graft classification system, described in table 2, has been developed to describe these groups based on their material makeup.[92] Allograft-based bone graft substitutes can be used

alone or in combination with other growth factors or materials. Additionally, natural and recombinant growth factors are another source and can be used alone or in combination with other materials. The utilization of cells, of particular interest, various stem cell types, to generate new tissue either alone or seeded onto a support matrix provides another feasible bone graft substitute option. Various ceramics such as calcium phosphates and bioactive glasses used alone or in other combinations are another viable option for bone graft substitutes as they can mimic the inorganic portion of native composite bone tissue if they are fabricated in an optimal way. Polymers are another viable option as a bone graft substitute as they are relatively easy to manufacture and can be degradable or nondegradable depending upon their application for use. Lastly, hydrogels, such as collagen, serve as another alternative and may be useful for cell encapsulation and allow for degradation where the bone cells own extracellular matrix may secure the growth of a new extracellular matrix to replace the initial suspended structure. Further discussion of each class of bone graft substitutes is provided in the following sections. When considering the selection of biomaterials for bone graft substitutes, a few key properties are worth noting including biocompatibility, biodegradability, mechanical properties, osteoconductivity, osteoinductivity, osteointegrity, osteogenicity, and porosity. These terms are defined below.[92]

**Biocompatibility** – Biocompatible grafts do not elicit an immune response, and therefore minimize the host's natural tendency to eliminate the foreign species.

**Biodegradability** – Biodegradable scaffolds are capable of gradual decomposition so that newly formed tissue may appropriately fill in the defect site, and therefore eliminate the need for a second surgery to remove the original graft.

**Mechanical properties** – A graft should have the mechanical properties that are similar to those of the native bone. While a weak graft may not have sufficient load-bearing capabilities, an overly strong graft may result in stress shielding that could lead to the resorption of the newly forming bone.

**Osteoconductivity** – This property refers to a graft's ability to support the attachment, proliferation, and migration of new osteoblasts and osteoprogenitor cells onto its surface and has an interconnected pore system that allows these cells and others to migrate throughout the structure.

**Osteoinductivity** - This property describes the ability of a graft to induce non-differentiated stem cells or osteoprogenitor cells down the osteoblastic lineage. A graft may possess this capability via the addition of growth factors or other inductive agent.

**Osteointegrity** – An osteointegrative graft can bond to the surrounding tissues through new tissue growth and/or mineral formation. A graft stably fixed in position is necessary to direct the proper localized bone formation while accepting the required mechanical responsibilities.

**Osteogenicity** – An osteogenic graft is one that is cellularized with osteoblast-lineage cells, and furthermore supports the mineralization of the cells' collagen-based ECMs.

**Porosity** – An appropriate and interconnected pore structure provides a means for cellular migration and to transfer nutrients and waste between the cells on the scaffold and the surrounding environment. Without proper molecular transport, cells become starved of required nutrients and poisoned with generated toxins.

#### 1.4.3.1. Allograft-based

Prior to the 1980's, allograft tissue was mainly used as a substitute for autografts for large defect sites. However, since then the use of allograft tissue has increased from approximately 5,000-10,000 cases in 1985 to almost 150,000 cases in 1996.[96] Between methods of donor screening and tissue processing, risk of disease transmission from allograft tissue has been reduced and therefore become a more attractive alternative to the autograft. As the clinical acceptance of allograft tissue has increased, numerous products have emerged that are allograft-based but also used in combination with other materials and/or growth factors.[6,92,97,98]

Demineralized bone matrix (DBM) is another clinically used bone graft substitute produced by acid extraction of allograft cortical bones.[99,100] DBM is attractive as it exhibits both osteoinductive and osteoconductive properties.[6,15,89,100] The effectiveness of DBM comes in part due to the osteoconductive scaffold in addition to osteoinductivity provided by the presence of endogenous growth factors including bone morphogenic proteins (BMPs), fibroblast growth factor 2 (FGF-2), insulin growth factor 1 (IGF-1) and tumor growth factor beta (TGF-β).[99,100] Additionally, DBM serves as an effective cell carrier as it does not

stimulate a large immunological response from host cells from the removal of antigenic surface structure of bone during the demineralization processing. DBM has exhibited angiogenic properties as it has been shown to vascularize fairly quickly.[101] Various commercial forms of DBM are available clinically including powder, granules, gel, putty, and strips, and additional products are currently under FDA approval or review. Similar to allografts, osteoinductive potential of DBM can be affected by processing methods, sterilization, and storage. Additionally, as DBM is an allogenic material, risk of disease transmission such as HIV exists similar to allografts.[99,100] Another drawback to DBM is structural integrity due to its poor mechanical properties.

#### 1.4.3.2. Factor-based

Factors and proteins in bone are responsible for regulating cellular activity by binding to receptors on cell surfaces resulting in the stimulation of the intracellular environment. Generally, this translates to a protein kinase that induces a series of events resulting in the transcription of mRNA and ultimately into the formation of a protein to be used intra- or extra-cellularly. Many factors act simultaneously on a cell which results in the controlled production and resorption of bone. Factors residing in the extracellular matrix of bone include transforming growth factor-β (TGF-β), insulin-like growth factor (I and II)(IGF), platelet-derived growth factor (PDGF), fibroblast growth factor (FGF) and the bone morphogenetic proteins (BMP's). The mentioned factors have been isolated and some have been synthesized, allowing for the investigation of function of the factors both alone or in combination. The capability of isolating appropriate factors from bone, synthesizing them in large quantities, and

reapplying them in concentrated amounts to accelerate bone healing has produced many future possibilities for bone graft substitutes.[92]

While factor-based therapies have demonstrated advantages in bone defect repair and regeneration, some distinct disadvantages remain including high manufacturing cost, risk of contamination, potential immunological response, protein instability,[102–104] and the risk of uncontrolled bone growth or cancer.[92,105] An alternative to factor-based therapies is the use of 'small molecules', which are lower-molecular-weight organic compounds than their full protein counterparts (typically <1,000 Da). The use of small molecules is a relatively new area of research that is growing rapidly, and their attractiveness is in part due to their capability of diffusing across cell membranes to reach intracellular targets.[106,107] Additionally, small molecules exhibit beneficial qualities not inherently found with protein growth factors including being more stable, soluble, nonimmunogenic, affordable, and requiring a lower effective dose[108] while still exhibiting the same efficacy as the full protein.[92]

#### 1.4.3.3. Cell-based

Cell-based strategies allow researchers to investigate the use of delivering exogenous cells to a tissue defect using a suitable scaffold to accelerate tissue regeneration. Cells seeded within a biomaterial scaffold can be cultured in vitro in bioreactors prior to implantation or by directly seeding the cells on the scaffold before implantation. Cells have also been shown beneficial to regenerate bone when directly injected into the defect in the absence of biomaterials.[109–111] With the emerging capabilities of regenerative medicine, various sources of stem cells have been considered to meet patient-specific demand for bone tissue

engineering. Stem cells are attractive candidates based on their proliferative and regenerative capabilities hence avoiding certain supply limitations of adult somatic cells. Commonly studied stem cells for these applications include mesenchymal stem cells (MSCs), induced pluripotent stem cells (iPSCs)[112], and adipose-derived stem cells (ADSCs). In 2006, Yamanaka et al. revealed a significant breakthrough discovering how adult somatic cells treated with the right factors could be engineered back to a pluripotent state capable of producing any cell in the body. These cells induced back to an earlier cell lineage became known as iPSCs and carry the potential for many regenerative capabilities.[113]

#### 1.4.3.3.1. Mesenchymal stem cells (MSCs)

MSCs can be differentiated *in vitro* to the osteogenic lineage by being cultured in the presence of certain additives including TGF-β, BMP-2, -4, and -7. Phenotypic assays and staining can confirm the osteoblast-like cell phenotype of the stem cell.[114] MSCs have been defined through the expression of various cluster of differentiation (CD) markers and have been isolated from a number of adult sources including bone marrow,[115] peripheral blood,[116] umbilical cord blood,[117] synovial membrane,[118] adipose tissue,[119] brain, skin, heart, kidneys, and liver.[120] Of common interest are bone marrow-derived mesenchymal stem cells (BMSCs), which are multipotent stem cells capable of differentiating into several mesenchymal lineage-derived cell types including osteoblasts.[121] An advantageous use of BMSCs is that they can be obtained via bone marrow aspiration, percutaneously. Additionally, proliferation and differentiation of stem cells derived from BMSCs can be increased by the addition of growth factors[122,123] or by seeding onto osteoconductive scaffolds prior to implantation, such as

collagen matrices.[124,125] The use BMSC-seeded scaffolds with growth factors such as BMP-2 has been shown to enhance healing of critical-size defect models in both rat[126,127] and rabbit.[128–130] While the potential regenerative capabilities of BMSCs appear vast, as with any bone graft substitute, limitations exist. Drawbacks include the pain and discomfort from the bone aspiration procedure and the difficulty in obtaining a sufficient number of cells required for the procedures, particularly in the case of large bone defect repair. Additionally, studies have shown that various factors can significantly limit the actual amount and quality of MSCs obtainable for clinical application. Approximately four to six weeks are required for cell expansion before clinical treatment, yet a maximum of 24-40 population doublings are reached before the cells result in a senescence-associated growth arrest. As donor age and systemic disease increases, osteogenic differentiation potential *in vitro* and bone forming efficiency *in vivo* significantly decreases. Further knowledge about common markers is needed to help identify and define MSCs isolated from different sources.[131,132]

#### 1.4.3.3.2. Adipose-derived stem cells

ADSCs offer an attractive source of stem cells as the cells can be rapidly expanded and as supply limitations and ease of harvesting is less problematic given the ready access of patient adipose tissue deposits under the dermal layers. ADSCs are multipotent cells easily isolated from fat subcutaneously that can be induced to differentiate into the osteogenic lineage.[133] Studies have shown promising results using ADSCs in animal defect models. Implantation of poly(lactic-co-glycolic acid) (PLGA) scaffolds seeded with ADSCs in rat calvarial defects resulted in complete healing of the defect in 3 months.[134] Successful repair

of critical-size cranial defects in canines[135] and rabbits[136] by delivery of ADSCs via coral and nano-hydroxyapatite-collagen/PLA composites, respectively. While ADSCs do not face the supply limitations of other cell types, drawbacks include lower osteogenic potential compared to BMSCs, as indicated in various *in vitro* and *in vivo* studies.[133] The major challenge in finding efficacy in cellular therapies is both the identification of the cell sources as well as appropriate scaffolds for delivery and implantation to the bone defect site in order for cellular differentiation into osteoblasts and the formation of neo-vasculature.[137,138] In addition to MSCs, iPSCs, and ADSCs, other stem cell types including human umbilical vein endothelial cells (HUVECs),[139] muscle derived stem cells (MDSCs),[140] embryonic stem cells (ESCs),[141] and endothelial progenitor cells (EPCs)[142] are also currently under investigation; however, to date, none of these alternative cell sources have provided significant evidence to surpass the osteogenic potential of BMSCs.

#### 1.4.3.4. Ceramic-based

Currently available ceramic-based bone graft substitutes include products containing calcium sulfate, bioactive glass, and calcium phosphates. Ceramic-based bone graft substitutes are relevant, especially calcium phosphates, because the primary inorganic compound of bone is calcium hydroxyapatite (HA), a subset of the calcium phosphate group. As a result, the particular manufacturing methods of calcium phosphates can come close to mimicking the natural matrix of bones depending on the scaffold's structure and porosity. They are manufactured in a variety of types including coralline HAs, synthetic HAs, and tricalcium phosphates, which can be processed into various workable forms such as solid matrices,

injectable pastes, or putties. Calcium phosphates exhibit relevant properties to bone graft substitute applications as they are osteoconductive, osteointegrative, and in some cases osteoinductive.[143] It comes as no surprise that HA-based biomaterials are the most widely used bone graft substitutes because of their unique properties.[144]

Studies have shown that MSCs cultured and seeded on HA constructs successfully differentiate into osteoblasts which results in bone tissue growth on the HA surface.[145] Calcium phosphate cement (CPC) is commonly manufactured as an injectable paste and is of particular interest. CPC is a mixture of tetracalcium phosphate and dicalcium phosphate anhydride.[146,147] The cement is unique due to its ability to react at body temperature to form a paste containing crystals of calcium phosphates and upon implantation can form HA within the body.[146] The cement is advantageous as it is a freely moldable and adaptable material, making it suitable for irregularly shaped bone defects. Osteoblasts' proliferation and differentiation has been found to have dependence upon not only calcium phosphate composition, but also the structure and crystallinity of the scaffold which can be modified to particularly specifications during the fabrication process. Higher crystallinity HA has been found to have lower efficacy for *in vitro* culturing of rat osteoblasts as an early increase in proliferation was seen; however, a subsequent drop off was evident as culture time increased.[148] Lower crystallinity HA scaffolds have shown better effectiveness as cultured rat osteoblasts experienced gradual yet increased proliferation as time increased as the scaffold more closely mimics natural bone in overall crystallinity in comparison to highly crystalline forms.[149–151]

Studies have shown a direct relationship exists between reduced crystallinity and increased healing rates.[152] Another advantageous property of lower crystallinity calcium

phosphates is that they are more soluble in body fluid as well as *in vitro* analogues in comparison to higher crystallinity calcium phosphates, resulting in a higher ion concentration near the scaffold,[148] and a plate-like precipitation on the scaffold surface, leading to increased bone repair activity.[153] As with any biomaterial, certain favorable biological properties have negative tradeoffs. In particular, ceramics, including crystalline HA, are extremely brittle resulting in failure under load-bearing situations.[151,154] Additionally, the processing of ceramics for scaffold formation often requires exposures to high temperatures which complicates the incorporation of biological molecules. As native bone tissue demonstrates mechanical resilience as it naturally is a composite material composed of its flexible organic and rigid inorganic counterparts, to combat the brittle properties of ceramics, they are often combined with other materials to form a composite for enhanced mechanical integrity.

#### 1.4.3.5. Polymer-based

Polymer-based solutions are considered as good candidates for bone grafting materials due to their controllable mechanical properties and biocompatibility. By controlling processing, chemically modified polymer materials have the advantage to suit biological applications through specific functionalization in addition to degradation modification. As with any biomaterial scaffold, the polymer biomaterial must suit the mechanical demands of the defect in addition to allowing for little to no immune response from its degradation products. Polymers used today can be loosely divided into two categories: natural and synthetic polymers, which can be further divided into degradable and nondegradable. Hydrogels are another representation of polymeric structures which consist of networks of

natural or synthetic hydrophilic polymer chains capable of containing over 99.9% water by mass. Hydrogels will be discussed further in the following section.

Natural polymers are derived from living sources such as animals, plants and microorganisms. Polysaccharide-derived polymers such as chitan and chitosan, hyaluronic acid (HA), alginate, starch and cellulose-based polymers have been on the forefront of research for the development of scaffolds for bone, cartilage, and skin regeneration.[155] Collagen and chitosan are two commonly used natural polymers in bone tissue engineering applications. Collagen, a natural polymer that is vastly present in connective tissues, has been used alone or in combination with other materials in numerous bone graft substitute applications and is a main focus of this thesis. As collagen is a main organic component of the extracellular matrix in bone tissue, it is highly attractive as a bone graft substitute and has been used in combination with other materials for clinical procedures.[100] Collagen sponges, typically made from bovine collagen, are manufactured by numerous companies with or without other growth factors and/or materials and are commonly used in bone defect sites to promote bone growth and healing such as in spinal fusion surgeries.[89,156–159] Medtronic (U.S.A.) manufactures a product known as InFUSE™ Bone Graft which is a collagen sponge that serves as an osteoconductive carrier of bone morphogenetic protein (BMP-2) for spinal fusions.[160,161] Natural polymers are advantageous for tissue engineering applications because they can mimic the endogenous extracellular matrix and surrounding tissues recognize and metabolize their products through common pathways. While natural polymers offer many advantages, downsides include the possibility of causing immunological responses, lot variability among different supply sources, and inferior mechanical properties to synthetic polymers.[92] Particularly, the compressive

strength of collagen-based bone substitutes is typically weaker than cancellous bone, rendering them unsuitable for load bearing bone defects.[162]

Synthetic polymers a currently clinically available as options for bone grafting materials and can be manufactured into various shapes for optimum surface textures and pore sizes conducive to tissue formation. Degradable polymers are commonly used in tissue engineering applications where the natural extracellular matrix will eventually replace the scaffold. Importantly, the tissues surrounding the scaffold must be capable of processing the degradation products from the polymer via metabolization or excretion, otherwise an immunological response may occur. Synthetic polymers can be designed with chemical functional groups that allow for tissue ingrowth. Aliphatic polyesters including poly(lactic acid) (PLA), poly(glycolic acid) (PGA), and their copolymer poly[(lactic acid)-co-(glycolic acid)] (PLGA) are the most widely used synthetic polymers in tissue engineering and are well characterized having gained FDA-approval for certain clinical applications such as sutures. PLGA has been studied in multiple tissue engineering applications including bone,[163] cartilage,[164] ligament/tendon,[165] nerve,[166] and skeletal muscle.[167] The degradation rates of these polymers can be controlled by adjusting their molecular weights.[168] These polymers are highly attractive due to their ease of processing and formability to suit a range of applications. While ceramics require heating to extremely high temperatures for processing,[169] hydroxyesters have relatively low glass transition temperatures therefore being able to be processed using conventional heating methods.[168] Specific structural and chemical properties can be achieved by tissue engineers by methods such as solvent-casting, porogen-leaching, and electrospinning.[168]

#### 1.4.3.6. Hydrogels

Hydrogels are of particular interest to this work as they can be used for space-filling scaffolds, for cell delivery, and for bioactive molecule delivery.[170] As hydrogels are another representation of polymeric structures, they provide a great method to create a three-dimensional environment for cells to migrate along their hydrophilic polymer chains in an environment that can contain over 99.9% water by mass. A major focus of this work is the capability to deliver an appropriate cell source to a bone defect area for remote mechanical stimulation to accelerate bone healing and regeneration. Hydrogel-based products have been greatly improved over recent years such as for soft contact lenses which are typical made from poly(hydroxyethylmethacrylic) acid [poly(HEMA)]. Other biological adhesives have been developed from reconstituted fibrin or albumin for use in surgical procedures. Applications for hydrogels have been investigated for bone, cartilage, intervertebral, and cardiac regeneration. Where adult muscle stem cells typically lose their pluripotency and undergo massive cell death within the first weeks of culture on rigid plastic culture dishes, when they were cultured on chemically crosslinked bioactive poly(ethylene glycol) (PEG) hydrogels, the cells showed evidence of self-renewal and were engrafted with substantially better integration in a muscle implant model.[171] Additionally, 'smart' hydrogels are an interesting biomaterial currently under research for many applications due to their ability to change shapes. Smart hydrogels are able to dynamically shrink, swell, or degrade based on exposure environmental stimuli including pH, temperature, and other activators. As their smart capabilities allow them to be maneuvered through small, tight pathways, they are often investigated for vascular applications.[172] Collagen hydrogels are attractive candidates for scaffolds in bone tissue engineering and particularly for this thesis.

#### 1.4.3.7. Composites

As bone tissue inherently is a composite material made of collagen proteins which provide an elastic phase to a more rigid and stiffer calcium phosphate matrix, in order to engineer bone graft substitutes to mimic natural and physiological conditions, in many cases, composites, or substances containing two or more constituent materials, can best suit the application at hand. Where one constituent material alone could not provide the mechanical integrity needed for an application on its own, often the combination of the two or more materials provides the strengths of each of the materials and minimizes each constituent material's weaknesses. Composite-based bone graft substitutes have shown promising results in bone tissue engineering applications. As bone is largely made of type I collagen and HA and both materials are osteoconductive, together they can be manufactured together as a composite material capable of supporting bone regeneration.[173] It has been shown that collagen-HA composites provide higher osteogenic potential towards human osteoblast-like cells in comparison to HA scaffolds alone.[174] As the use of composites can significantly modulate the mechanical properties, the ductile properties of collagen have been shown to increase the fracture strength of HA. Collagen-based matrices can have their stability significantly improved by chemical cross-linking.[124,175–178] The use of aldehydes can crosslink the amine groups within collagen; however, potentially toxic residues can remain if the process is not appropriately optimized resulting in the implantable collagenous grafts being less acceptable. Additionally, polymer-ceramic composites, as with bone, are capable of providing the benefits of each material while counteracting each's limitations. It has been shown that

polymer-ceramic composite scaffolds have successfully been used *in vitro* and *in vivo* to differentiate stem cells into osteoblasts.[179]

### 1.5. Bone Tissue Engineering

Tissue engineering involves the application of biological, chemical and engineering principles towards the development of biological substitutes for the repair, restoration, or regeneration of tissue form and function.[24] The field of bone tissue engineering investigates the combination of interaction of cells with specific biomaterials and/or growth factors to restore bone to its original and functional state following instances of fractures, trauma, or

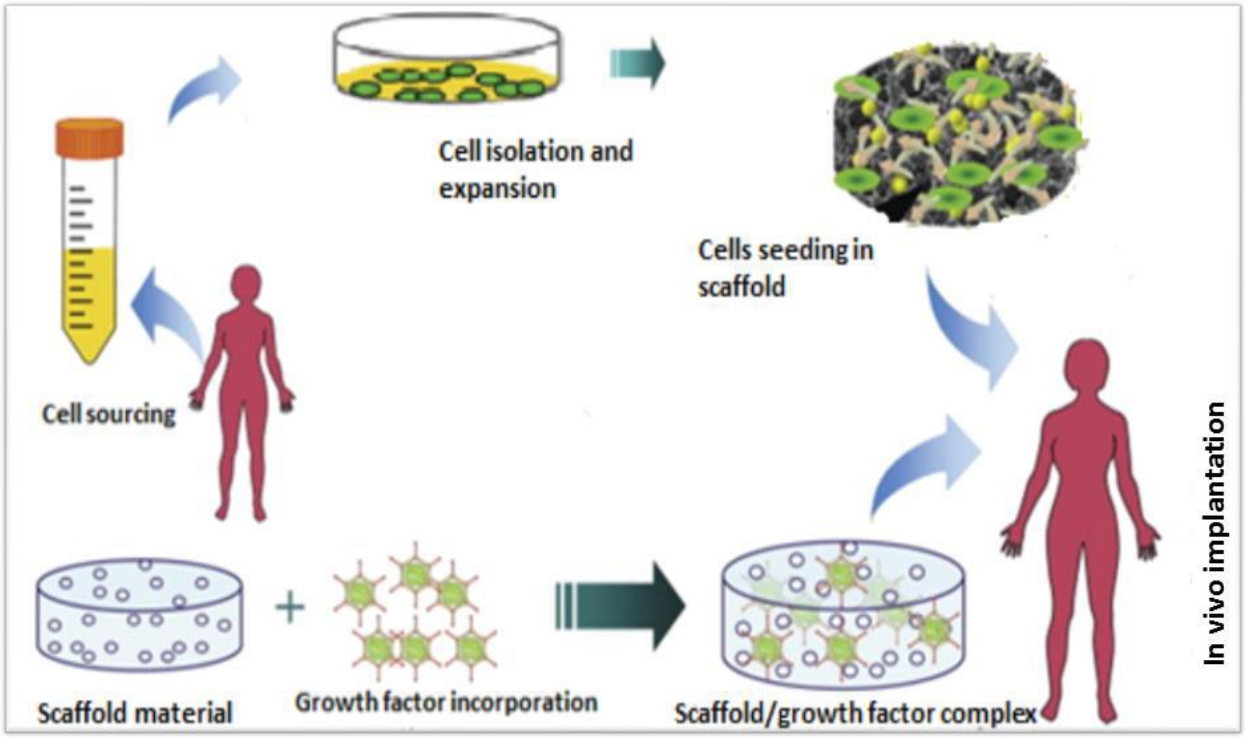


**Figure 9. Tissue engineering paradigm. Cells are isolated from donor/source, seeded in combination with appropriate growth factors onto the biomaterial scaffold, and the construct is implanted into the host defect site.**[180]

extraction of tissue due to diseased states. The tissue engineering paradigm can be seen in figure 9 displaying the three main components for tissue regeneration: the biomaterial scaffold that serves as a substrate onto which cells and biological molecules can reside; the growth factors or small molecules that function to influence cellular behavior; and the patient-specific cells responsible for building the tissue.[180] The design of a scaffold should involve the consideration of the following critical criteria: 1) suitable biomaterials should be selected in regards to both the tissue type to be replaced and the degradation time to match the ingrowth of newly forming tissue; 2) appropriate initial mechanical strength and stiffness to substitute for the mechanical function of the defect area where the damaged tissue is to be repaired/regenerated; 3) optimization of the scaffold surface to encourage cell attachment, proliferation, differentiation, and migration through the scaffold; 4) minimal to no immune response, neither from the initial intact biomaterial nor its degradation by-products; 5) interconnected pore structure so that both cell migration and proliferation in initial stages and consequently ECM infiltration for the desired tissue is supported without compromise of mechanical integrity; and, 6) the scaffold should be reproducible at an economic cost and reasonable efficacy.[180] Critical sized bone defects are incapable of healing on their own due to the size of the defect and the difficulty in cell migration to effectively fill the void. When choosing appropriate and effective bone tissue engineering experiments, one must consider the location and mechanics of the bone in need of being regenerated. For example, cortical bone and trabecular bone each have different storage moduli. If an implant is chosen that is too strong for the defect, commonly seen with metal biomaterials, a phenomenon known as stress shielding[181–183] can occur where the implant or scaffold is taking on the load of the typical

weight bearing area of the native tissue, ultimately causing it to not heal properly due to the lack of stresses the bone cells need to build and remodel their tissue.

Researchers factor in the desired properties of an optimal biomaterial as discussed in the bone graft substitutes section when designing and fabricating scaffolds for bone tissue engineering applications. To reiterate, the properties included mechanical properties, biodegradability or bioresorbability, biocompatibility, porosity, osteoconductivity, osteointegrity, osteoinductivity, and osteogenicity. To achieve optimal levels for cellular attachment, growth, proliferation, migration, etc. as well as incorporation into host tissues, scaffolds are designed with optimal materials and fabrication techniques. Particularly, the scaffold structure including topographical features at both the micro and nano scale is a promising approach to control the cellular function towards tissue engineering applications. In particular with native bone tissue, bone cells live within the ECM containing an array of organized nanofibers where this structure acts as a support system that can guide cellular functions including proliferation, differentiation, adhesion, and migration by way of physical cues.[184] Therefore, evidence has shown that scaffold topography alone, independent of the substrate chemistry, may have various modulatory effects on cellular functions.[185] By using various fabrication methods, unique micro and nano topographies have been created to evaluate how topography effects cellular functions.[186] Evidently, topographical cues have been correlated with cell shape, alignment, migration, and proliferation.[187] Additionally, nanotopography has been shown to be a regulator of microRNA expression, gene expression, and cellular differentiation.[188]

Considering the vast array of parameters in tissue engineering applications studies including differences in cell sources, the materials used in scaffold fabrication, fabrication

methods resulting in size and shape differences, environmental conditions such as growth media and study time points, establishing a consensus on how specific cell types respond to scaffold topography has been found difficult. Many fabrication techniques are used to aid in the formation of biomimetic scaffold structures. Biomimetics refers to human-made substances, devices, processes or systems that imitate nature to solve complex human problems. As species and their systems have evolved in nature over thousands or more years, many of nature's technology can be harnessed to solve complex problems in engineering and in particular the field of medicine, so in essence 'reinventing the wheel' can be avoided for efficiency in resources – mainly time and funding as both are very costly in research. In summary, when designing a tissue engineering scaffold, researchers must consider the physical, chemical, and biological properties of the biomaterial scaffold in respect to the graft's potential ability to facilitate the initial and prolonged functional tissue growth.

### 1.5.1. Cell-based Strategies

The use of cell-based treatments for bone repair and regeneration were discussed previously in detail in the bone graft substitutes section. Stem cell types including MSCs, iPSCs, ADSCs, MDSCs, HUVECs, ESCs, and EPCs are some of the many cell sources commonly investigated for bone tissue engineering applications. To reiterate, the implementation and delivery of cells to a defect whether it be for bone tissue engineering or other tissue engineering applications, must involve a delivery system to localize and maintain cell viability for functional tissue regeneration and growth, which is a main focus of this work. While it appears intuitive that large scale tissue defects require a support matrix to maintain

cells locally within the defect, other applications using a direct injection of cellular suspension have gained common interest lately for treatment of degenerative chondral lesions and osteoarthritis within joints. Platelet-rich plasma (PRP) therapy alone or in combination with MSC therapy have been used clinically as intra-articular injections for degenerative osteoarthritis (OA) for patellofemoral joint (PTF) degeneration and in other joints as well. PRP therapy has shown efficacy in treating pain and improving functionality in joints with cartilage lesions or OA,[189–191] as well as evidenced in diagnostic imaging of cartilage integrity using magnetic resonance imaging (MRI).[192] Additionally, PRP therapy efficacy has been seen in the treatment of other tendon and ligament disorders including tendonitis[193] and anterior cruciate ligament (ACL)[194] injury.

### 1.5.2. Scaffolds for Bone Regenerative Engineering Strategies

#### 1.5.2.1. Electrospinning

Electrospinning is a method to create scaffolds that uses and electrical field to control the formation and deposition of polymer and/or composite fibers on a target surface.[195] Figure 10 illustrates a schematic of a typical electrospinning setup. Electrospinning works by charging a droplet of polymer solution pumped at an appropriate rate out of a needle and syringe. The droplet of polymer gets charged through a high voltage source which is connected to the metal needle, and the droplet will elongate to form a Taylor cone. When the solution

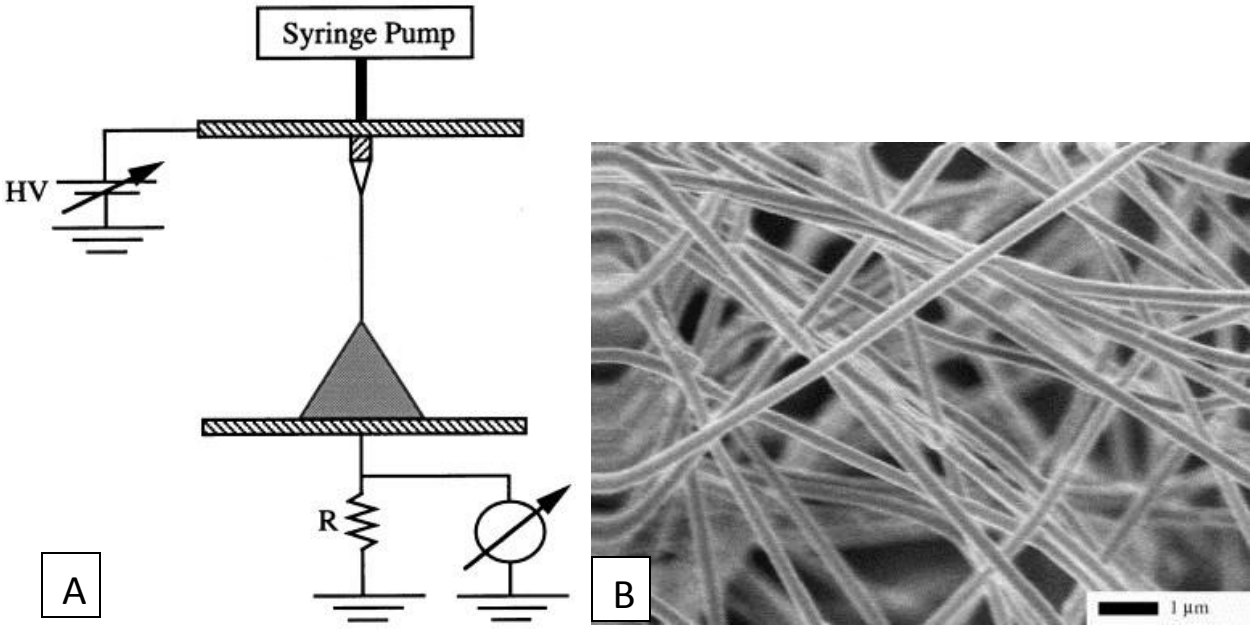


**Figure 10. Schematic representation of an electrospinning setup with high voltage applied to polymeric solution sprayed on to a grounded collector (A). Polymeric nanofibers under SEM microscopy.**[195]

reaches the optimal voltage, a fibrous jet emerges from the Taylor cone and is attracted to the grounded collector, which is commonly a flat piece of aluminum metal due to its conductive properties. While the jet initially follows a straight path, the bending instability of the electrified polymer leads to a whipping motion, during which electrical forces cause the jet stream to stretch and thin.[195,196,197] As the solvent evaporates, micro or nanofibers will be formed from the jet and are pulled toward the grounded collector where they form a nonwoven mat. Various parameters can affect the formation of fibers and can be adjusted depending on the desired properties of the scaffold to be manufactured. Parameters include humidity, voltage applied, polymer charge, polymer solution viscosity, and distance between the needle

tip to the grounded collector. When parameters are not optimal for a given setup, nanofibers will not develop resulting in electrospraying rather than electrospinning and fiber deposition.

Electrospun nanofibers are an attractive biomaterial scaffold as their nanoscale diameter and high surface area-to-volume ratio offer biomimetic properties, which are similar to the natural cellular ECM. Electrospinning is a fairly simple and affordable method for scaffold design and allows for the use of biodegradable polymers and materials which ultimately allow for scaffold incorporation into host tissues as well as controlled release of various loaded bioactive molecules, such as small molecules, proteins, drugs, DNA, or RNA.[198,199] A large variety of polymers are feasible for use in electrospinning and the production of nanofibers as they are well documented in literature.[200] Some of these polymers include natural polymers such as chitosan[201], gelatin[199], and collagen[202]; while synthetic polymers have been successfully manufactured into nanofibers such as poly (epsilon-caprolactone) (PCL)[203], poly (lactic-co-glycolic acid)[204], and poly (lactic acid)[205] which are commonly used for regenerative applications.

#### 1.5.2.2. Microspheres

Microspheres are readily made by an emulsion solvent extraction/evaporation method.[206,207] This is achieved by emulsifying a polymer solution in a non-solvent containing stabilizer. PLGA, a commonly used polymer in biomedical applications, can be dissolved in a solvent such as methylene chloride, and emulsified in an aqueous solution containing poly vinyl alcohol, which serves as the stabilizer. The emulsion process is commonly prepared by

either stirring or sonication of the two solutions. Once the polymer solution is emulsified, the organic solvent is given time to evaporate to form solid microparticles.

Microspheres in biomedical applications are commonly used as an injectable system for controlled drug delivery or can be sintered, a heating process to make the microspheres coalesce into a porous mass, under various conditions to fabricate three-dimensional matrices for tissue engineering applications.[208,209] Various methods can be used to sinter microspheres into a three-dimensional scaffold including heat sintering, solvent/non-solvent sintering, as well as solvent vapor treatment.[210–213] The release of molecules from microspheres can be controlled by several factors including the molecular weight of the polymer used.[211] Sintered scaffolds have been used as drug, protein, and peptide delivery vehicles, as well as for gene therapy.[214–216] Advantages of using sintered microsphere scaffolds include ease of fabrication, control over morphology, pore interconnectivity, and the ability to control the release of various encapsulated bioactive molecules leading to the facilitation of cellular infiltration and migration into the scaffold from host tissue.[208,217,218]

## 1.6. Ultrasound Theory

### 1.6.1. Physics of Sound

There were multiple important historical findings that lead to the understanding of sound and the discovery of ultrasound. Dating back the furthest, Sir Isaac Newton first proposed his theory that sound is a wave in 1687.[219] About two hundred years later in 1877, Lord Rayleigh discussed the field of modern acoustics.[220] As one of the last key findings in

1880, the Curie brothers discovered the piezoelectric effect[221] which ultimately led Paul Langevin to develop one of the first uses of underwater ultrasound at a frequency of about 150 kHz.[222] In general terms, sound can be described as a mechanical wave that moves through a medium such as gases, liquids, or solids. The wave travels at a particular velocity depending on the density and temperature of the medium. For example, at room temperature, sound travels through water around 1500 meters per second. A common parameter of sound is frequency, which is the amount of cycles per second. Humans can hear a particular range of frequencies. The 'ultra' in ultrasound is termed so because it is at a higher frequency beyond the limits of human hearing which is approximately at 20 kHz or higher.[223–226]

### 1.6.2. Bioeffects of Ultrasound

This section discusses the noncavitational, nonthermal bioeffects of ultrasound. These bioeffects are produced in the absence of cavitation bubbles or other gas bodies in the exposed sample. There are three main mechanisms of action: acoustic radiation force; radiation torque or acoustic streaming. Ultrasound beams in fluid media have also been shown to be accompanied by acoustic streaming, or time averaged velocity (i.e. fluid flow in or surrounding the beam and generally moving in the direction of beam propagation).[227] Acoustic radiation force (ARF), or acoustic pressure, occurs when a body is irradiated by an ultrasonic beam resulting in an experienced force. It is defined as a steady force caused by radiation.[228] The radiation force was first measured in 1903.[229,230] The force that is experienced is dependent upon the intensity of the source, the beam field, and the physical properties of the body being irradiated.[231] For this particular study, radiation force occurs when biological tissue responds

to a force by moving in the direction of the incident sound wave. Acoustic radiation force has the ability to deform the biological tissue or set it in motion.[228] Tissues with low physical strength may lose their structural integrity if the force is great enough to cause the tissue to tear or be disrupted. If the wave comes into contact with an object that absorbs the energy completely, then a force is imparted upon the object. This occurs because a traveling acoustic wave carries energy and momentum from its source. Measuring this force is a common method for quantifying the output of clinical ultrasound.[230,232–234] Additionally, Torr showed that the observed force is the result of "the transfer of wave momentum".[229] We hypothesize that the beneficial bone healing effects of ultrasound results from the mechanical load the ultrasound imparts on the cells and extra-cellular matrix.

### 1.6.3. Mechanotransduction

All living organisms experience mechanical forces, from the cellular level all the way to the organism's entire structure as a whole. Forces take part in occurrences at molecular- and cellular-level structures in all tissues in a phenomenon coined as mechanotransduction, where bone tissue is of no exception and is researched greatly.[235–241] As this thesis is centered around bone tissue engineering and the link of acoustic radiation force via ultrasound and its efficacy, mechanotransduction is of great interest, which has been defined as the "process of converting physical forces into biochemical signals and integrating these signals into the cellular responses".[242] Mechanotransduction commonly involves a series of discrete steps which lead to the general objective of growth.[243]

Examples of mechanotransduction in the body at various tissue levels have been well cited in literature. Osteoblast proliferation and increased matrix deposition has been evidenced from mechanical stimulation of the skeleton by exercise.[244] Exercise also has been shown to stimulate chondrocyte proliferation and increase cartilage synthesis.[245] Increases in mechanical pressure in the heart results in compensatory fibroblast proliferation and cardiomyocyte hypertrophy.[246] However, when mechanosensitive tissues experience the absence of mechanical stimulation, tissue degradation results.[243] Immobilization or microgravity leads to acute, rapid, and severe bone loss in humans and animals,[247] and disuse of a limb leads selectively to bone degradation in that limb[248] which is due to the lack of stimulation of the osteocyte, the key mechanosensitive cell.[243] Furthermore, the significance of mechanotransduction in bone is evidenced clearly during spaceflight as reduction in bone formation,[249] mineral content,[250] and bone matrix protein production[251] result from skeletal unweighting.

While mechanotransduction is known to play a crucial role in the physiology of many tissues, the process of mechanotransduction of bone can be divided into four stages: 1) mechanocoupling; 2) biochemical coupling; 3) transmission of signal; and 4) effector cell response.[241] Mechanocoupling refers to the physical transduction of mechanical energy in a manner that it can be detected by cells. An example of this in animals is where bones of the middle ear transduce sound waves in air into stress waves within fluid of the cochlea. Additionally, the mechanical loads *in vivo* in bone cause deformations that result in the stretching of bone cells within and lining the bone matrix resulting in fluid movement within the canaliculae of bone. The phenomenon of dynamic loading causes extracellular fluid flow and creates streaming potentials within bone and is most effective for stimulating new bone

formation *in vivo*.[252,253] Bone cells *in vitro* exposed to fluid flow or mechanical stretch are stimulated to produce secondary messangers.[254]

Biochemical coupling is the coupling of cell-level mechanical signals into intracellular biochemical signals. Possible mechanisms for these include force transduction through the integrin-cytoskeleton-nuclear matrix structure, stretch-activated cation channels within the cell membrane, G protein-dependent pathways, and linkage between the cytoskeleton and the phospholipase C or phospholipase A pathways.[241] It is theorized that the entire cell is a mechanosensor based on the tight interaction of each of these pathways and that there are numerous pathways available for the transduction of a mechanical signal.[241] The third distinct step in the process of mechanotransduction is the transmission of signal where osteoblasts, osteocytes, and bone lining cells may act as sensors of mechanical signals subsequently to communicate the signal through cell processes connected by gap junctions.[241] These bone cells can produce paracrine factors to cause osteoprogenitors to differentiate into osteoblasts and attach to the bone surface. Additionally, insulin-like growth factors and prostaglandins are studied as intermediaries in signal transduction.[255,256] In the final step of the process of mechanotransduction, the effector cell response exhibits the effects of mechanical loading as expressed by the magnitude, duration, and rate of applied load. As with the calculus theory and the notion of the area under the curve, the same effect on bone formation is seen with longer duration and lower amplitude loading in comparison to short duration and higher amplitude loading.[241,257] In order for the stimulation of new bone formation, loading must be cyclic; however, aging greatly reduces the osteogenic effects of mechanical loading, and hormones can affect the sensitivity of the sensor or effector cells to mechanical loads via interaction with local mechanical signals.[241]

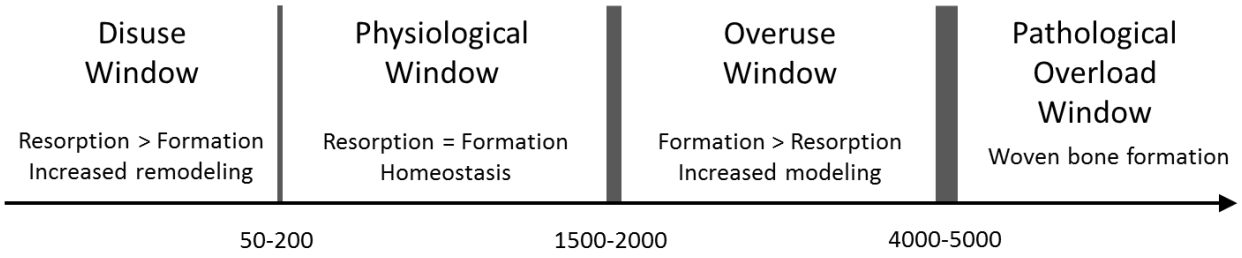


**Figure 11. The four mechanical usage windows defined by mechanostat theory (adapted from Burr and Martin).**[268]

As discussed previously, bone mass and architecture is controlled in part by adaptive mechanisms sensitive to their mechanical environment. The theory that mechanical forces shaped the architecture of the skeleton emerged in the 19th century in the works of Roux[258] and Meyer.[259] However, literature's most famous ties with bone adaptation theory is seemingly always tied with Julius Wolff.[260] Considering Meyer's observations concerning cancellous bone structure, Wolff proposed that the architecture of bone was indicative upon its mechanical stress. Furthermore, Wolff expressed that the form of bone is related to mechanical stress by a mathematical law known as Wolff's law of bone formation.[260] While today it is known today that some tenets of Wolff's law are incorrect,[261] the basic principles that mechanical forces affect the form of bone still remains largely accepted.[262,263] A more recent interpretation of Wolff's law proposed by Frost suggests that changes in bone structure are caused by a feedback system where changes in local mechanical signals trigger bone cells to change bone structure. Frost's "mechanostat" theory presents a distinction between modeling and remodeling processes and thresholds for activating lamellar or woven bone formation in which there is a window of mechanical usage that should be considered normal or physiological (figure 11).[262,264–268] If bone tissue experiences mechanical forces exceeding the upper boundary of

the physiological window, known as the minimum effective strain (MES), bone undergoes modeling, or sculpting, where its structure is changed to reduce local strains to a level below the MES.[241] Additionally, when forces on bone tissue are very large resulting in bone strains pushed into a pathological overload zone, woven bone formation will occur on bone surfaces. However, on the other end of the spectrum when forces are low enough producing a lower MES, bone tissue will be resorbed until the local strains are increased.[241] While mechanical forces resulting in strains on bone tissue is a main driving factor to bone formation/resorption, Frost suggested that various hormones and biochemical signals can alter the mechanostat phenomenon of bone thus altering the boundaries of the physiological window allowing normal mechanical usage to significantly increase bone mass and bone strength.[265] Much of this work focuses on certain mechanosensory pathways with preosteoblasts as mechanotransduction is a hypothesized bioeffect phenomenon from the stimulation of LIPUS via acoustic radiation force. Further discussion of this notion is discussed in the following sections.

### 1.6.4. Medical Ultrasound

In medical ultrasound equipment, a transducer consisting of a piezoelectric crystal converts a particular ultrasound frequency (1-12 MHz) as an electrical signal into a mechanical vibration resulting in acoustic energy. As the human body consists of a high percentage of water, this acoustic energy produced by the transducer can be used as a minimally invasive technique to propagate through the skin and various tissues at different impedances.[269] Medical ultrasound devices range in their functions and uses, such as surgical applications, diagnostics, for example imaging, and therapeutics for cancer treatment, kidney stones via

ablation, tissue swelling in physical therapy, and fracture healing.[270,271] Seemingly the most critical factor in medical ultrasound is the measurement of the acoustic energy output which leads to the key parameters: intensity and spatial intensity. Intensity refers to the total power output of a device (typically measured in Watts) while spatial intensity may be a more useful term in medical therapies as it indicates the device's power output normalized to a particular area (commonly measured in Watts/cm$^2$).[272–275] To refresh, power indicates energy per unit time. Ultrasound devices may be engineered at higher or lower intensities – whatever is optimal for the given treatment or diagnostic testing. Medical ultrasound units can have output intensities range from milliwatts all the way to 1,000 watts or more depending on their application. If compared to household appliances as a way to put the output intensities into perspective, medical ultrasound devices have somewhat similar output when taking the example of two common household devices: a 5 watt LED lightbulb and a 1,000 watt microwave. While the 5 watt LED lightbulb barely produces any heat, it is still a few orders of magnitude higher than some types of medical ultrasound devices such as low intensity pulsed ultrasound, the therapeutic device for fracture healing, which operates at a spatial intensity of only 30 mW/cm$^2$ and will be discussed further in the following section and is the focus of this research. However, as the 1,000 watt microwave uses a lot of power, it is capable of producing high amounts of heat in a short period of time as its intended purpose is to cook or heat food rapidly. The high wattage microwave power output is similar to the high end of the spectrum of medical ultrasound, such as high intensity focused ultrasound (HIFU) which is used for thermal ablation of tissues where HIFU systems have been shown to operate in the 100s to 1,000s Watts of total output and 1,000s to 10,000s Watts/cm$^2$ of spatial intensity resulting in tissue temperature increases up to 100°C.[276,277]

### 1.6.5. Ultrasound for Fracture Healing (LIPUS)

#### 1.6.5.1. History and Background

In the mid-1990s the U.S. Food and Drug Administration (FDA) approved the use of low intensity pulsed ultrasound (LIPUS) devices for therapeutic applications, specifically for fresh fractures in 1994 and for non-union fractures in 2000.[269] Clinical evidence has shown the beneficial effects of LIPUS as fresh fracture healing time is reduced by 38%[278] and non-union defects heal at an 85% success rate.[279] While the use of LIPUS has proven beneficial in bone repair, the exact mechanism behind its success still remains unclear. Further investigation into LIPUS parameters as well as cellular and environmental effects may provide insight into this phenomenon, as is a major theme of this thesis.

As the name implies, LIPUS is an acronym for low intensity ultrasound, as opposed to high intensity ultrasound used in other medical applications (see Medical Ultrasound). Clinically, LIPUS is applied transdermally over the fracture site for twenty minute daily treatments for the duration of the fracture healing time determined by the clinician. Given that the LIPUS treatment was to be applied over one area for a substantial duration of time without considerable heating or other damaging effects, the FDA set a spatial intensity of 30 $mW/cm^2$ of which the devices must not exceed, which is orders of magnitude lower than high intensity focused ultrasound (HIFU).[280] The low spatial intensity was determined by the FDA in part so that local tissue heating would not exceed 1 °C.

As a therapeutic ultrasound device is essentially an electromechanical device, general knowledge of electrical engineering principles, particularly in signals, is necessary to

understand the basics of the system – how an electrical signal (waveform) is converted into a mechanical impulse via a transducer as a medical therapy for fracture healing. The following parameters are essential in the understanding and engineering of an ultrasound system:[281–283]

AMPERE - A unit of measure for the flow of current in a circuit. One ampere is the amount of current flow provided when one volt of electrical pressure is applied against one ohm of resistance.

AMPLIFIER - A device of electronic components used to increase power, voltage, or current of a signal.

AMPLITUDE - A term used to describe the maximum value of a pulse or wave. It is the crest value measured from zero.

BURST MODE - The function generator generates N cycles of a waveform every t seconds.

BURST WIDTH - The length of time a signal is burst as it goes through N cycles. Also known as pulse width.

CALIBRATION - The determination or rectification of the graduations used on a testing instrument.

CARRIER SIGNAL - The base waveform that is used to pulse durations of the signal during burst mode.

CURRENT - The flow of electric charge such as in an electric circuit this charge is carried by moving electrons in a wire. The SI unit for measuring an electric current is the

ampere, which is the flow of electric charge across a surface at the rate of one coulomb per second.

CYCLE - The change in an alternating electrical sine wave from zero to a positive peak to zero to a negative peak and back to zero.

DUTY CYCLE - The ratio of time a load or circuit is ON compared to the time the load or circuit is OFF. Duty cycle, sometimes called "duty factor," is expressed as a percentage of ON time.

ENERGY - The property that must be transferred to an object to do work. The SI unit for energy is the joule (J), where 1 joule is equal to 1 newton-meter.

FREQUENCY - The number of pulse or wave cycles that are completed in one second (measured in Hertz). Frequency is equal to the inverse of the period.

FUNCTION GENERATOR - Electronic test equipment or software used to generate different types of electrical waveforms over a wide range of frequencies. Some of the most common waveforms produced by the function generator are the sine, square, triangular and sawtooth shapes.

HYDROPHONE - A microphone designed to be used underwater for recording or listening to underwater sound. Most hydrophones are based on a piezoelectric transducer that generates electricity when subjected to a pressure change. Such piezoelectric materials, or transducers, can convert a sound signal into an electrical signal since sound is a pressure wave.

INTENSITY - The power output of a device.

OHM - The standard unit for measuring resistance to flow of an electrical current. Every electrical conductor offers resistance to the flow of current, just as a tube through which water flows offers resistance to the current of water. One ohm is the amount of resistance that limits current flow to one ampere in a circuit with one volt of electrical pressure.

OSCILLOSCOPE - A type of electronic test instrument that allows observation of constantly varying signal voltages, usually as a two-dimensional plot of one or more signals as a function of time. Other signals (such as sound or vibration) can be converted to voltages and displayed.

PERIOD - This is the length of time in seconds that the waveform takes to repeat itself from start to finish. The period is equal to the inverse of the frequency.

POWER - The energy per unit time, commonly measured in watts.

PIEZO ELECTRIC DEVICE - A device made of crystalline materials, such as quartz, which bend or distort when force or pressure is exerted on them. This pressure forces the electrons to move.

PULSE - A signal that is produced by a sudden ON and OFF of direct current (DC) within a circuit.

PULSE REPETITION FREQUENCY - The frequency at which the carrier signal is repeated or burst. Also, this parameter may be referred to as pulse rate or signal repetition frequency.

RESISTANCE - The opposing or retarding force offered by a circuit or component of a circuit to the passage of electrical current through it. Resistance is measured in ohms.

SPATIAL INTENSITY - The power output normalized to an area. For LIPUS applications the units are commonly $mW/cm^2$.

VOLTAGE - That force which is generated to cause current to flow in an electrical circuit. It is also referred to as electromotive force or electrical potential. Voltage is measured in volts.

WATT - A unit of measure for indicating the electrical power applied in a circuit. It is obtained by multiplying the current (in amperes) by the electrical pressure (in volts) which cause it to flow. That is: watts = amperes x volts. 1 watt is equal to 1 joule per second.

WAVE - A signal that is produced by varying a continuous flow of current within a circuit. Waveforms can be created by either AC or DC current.

WAVEFORM - A graphical representation of electrical cycles which shows the amount of variation in amplitude over some period of time.

LIPUS is typically applied by using a low amplitude 1 or 1.5 MHz sinusoidal carrier wave to meet the appropriate spatial intensity and pulsed at 1 kHz (pulse repetition frequency or PRF) at regular intervals (20% duty cycle) as opposed to a continuous wave. Figure 12 shows the typical LIPUS waveform. To better explain the signal parameters, every millisecond (the inverse of the PRF), a 1 MHz frequency signal is turned on for 200 microseconds and then turned off for 800 microseconds. The ratio of time that this 1 MHz carrier wave is on (200

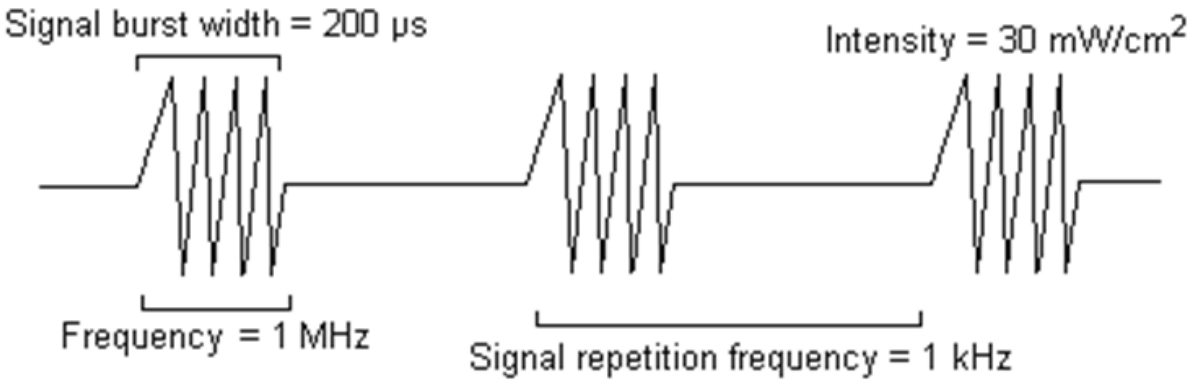


**Figure 12. Drawing of a typical LIPUS waveform signal used in fracture healing therapy.**

microseconds) over the total time period that it pulses at (1 millisecond or 1,000 microseconds) is termed the duty cycle and equates to 20% as noted above. A signal that is pulsed at the same rate (1 millisecond) but is kept on for 500 microseconds and off for the remaining 500 microseconds of the period, intuitively equates to a 50% duty cycle. A signal that remains on all of the time is continuous, resulting in a 100% duty cycle.

#### 1.6.5.2. LIPUS *in vitro* and *in vivo* studies

While the use of LIPUS therapy for fracture healing has been studied extensively over the last couple of decades, researchers still remain unclear on a biological mechanism leading to its efficacy. This section summarizes some of the well-cited studies. One theory behind LIPUS therapy efficacy suggests that LIPUS induces greater blood flow at the defect site resulting in promoting better *in vivo* healing, but various *in vitro* studies have shown that LIPUS is responsible for further actions and various biochemical signal responses. To name a few, LIPUS has been shown to increase osteoblast production of vascular endothelial growth factor and fibroblast growth factor,[284] promote chondrocyte aggrecan and type II procollagen synthesis,[285] inhibits

osteoclastogenesis,[286] stimulates PGE2 and COX-2 expression,[287] and elevates intracellular calcium,[285] osteocalcin, and gene expression for alkaline phosphatase, TGF-β, osteopontin, and BMP-7.[269,288] With all of this taken into consideration, no definitive mechanism behind LIPUS' clinical efficacy has been identified. For ease of display, some of the well-cited *in vitro* and *in vivo* LIPUS studies are listed below in table 3.[269]

| Study | Study Type | Animal Model or Cell Type | Treatment | Outcome |
|---|---|---|---|---|
| Takikawa et al. (2001) | In vivo | Rat tibial nonunion animal model | Low-intensity pulsed ultrasound 20 min/day for 2, 4, and 6 wk | 13.3% of nonunions healed after 2 wk; 31%, after 4 wk; 50%, after 6 wk |
| Warden et al. (2006) | In vivo | Rat femoral fracture animal model | Low-intensity pulsed ultrasound 20 min/day for 5 days/wk | 17% increase in bone mineral density after 40 days of treatment |
| Li et al. (2007) | In vivo | Rat ulnar stress fracture animal model | Low-intensity pulsed ultrasound 20 min/day for 5 days/wk | Peak in bone formation after 4 wk but increases at 8 wk as well compared with untreated limbs |
| Rawool et al. (2003) | In vivo | Dog ulnar fracture animal model | Low-intensity pulsed ultrasound 20 min/day for 1 wk | Threefold increase in blood flow around fracture site |
| Takayama et al. (2007) | In vitro | Osteoblast proliferation and differentiation | Low-intensity pulsed ultrasound 20 min/day for varied durations | Increased expression of alkaline phosphatase, Runx2, Msx2, Dlx5, Osterix, bone sialoprotein, mineralized nodule formation, and calcium content within nodules |
| Sena et al. (2005) | In vitro | Rat marrow stromal cell gene expression | Low-intensity pulsed ultrasound for 3 hr | Increased gene expression of c-jun, c-myc, COX-2, Egr-1, TSC-22, osteonectin, and osteopontin |
| Sant'Anna et al. (2005) | In vitro | | Low-intensity pulsed ultrasound for 20 | Increased gene expression of Cbfa- |

| | | | | |
|---|---|---|---|---|
| | | Rat marrow stromal cell gene expression | min/day for 1, 3, 5, and 7 days | 1/Runx-2, insulin-like growth factor, alkaline phosphatase, osteopontin, transforming growth factor-β, and BMP-7 |
| Reher et al. (2002) | In vitro | Human mandibular osteoblast protein expression | Ultrasound of varied intensities for 1, 2, 4, 6, 8, 12, 18, and 24 hr | Increased expression of prostaglandin $E_2$ and nitric oxide |
| Parvizi et al. (2002) | In vitro | Rat chondrocytes | Low-intensity pulsed ultrasound for 2 sec through 10 min each day for 3 days | Increase in intracellular $Ca^{2+}$ |
| Li et al. (2006) | In vitro | Rat calvarial cells | Low-intensity pulsed ultrasound for 15 min | Increase in intracellular $Ca^{2+}$ |
| Yang et al. (2005) | In vitro | Mouse osteoblast cells | Low-intensity pulsed ultrasound for 10 min/day with varied intensity | Increase in α2, α5, and β1 subunits |
| Tang et al. (2006) | In vitro | Mouse osteoblast cells | Low-intensity pulsed ultrasound for 20 min/day | Increase in α2, α5, β1, and β3 subunits and phosphorylation of focal adhesion kinase |

**Table 3. In Vivo and In Vitro Studies Evaluating the Effectiveness and Mechanism Behind Low-Intensity Pulsed Ultrasound Treatment for Bone Repair**[269]

# 2. PROJECT OVERVIEW AND SPECIFIC AIMS

## 2.1. Project Overview and Specific Aims

The goal of this thesis was to find more conclusive evidence as to how LIPUS is effective at bone healing in addition to optimizing the currently used clinical therapy. We developed and characterized our own highly tunable ultrasound system as well as a hydrogel scaffold system for tissue mimetics. A series of experiments evaluated the response of our adjustable ultrasound system to: cells alone; hydrogels alone; cell-hydrogel encapsulation; and cell-hydrogel encapsulation implantation into a mouse calvarial model. We hypothesized that LIPUS imparts a physical load via acoustic radiation force on cells and results in a mechanical deformation of the construct it acts on. Additionally, the use of collagen hydrogels with encapsulated cells implanted into a defect site such as in a mouse calvarial defect model, would result in enhanced healing with the remote mechanical stimulus of LIPUS treatment in comparison to groups without treatment. The study is organized into specific aims as detailed below.

**Specific Aim I:** To characterize a tunable ultrasound system and collagen type I hydrogel scaffold system.

It his hypothesized that acoustic radiation force and hence spatial intensity is directly proportional to amplitude and duty cycle and hydrogel deformation. Furthermore, it is hypothesized that hydrogel storage modulus is directly proportional to hydrogel collagen concentration. A hydrophone will be used to calibrate the ultrasound system's output, and a rheometer will test the viscosity of the hydrogels based on their collagen

concentration constructed at a range of optimal working viscosities. Encapsulated fluorescent beads will be tracked at four different collagen concentrations via imaging before, during, and after ultrasound treatment at the clinical parameters as well as other duty cycles and intensity.

**Specific Aim II:** To evaluate the effect of LIPUS *in vitro*.

It is hypothesized that the clinical LIPUS treatment will enhance certain osteogenic expression of MC3T3 cells. Furthermore, it is hypothesized that mechanosensory marker COX-2 expression will be dependent upon LIPUS treatment and intensity. Ultrasound treatment will be administered to MC3T3 cells cultured on TCP and encapsulated in three different concentrations of collagen hydrogels. RT-PCR analysis will be performed for up to 21 day time points for osteogenic markers and short term time points for COX-2 expression.

**Specific Aim III:** To evaluate *in vivo* effects of LIPUS in a critical sized defect combined with an implantable collagen hydrogel.

It is hypothesized that the combined treatment of LIPUS with an injectable BMSC-encapsulated collagen hydrogel will provide enhanced healing in a mouse calvarial defect model in comparison to no LIPUS treatment. Samples will be evaluated with x-ray imaging, and histological analysis will be performed on samples to evaluate the extent of donor cell survival, new bone formation, mineralization, and remodeling.

## 2.2. Preliminary Data

### 2.2.1. Ultrasound System Setup

In order to be able to run ultrasound experiments, an ultrasound system was designed and setup on a wheeled cart for portability. As commercially available clinical ultrasound devices to treat fractures and fracture non-unions are limited to only one output parameter (such as the Exogen unit from Smith and Nephew), the system was designed to have a high degree of control and verification over system output parameters. Preliminary studies verified the output parameters of the equipment and their relevance to clinical medicine. The waveform signal was produced by an Agilent 33210A 10 MHz waveform generator (Agilent Technologies, Santa Clara, CA). The signal was amplified to a desired output level by using an ENI 403LA Broadband Power Amplifier (37dB, .15-300MHz, 1V Max) (Manufacturer, City State), which was subsequently sent to a 1 MHz unfocused immersion transducer with a 0.75" nominal element size (Olympus NDT, Inc. Waltham MA) to generate ultrasound. The clinically relevant output and calibration of the transducer was performed by selecting appropriate parameters from the waveform generator: carrier frequency, pulse repetition frequency, duty cycle, and amplitude. The portability of the ultrasound system allowed for convenience and efficiency when calibrating various ultrasound transducers on the bench top, performing cell studies in the culture hood, and transporting the system for in vivo studies.

#### 2.2.1.1. Heating Effects

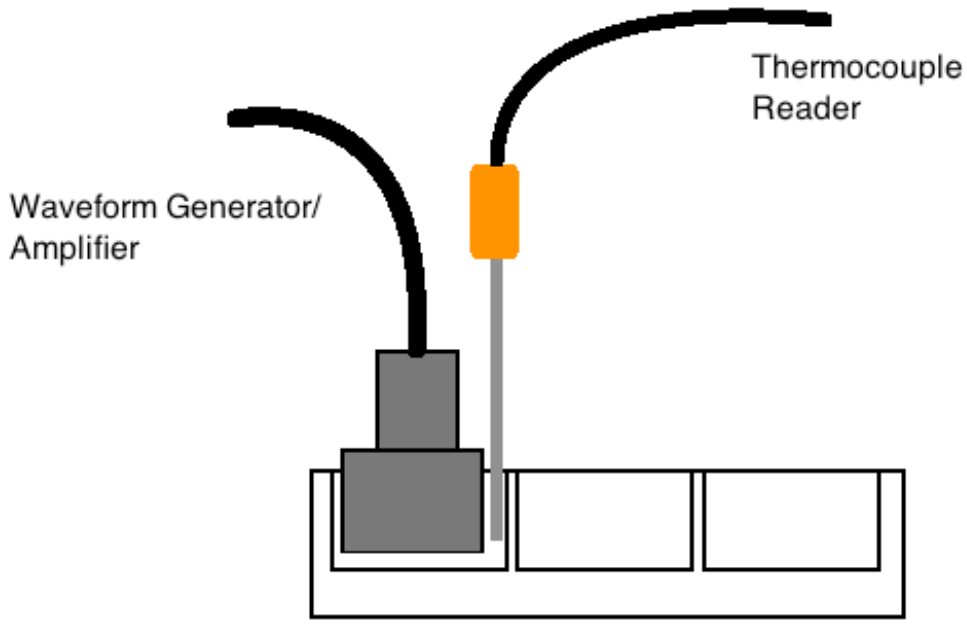


**Figure 13. A schematic of the temperature testing setup with an ultrasound transducer and thermocouple submerged in DI water.**

One possible concern of ultrasound treatment on healthy tissue is excessive heating; however, a small amount of heating could be beneficial and promote blood flow. Higher intensity ultrasound can raise temperatures considerably (Medical Ultrasound). Given both scenarios, local temperature was monitored to answer two questions: 1) does LIPUS raise local temperatures significantly enough to result in harm to cells for in vitro experiments; and 2) can local heating be responsible for effects seen during testing.

Important to note is that the FDA mandates that local temperatures for LIPUS treatment not increase by more than 1°C. An initial experiment was run to apply ultrasound at different intensities (amplitudes) to water in six-well plates incubated at 37°C to provide a baseline for various ultrasound intensities. To reproduce the parameters of the clinical LIPUS settings, the waveform generator was set to produce a 1 MHz signal with a 20% duty cycle and a 1 kHz

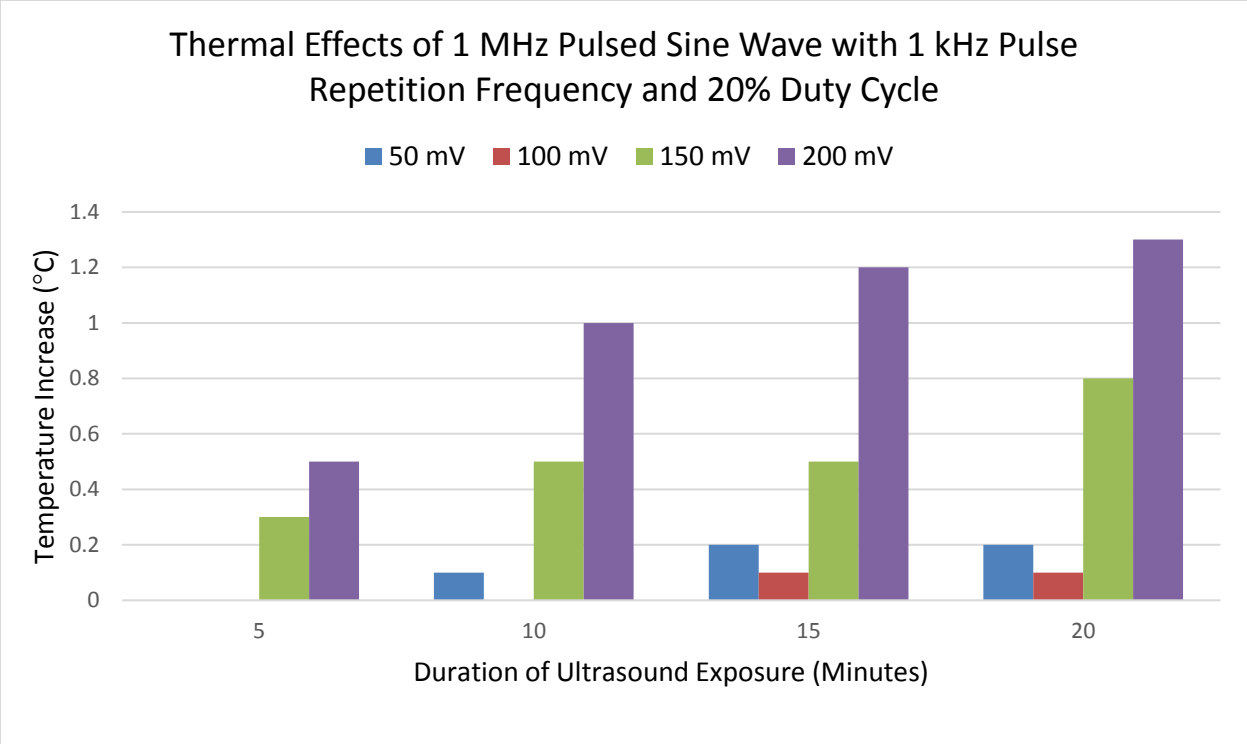


**Figure 14. Temperature increase from ultrasound exposure at various amplitudes over 5, 10, 15, and 20 minutes.**

pulse repetition frequency. The setup consisted of 6-well plates filled with DI water which were allowed to equilibrate at 37°C overnight. Next, the transducer was submerged into a well and run with the specified parameters at amplitudes of 50, 100, 150, and 200 mV for 20 minutes. The temperature of the water was measured in each well at the start of each run and then at 5 minute intervals for the duration of exposure. A schematic of the setup can be seen in Figure 13. Temperature change is plotted in Figure 14. Importantly, all sets of parameters

except for 200 mV after 15 minutes did not result in a temperature increase of greater than 1°C, therefore verifying the FDA mandated limit for local heating by an ultrasound device was not exceeded. Additionally, even at the most extreme conditions tested, the temperature rise barely exceeded 1.25°C after 20 minutes of exposure to an intensity greater than currently used clinically for LIPUS devices. Also, these conditions were tested in a static well of fluid which are more extreme than an in vivo environment where the body is able to transfer excess heat away from local tissues through fluid flow.

#### 2.2.1.2. Force Measurements

Given the correlation between ultrasound and bone healing and how previous work has shown that high intensity ultrasound produces a measurable acoustic radiation force,[289] the purpose of the following experiments was to investigate if low intensity ultrasound (<1 W/cm$^2$ spatial intensity) produces a detectable physical force as well. Also, testing would verify the system could produce a controlled and measurable force which may be beneficial to understanding bone repair in regards to the cellular and environmental response to the force. In order to measure the force produced by the ultrasound system, a setup was engineered from raw materials using a small ~12" tall table with four legs which held a Mettler Toledo digital scale. On the bottom of the scale, from the weigh hook hung a clip which held two wires that suspended a cone target. The cone was situated in an insulated water bath bucket, and the transducer was immersed and positioned directly and uniaxially approximately 1/8" above the cone secured by a clamp and ring stand. The transducer produced an ultrasonic beam which

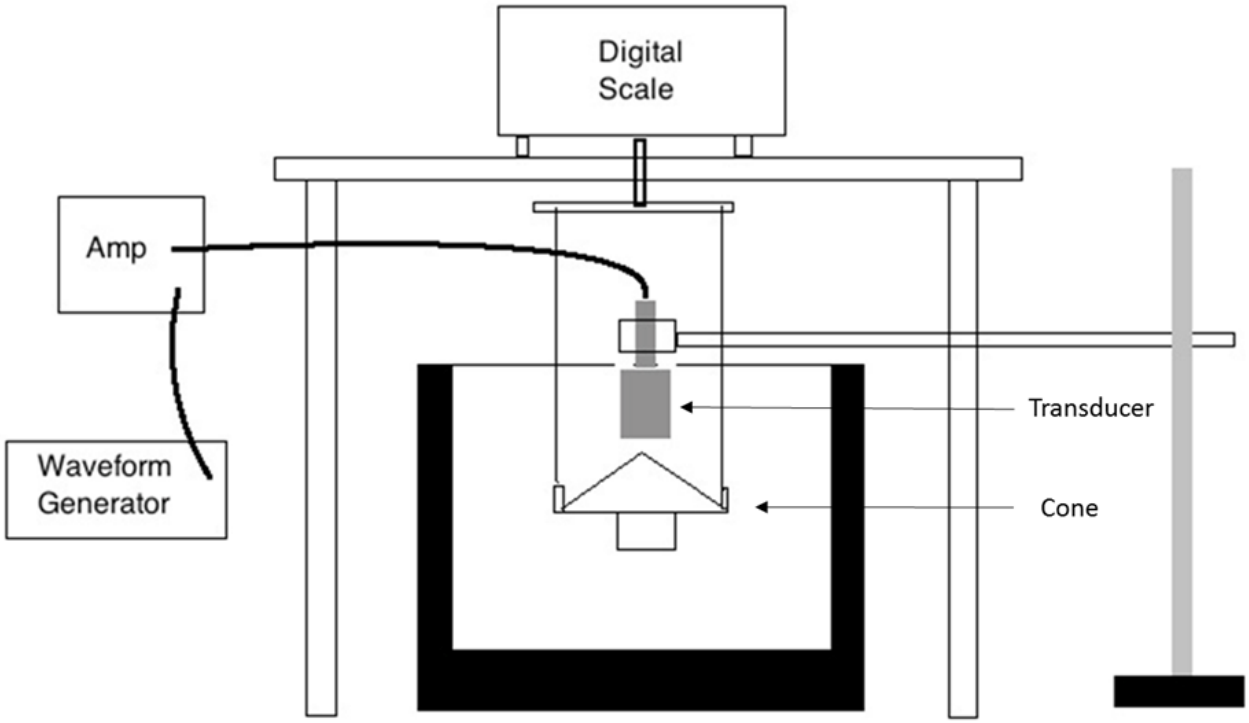


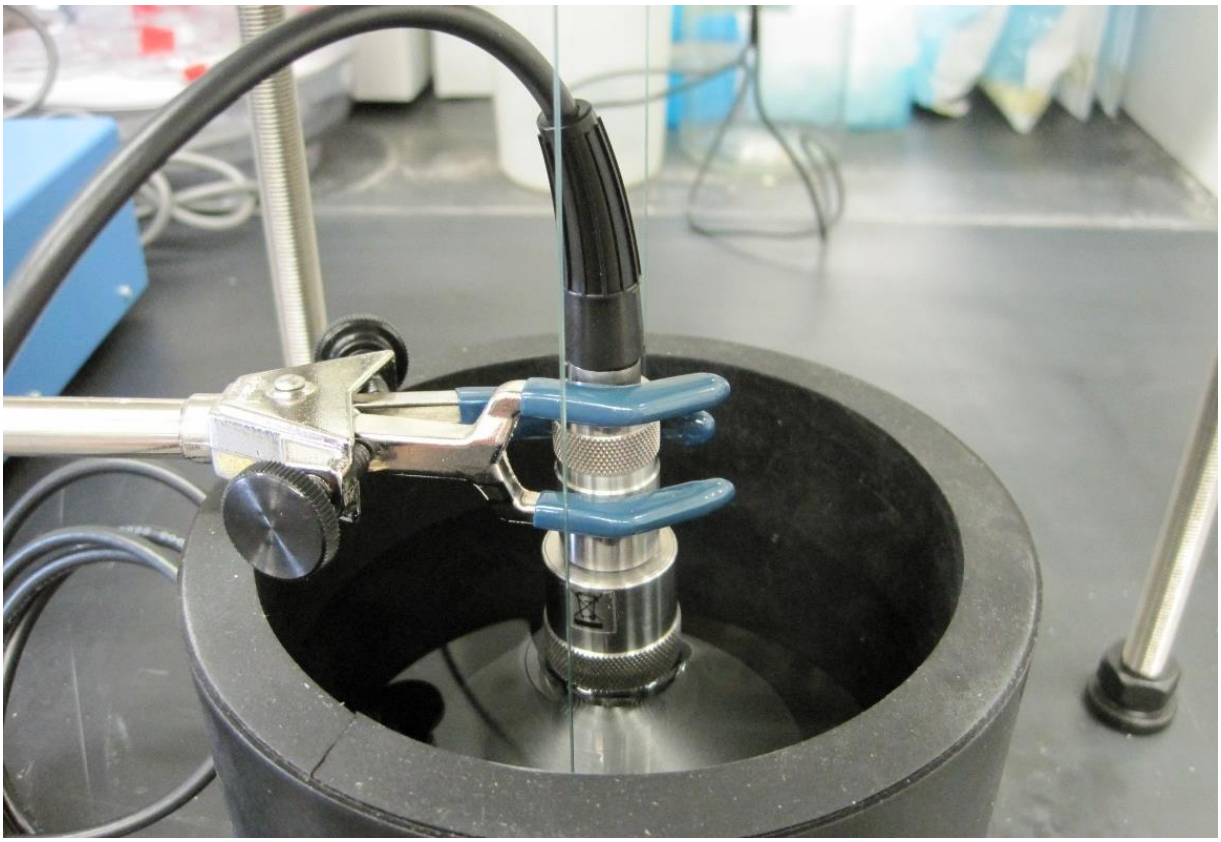

**Figure 15. Mass balance setup showing a schematic drawing (top) and the transducer suspended over the hanging cone in water within an insulating rubber bucket (bottom).**

image of the setup can be seen in figure 15. With the following equations, the intensity of the ultrasound beam was calculated from the measured load at each amplitude and duty cycle:

$$p = Wgc$$

where:

$$p = power\ \left[\frac{ergs}{sec}\right]$$

$$W = measured\ mass\ [grams]$$

$$g = acceleration\ due\ to\ gravity\ [dynes]$$

$$c = speed\ of\ propagation\ of\ sound\ \left[\frac{cm}{sec}\right]$$

Further simplifying and assuming constant values for $g$ and $c$, the following equation is yielded:

$$P = 14.65w$$

where:

$$P = power\ of\ ultrasound\ beam\ [Watts]$$

$$w = force\ of\ the\ ultrasound\ beam\ [grams]$$

Beam power can be converted into spatial intensity (I) by dividing by the cross-sectional area of the beam. Given that spatial intensity is normalized to the size of the transducer, it is a universally recognized and standard measurement allowing for clinical comparisons of ultrasound systems. As discussed earlier, the FDA approved the use of LIPUS treatment for fracture healing applications with a spatial intensity of 30 mW/cm$^2$. With the transducer used in this study having a nominal element size (diameter) of 0.75" or 1.905 cm, spatial intensity was calculated by dividing the power of the ultrasound beam by the cross-sectional area of the beam:

$$I = \frac{P * 1000}{0.25\pi 1.905^2}$$

where:

$$I = spatial\ intensity\ \left[\frac{mW}{cm^2}\right]$$

$$P = power\ of\ the\ ultrasound\ beam\ [Watts]$$

Notably, the FDA approved spatial intensity of 30 mW/cm$^2$ would result in a load of 6 mg, or 0.059 N. Using clinically prescribed parameters, loads were measured for a series of amplitudes (peak-to-peak voltage values) of a 1 MHz carrier signal with a pulse repetition frequency of 1 kHz at a 20% duty cycle. Importantly, a 1 kHz pulse repetition frequency

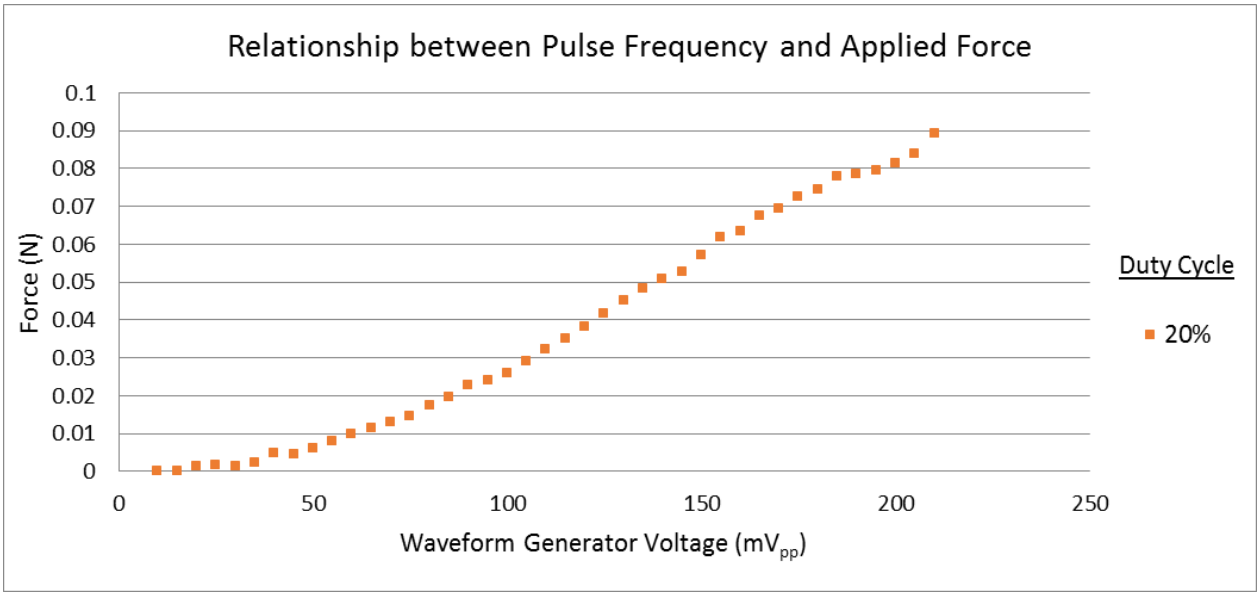


**Figure 16. A plot of applied force as a function of amplitude of a 1 MHz carrier signal, 1 kHz pulse repetition frequency, and 20% duty cycle.**

equates to a 1 ms, or 1000 µs, burst period. Hence a signal with these parameters at a 20% duty cycle results in a signal burst of 200 µs and a pause of 800 µs. Measured loads can be seen in figure 16. A measurable physical load was present when LIPUS was applied using the clinical parameters. Additionally, it is observed that as amplitude increases, the measured load

increased as well. In order to produce the clinically relevant intensity of 30 mW/cm$^2$, an amplitude of ~160 mVpp is necessary at the 20% duty cycle. A linear relationship was determined between the applied voltage and the resulting load for the waveform tested. Importantly, the significance of the data is that there is a predictable force output given certain input parameters and that a wide range of physical loads can be produced with accuracy by varying amplitude. Given that the system is highly tunable, its potential use for experiments or therapies may be vast and go far beyond orthopedic applications.

#### 2.2.1.3. Cell Viability from LIPUS Treatment

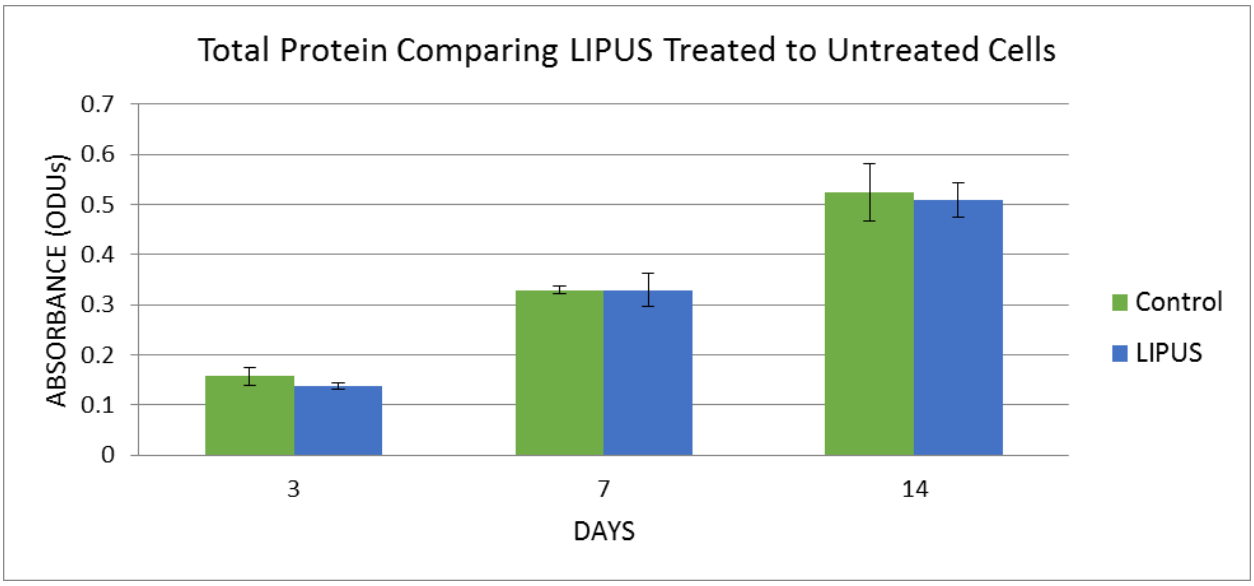


**Figure 17. Total protein assay to investigate cell viability of MC3T3 cells treated with and without LIPUS over 3, 7, and 14 days.**

In order to test the viability of the designed ultrasound system for in vitro cell studies, MC3T3 osteoblast-like cells were cultured on tissue culture polystyrene (TCP) for 3, 7, and 14 days. An amount of 50,000 cells were cultured per well in 6 well plates (n=3) with α-MEM

media supplemented with 10% fetal bovine serum (FBS) and 1% Penicillin/Streptomycin (P/S). The experimental group was treated with the clinically prescribed parameters of LIPUS for 20 minutes per day. The group receiving no treatment was the control group. Proliferation of MC3T3 osteoblasts was determined by using a total protein assay (Thermo Scientific), and compared to cells not exposed to LIPUS over the same time period, to assess any effects of LIPUS on proliferation as plotted below in Figure 17. Importantly, groups treated with LIPUS did not experience any negative effects in terms of proliferation over the 14 day time period.

### 2.2.2. LIPUS Deformation of Cells and Gels

Ultrasonic radiation force was produced using a 1.2 MHz unfocused immersion transducer with a 1" nominal element size (Olympus NDT, Inc. Waltham MA) while submerged in cell culture media (DMEM). An ultrasound signal was generated with a carrier frequency of 1 MHz and amplitude that ranged from 20mV–500mV, which was pulsed at 1 kHz. The purpose of this study was to determine what mechanical effects, if any, that LIPUS imparts on cells and 3-dimensional (3-D) scaffolds in the form of hydrogels via the use of fluorescent imaging. Imaging of GFP cells under LIPUS was performed using a Nikon optical microscope equipped with epifluorescence, and a water-cooled digital camera (Hamamatsu, Inc.). Images were collected and evaluated using Volocity Software (Improvision, Inc.).

#### 2.2.2.1. Macrophage Displacement from Ultrasound

LIPUS (50% duty cycle, 500mV amplitude) was applied to macrophages with GFP actin seeded on tissue culture polystyrene and submerged in cell culture media. Macrophage imaging before, during, and after LIPUS exposure (1 minute off, 2 minutes on, 2 minutes off; 10 μm z-stack images acquired every 30 seconds) revealed both cell deformation/displacement by approximately 1μm with subsequent partial recovery, and enhanced actin activity at the

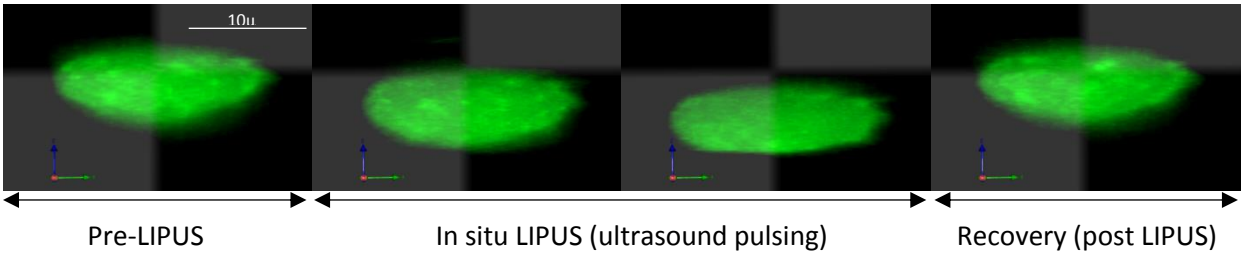


**Figure 18. X-Z plane images of GFP actin labeled macrophages before, during, and after exposure to a 1 MHz, 50% duty cycle, 500mV amplitude ultrasound treatment indicate evident Z-plane deformation and displacement with subsequent recovery after exposure ended.**

basal plane during and after LIPUS administration as seen in figure 18. Given that cellular deformation/displacement was evident from cells seeded on TCP, further investigation was necessary to report what mechanical effects LIPUS could have on 3-D hydrogel structures.

#### 2.2.2.2. Beads in Puramatrix

Puramatrix, a commercially available, self-assembling peptide hydrogel (BD), was used as a synthetic extra cellular matrix (ECM) and was reconstituted according to manufacturer's instructions. Briefly, the hydrogel stock solution (1% w/v) was sonicated for

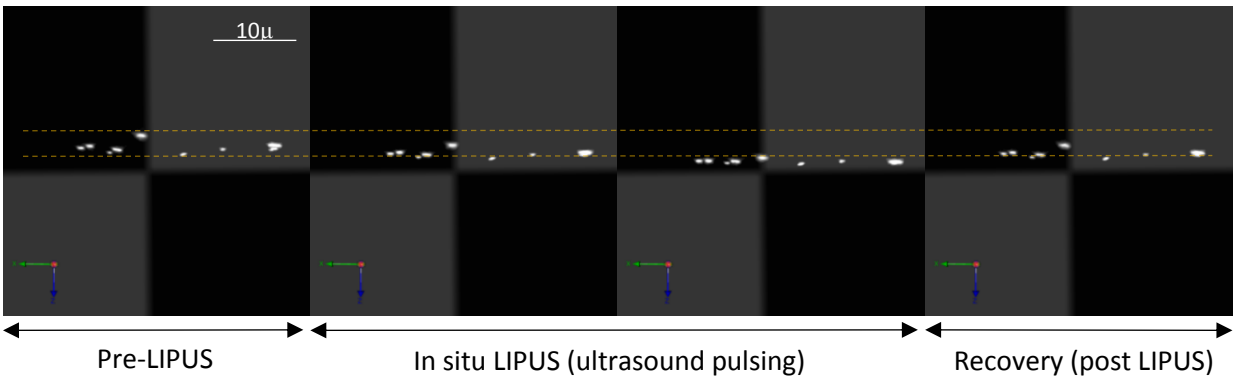


**Figure 19. Z-plane images of fluorescent particles within the Puramatrix hydrogel before, during, and after ultrasound treatment. Based on the initial position of the beads in the first frame on the left, dotted yellow lines were added to help identify particle movement throughout exposure and recovery periods.**

30 minutes and pipetted into a culture well plate. The solution was then diluted into three separate concentrations (1%, 0.5%, 0.25%), pipetted onto a glass cover slip, mixed with salt solution and allowed to gel for 30 minutes at room temperature. The salt solution was replenished twice over 60 minutes. To visualize the movement of the matrix under LIPUS stimulation, 10 µl of a fluorescent 1-µm diameter polystyrene (Fluoro-Max) bead suspension (Thermo Scientific) was pipetted into each well prior to gelation. Hydrogels were exposed to ultrasound with a carrier frequency of 1 MHz and an amplitude of 500mV, pulsed at 1 kHz. Duty cycle of the pulse ranged from 20%-100%. Using the same imaging parameters as indicated with the macrophage displacement, microscopy images acquired over time indicated a movement of beads of approximately 4 µm when subjected to a 1 MHz continuous (100% duty cycle) ultrasound signal as shown in figure 19. Bead displacement proved that acoustic radiation force does in fact result in deformable matrices which can be controlled by LIPUS intensity.

## 2.3. Detailed Summary of Research Objectives

### 2.3.1. Specific Aim I

For characterization of ultrasound and collagen hydrogels, tunable ultrasound system will be designed so that various parameters and output (most notably spatial intensity) can be controlled. A hydrophone will be used to calibrate the system's output during an amplitude sweep and at different duty cycles. Next, type I collagen hydrogels will be constructed at a range of optimal working viscosities. A rheometer will test the viscosity of the hydrogels based on their collagen concentration. Fluorescent beads will be encapsulated into four different collagen concentrations. The hydrogels will be fluorescently imaged before, during, and after ultrasound treatment at the clinical parameters as well as other duty cycles and intensity. Volocity image analysis software will acquire z-stack images of the samples throughout the runs and subsequently quantify bead deformation in total displacement as well as x, y, and z directions.

### 2.3.2. Specific Aim II

To evaluate the effect of LIPUS in vitro, MC3T3 cells will be cultured on TCP and encapsulated in three different concentrations of collagen hydrogels. Ultrasound treatment will be provided using the clinical LIPUS parameters for 20 minutes per day by submerging the transducers in culture media 3 mm above the cells on TCP or hydrogels. RT-PCR analysis will be performed with osteogenic markers for the TCP study with 3, 7, 14 and 21 day time

points. The same analysis will be performed for each concentration of hydrogels although the time points will be 1, 3, and 7 days. Additionally, shorter term studies will be performed where COX-2 expression, an indicator of mechanical transduction, will be detected in hydrogels immediately after LIPUS treatment and 30 minutes after treatment. Based on results, varying intensities may be used to analyze if COX-2 expression is affected.

### 2.3.3. Specific Aim III

In vivo analysis in the last study will show the efficacy of the combined treatment of LIPUS with an injectable BMSC-encapsulated collagen hydrogel over a healing time of 2 or 4 weeks in a mouse calvarial defect model. LIPUS will be administered for five of every seven days of the week with ultrasound gel coupled between the transducer and skin over the defect site. As this study is the first ultrasound in vivo experiment in our lab, it will be performed as a pilot study with a limited number of groups, but will lay the groundwork for future investigations. The groups will consist of the hydrogels with encapsulated cells without LIPUS treatment (control) and hydrogels with cells and with LIPUS treatment (experimental). Samples will be evaluated with x-ray imaging, and histological analysis will be performed on samples to evaluate the extent of donor cell survival, new bone formation, mineralization, and remodeling.

# 3. SPECIFIC AIM I: CHARACTERIZATION OF ULTRASOUND AND COLLAGEN HYDROGELS

## 3.1. Introduction

As indicated earlier, ultrasound is used clinically in many various modalities including diagnostics, therapeutics, surgical, and imaging. As an orthopedic laboratory, of particular interest to our research is the lower intensity ultrasound which has served as a beneficial therapy for fractures and non-union defects over the past two decades. However, the commercially available units such as the one manufactured by Smith and Nephew all use the same or similar therapeutic ultrasound parameters in terms of carrier frequency, pulse repetition frequency, duty cycle and spatial intensity as well as the duration of treatment. Additionally, the limited knowledge of how LIPUS works is left to studies investigating cellular signaling and the resulting macro scale bone formation.[290] In order for a comprehensive investigation of the beneficial effects of LIPUS, the steps between LIPUS therapy and ultimate bone formation/healing must be better understood to maximize the utility of this technology. The preliminary data has shown that LIPUS generates a measurable acoustic radiation force, and it is our hypothesis that this force may be the underlying mechanism initiating the cascade of events leading to healing. And in order to ultimately better understand ultrasound and its bioeffects, we needed to create a highly tunable system where we could control each of the parameters listed above, not only for the work in this thesis, but for many future studies to come as well.

And in combination of the currently clinically used LIPUS therapy, we needed a way to analyze the response of the physical force of LIPUS both in tissue mimetics where we proved the feasibility with the PuraMatrix and also with a relevant biomaterial scaffold which could be incorporated for bone tissue engineering. After some consideration, type I collagen seemed a logical choice in terms of workability and its capability for bone cell encapsulation. As bone is a composite tissue, it contains both organic and inorganic material. Type I collagen would be a good starting point to simultaneously characterize the ultrasound system via parameters affecting acoustic radiation force and additionally encapsulate bone cells, particularly osteoblasts which are native to collagen in bone formation and extracellular matrix. With a properly designed and characterized ultrasound system and naturally occurring three-dimensional scaffold such as a type I collagen hydrogel, we had the capability and laid the ground work to run many experiments. The characterized ultrasound system and collagen hydrogels could be used to address the relationship between LIPUS generated acoustic radiation force on: tissue deformation; cellular movement and/or deformation; cellular genetic response; and an *in vivo* defect in hopes to tie some of the results and concepts together. Importantly, by adjusting ultrasound parameters of interest along with collagen hydrogel composition, we could investigate how cells respond to different treatments and attempt to understand the underlying mechanisms of ultrasound efficacy.

## 3.2. Materials and Methods

### 3.2.1. Ultrasound System Characterization and Quantification of Force, Pressure, and Intensity

As discussed in the preliminary data, the tunable ultrasound system consisted of using a 1.2 MHz unfocused immersion transducer (Olympus), a waveform generator (Agilent), and an ENI RF amplifier (Bell Electronics) and calibrated with a mass balance & reflecting target cone setup and a 200 μm diameter needle hydrophone (Onda). A 1 MHz carrier frequency, 1 kHz pulse repetition frequency, and 20, 50 and 100% duty cycle was tested for output using an amplitude sweep in order to find the proper amplitude to produce a 30 $mW/cm^2$ spatial intensity (clinically approved intensity for fracture healing). The acquired data was used to calculate values for force, intensity and pressure which will be plotted against amplitude (input voltage). Importantly, best fit curves were calculated to provide the necessary calibration plots from the acquired data so that in vitro and in vivo studies can be performed with the desired output parameters based on the input settings on the waveform generator.

As shown in the preliminary data, the mass balance and cone setup was able to detect forces from the ultrasound system which can be translated into intensity. However, a hydrophone can provide a much higher resolution to detect instantaneous acoustic pressures in water.[291] The hydrophone has a membrane and based on its amount of deflection, can output a voltage detected by an oscilloscope. During the amplitude sweeps, voltages were recorded and used in an equation including the hydrophone calibration factor provided in documentation supplied by the vendor. The resulting hydrophone calculations were used to provide instantaneous pressure (kPa) which subsequent calculations were used to convert the pressure

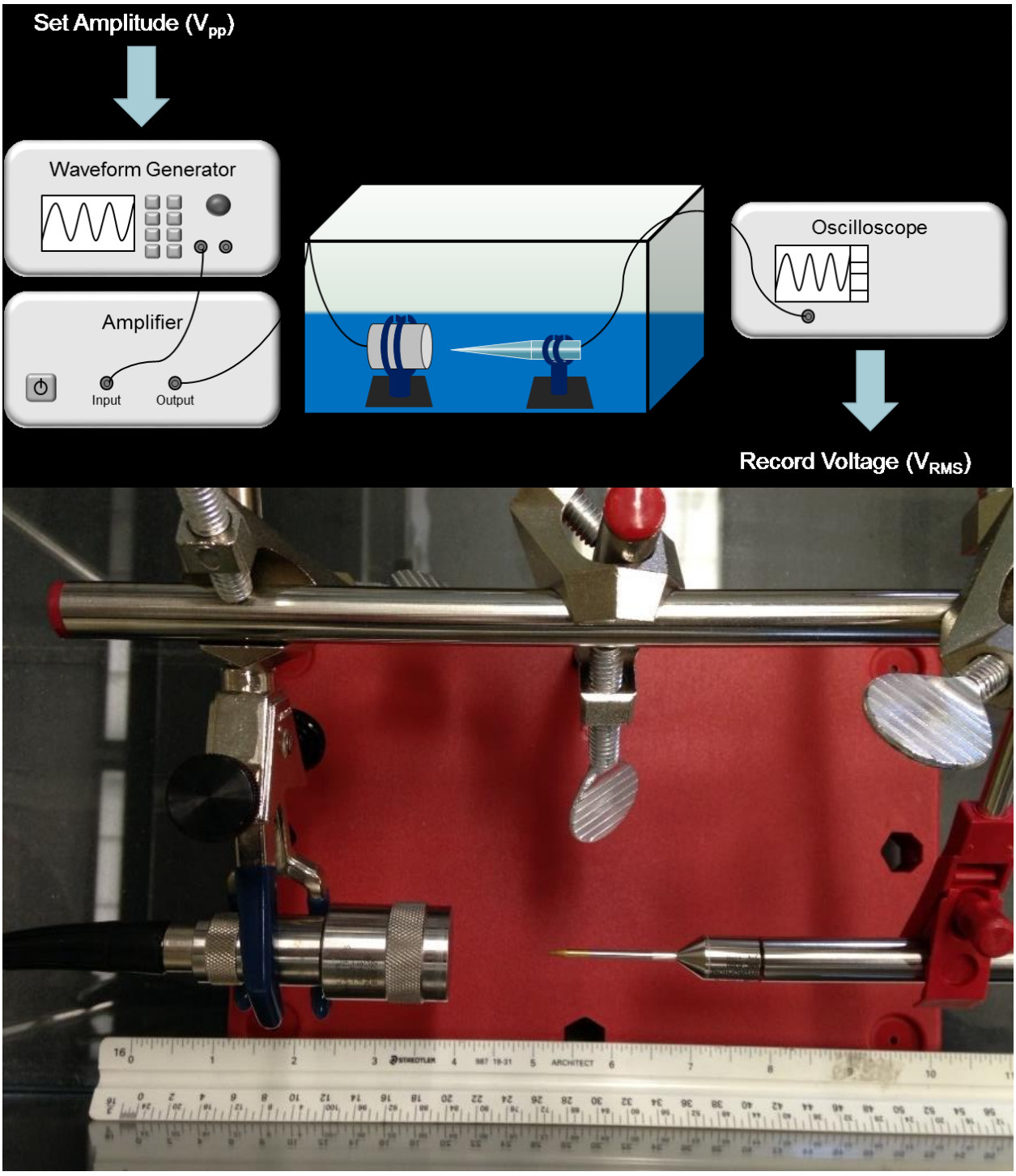


**Figure 20. Schematic drawing of the hydrophone testing setup (top) and a picture of the setup (bottom) with the clamps holding the transducer and hydrophone uniaxially and allowing for distance between the two pieces of equipment to be changed.**

transducer were oriented uniaxially with a clamp holder approximately 1/8" apart submerged under DI water in a fish tank to maintain consistency with cell culture and in vivo setups (figure 19). As can be seen in the equations below, the hydrophone's output voltage was converted into a pressure based on a sensitivity factor provided by the manufacturer. Additionally, the sensitivity factor is also dependent on the experimental frequency.

$$p = \frac{V}{M(f)} \qquad \text{(Equation 1)}$$

$p$: acoustic pressure [kPa]

$V$: measured voltage [mV]

$M(f)$*: sensitivity of hydrophone as a function of frequency [mV/MPa]

*Note: sensitivity factor must be corrected, see below.

However, as noted above, the sensitivity factor $M(f)$ is dependent on the experimental frequency and was calibrated by the manufacturer. Additionally, depending on one's setup, a corrected sensitivity factor must be calculated as indicated in the equation below taking into account the gain of the preamplifier (AH-2010, Onda), the experimental frequency, and the capacitance of the hydrophone (HNC-0200, Onda) and preamplifier [ALUM/NEMA, 1998; IEC 62127-2, 2007]. Once the corrected sensitivity factor was calculated, it was used in Equation 1 above to solve for pressure.

$$M_L(f) = G(f)M_C(f)\frac{C_H}{C_H + C_A} \qquad \text{(Equation 2)}$$

$G(f)$: gain of preamplifier

$M_C(f)$: sensitivity of hydrophone as a function of frequency [mV/MPa]

$C_H$: capacitance of hydrophone (pF)

$C_A$: capacitance of preamplifier (pF)

$M_L(f)$: corrected sensitivity factor of the hydrophone/preamplifier setup

To convert the calculated pressure values to the clinically relevant parameter, instantaneous acoustic intensity was converted by the equation below.

$$I = \frac{p^2}{\rho c} \qquad \text{(Equation 3)}$$

$I$: Instantaneous acoustic intensity [mW/cm$^2$]

$p$: acoustic pressure [kPa]

$\rho$: density of the propagating medium [$H_2O$ @ RT: 1000 kg/m$^3$]

$c$: velocity of sound in the propagating medium [$H_2O$ @ RT: 1480 m/s]

The calculated data for pressure and intensity was plotted against amplitude and best fit curves were calculated and added to provide the calibration plots. We hypothesized that as amplitude and duty cycle increased, intensity would increase as well.

### 3.2.2. Collagen Hydrogel Characterization via Rheology and SEM

In order to conduct cell studies and understand the relationship between gel stiffness and concentration, mechanical properties of various Type I rat tail collagen (BD Biosciences) hydrogels ranging from 1mg/mL - 5mg/mL, which resembled optimal viscosities for injectable

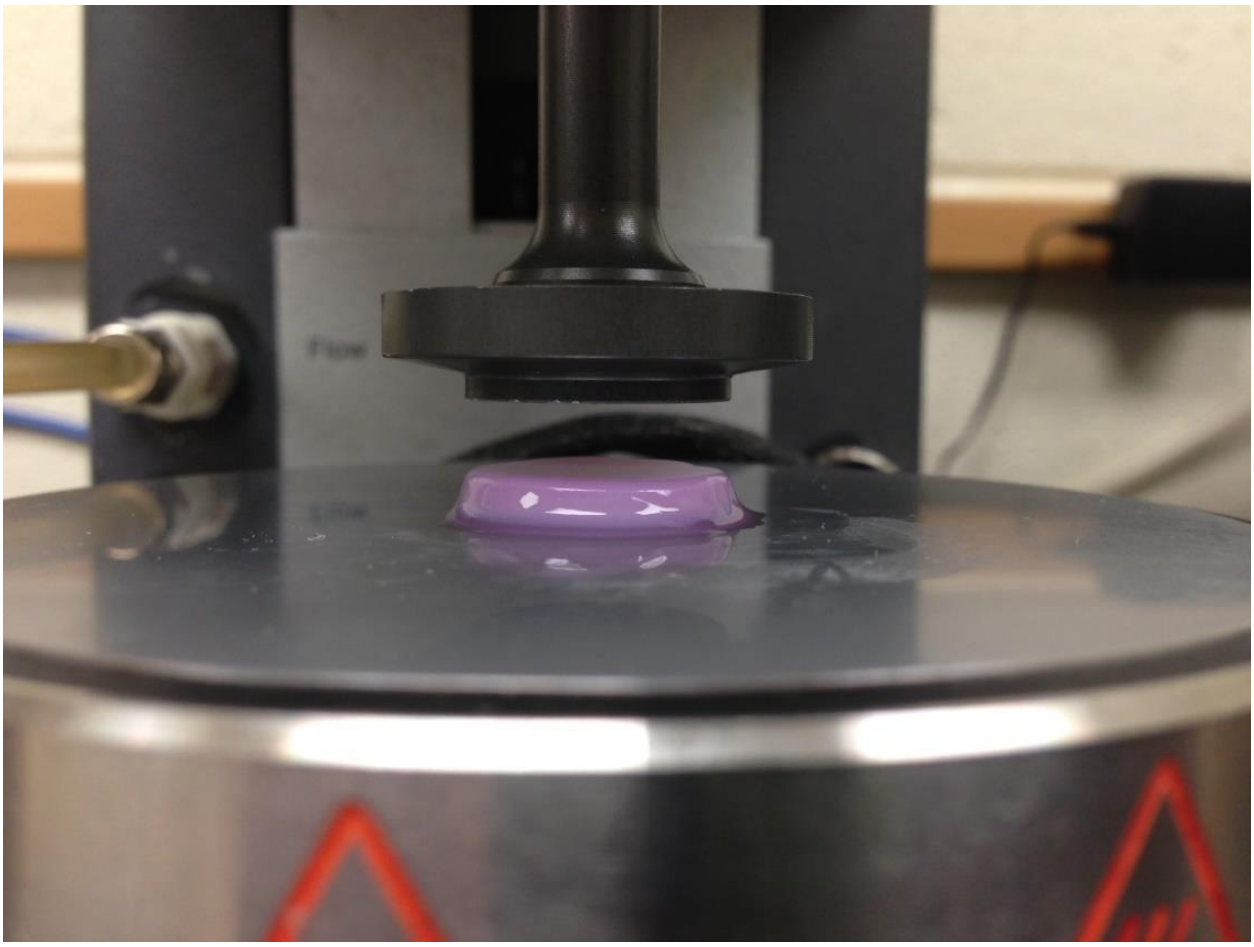

**Figure 21. Picture of the experimental rheometry setup after the collagen hydrogel was analyzed.**

bone tissue mechanics, were tested using a rheometer (TA Instruments). Important to note in terms of collagen hydrogel concentration is that the percentage composition of collagen is related to the mass (milligrams) per volume (milliliter) by a factor of 10. For example, 0.1% collagen is equivalent to 1 mg/mL collagen, and 0.2% collagen is equivalent to 2 mg/mL. The

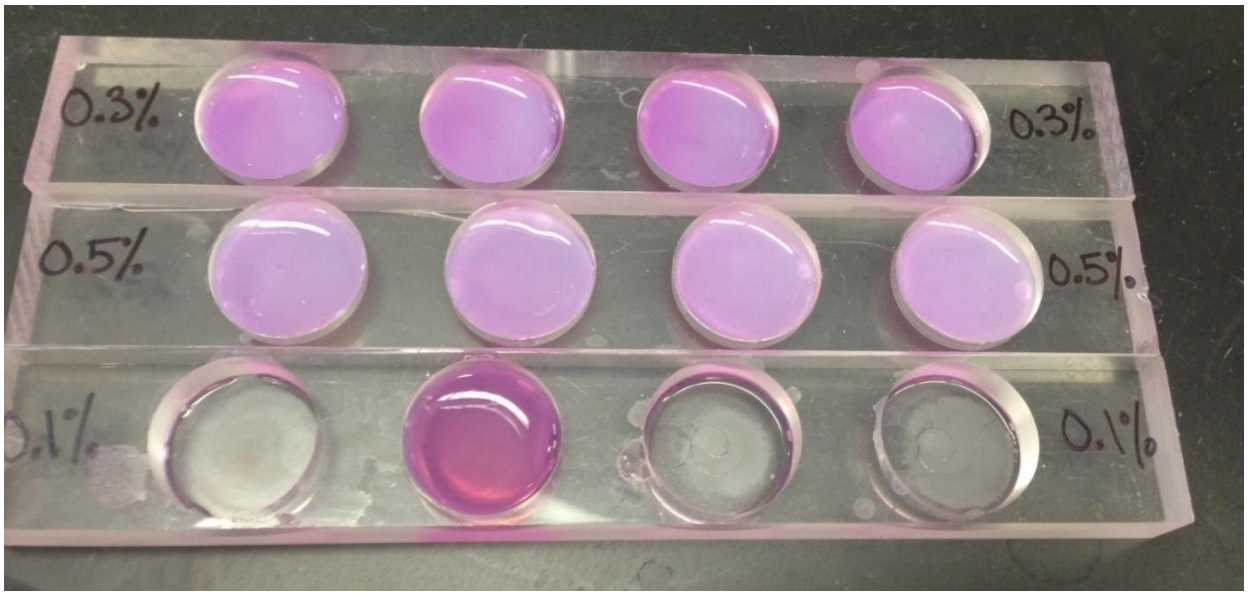


**Figure 23. Hydrogel molds made out of acrylic allowed for the uniform fabrication and transport of collagen hydrogels.**

**Figure 22. Hydrogels flash frozen in the liquid nitrogen setup (right) and then freeze-fractured and dehydrated in liquid nitrogen (left) before lyophilization.**

collagen hydrogels were made according to the manufacturer's protocol. The rat tail collagen stock solution was maintained in acetic acid at 4°C. The stock solution, NaOH, and two additional reagents were mixed on ice, and then were placed on the rheometer's stage between a preheated parallel-plate at 37°C where the solution quickly gelated (figure 21). The parallel-

**Figure 24. Freeze-fractured hydrogel cross-sectional pieces sputter-coated with gold-palladium.**

plate used had a 12mm diameter geometry and obtained the storage and loss modulus of collagen hydrogels. A maximum strain was set at 0.1% within the 10% linear viscoelastic regime for shear measurements.[292] An n =3 was used and the data was plotted.

Additionally, collagen hydrogels of the same concentrations as listed above were fabricated in molds in a 37°C incubator for 30 minutes (figure 22). They were then removed and individually flash frozen in liquid nitrogen and freeze fractured to image the cross sections (figure 23). The samples were lyophilized for 24+ hours and subsequently sputter coated with gold-palladium for 1 minute at 50mA (15nm thickness) (figure 24). Each concentration hydrogel was imaged on an SEM at magnifications of 100, 400, 1,000 and 2,000X in order to see the internal structure of the scaffolds.

### 3.2.3. Mechanical loading of hydrogels via ultrasound and quantification of deformation via fluorescent imaging

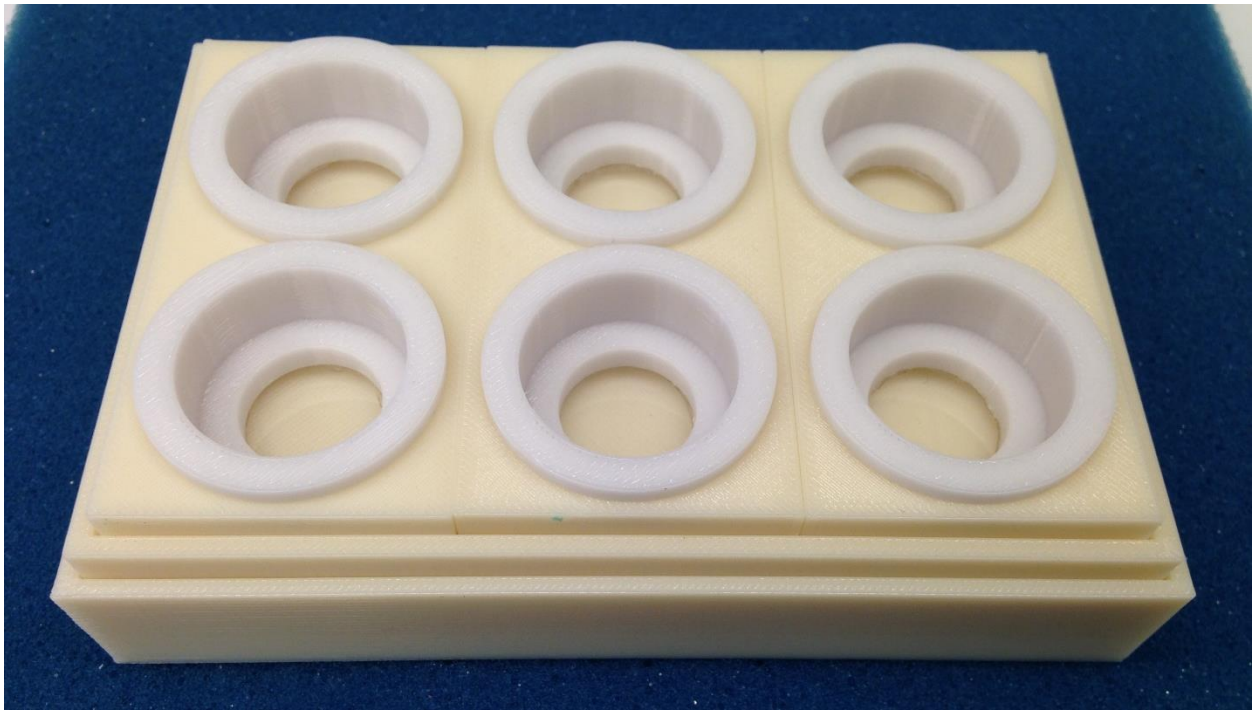

**Figure 25. 3-D printed culture inserts used to visualize the hydrogels undergoing LIPUS stimulation.**

Rat tail Collagen Type I hydrogels (0.5, 0.75, 1, and 2 mg/mL) were formed with encapsulated fluorescent 1µm beads and imaged with a water-cooled epifluorescent microscope using Volocity (Improvision) acquisition and quantification software. Hydrogels were manufactured in 3-D printed acrylic wells custom fit for the fluorescent microscope used (figure 25). Additionally, removeable holding plates were 3-D printed which each held two wells and could be stored in the larger 3-D printed base which could fit a total of six wells for ease of transport between hydrogel manufacturing within the incubator and the final microscopy setup destination (figure 26). For timing, the first 30 seconds had no treatment to establish a baseline, with the following 30 seconds subjected to ultrasound treatment, and the

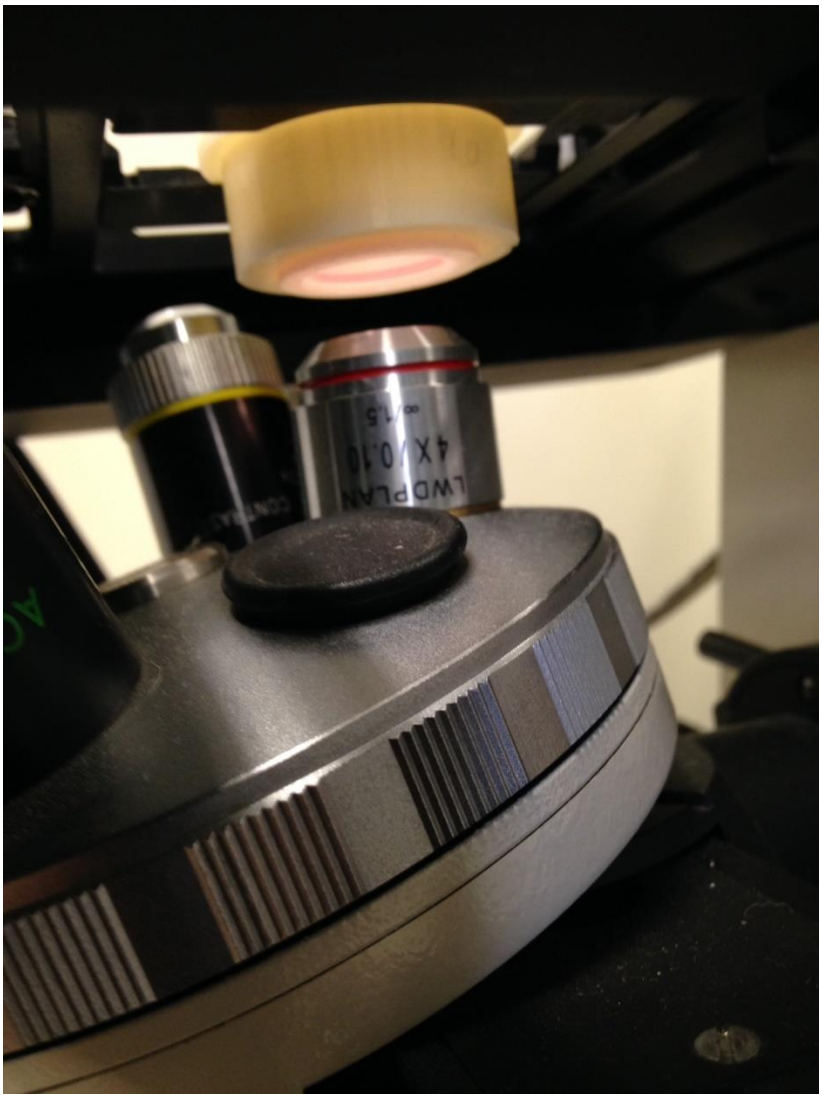


**Figure 26. 3-D printed culture insert with hydrogel undergoing LIPUS stimulation during fluorescent imaging.**

final 30 seconds no treatment was provided in order to visualize any scaffold deformation and relaxation. By acquiring z-stack images over time, fluorescent beads were tracked and movements were averaged to determine the average deformation of the various viscosity hydrogels under variable loads and quantified in the total directional movement, and the x, y, and z directional movements as well. Additionally, the various viscosity hydrogels were subjected to the clinical parameters for fracture healing as noted earlier (30 $mW/cm^2$ at 20%

duty cycle and 1 kHz pulse repetition frequency) and the amplitude was held constant for the 50 and 100% duty cycle runs. The ultrasound transducer was submerged in 2 mL of media centered within the well directly over the hydrogel being tested. The ultrasound transducer was positioned and lowered using adjustable clamps and ring-stand, and the fluorescent microscope was stabilized as it was situated on an air table to limit any environmental vibrations and noise. Also, a higher intensity LIPUS treatment was used with a stiffer gel (2 mg/mL) to verify that some deformation can still occur if the intensity/load is increased. Intuitively, we hypothesized that the lowest viscosity hydrogels would experience the greatest deformation in addition to higher duty cycles causing greater deformation.

## 3.3. Results

### 3.3.1. Ultrasound System Characterization and Quantification of Force, Pressure, and Intensity

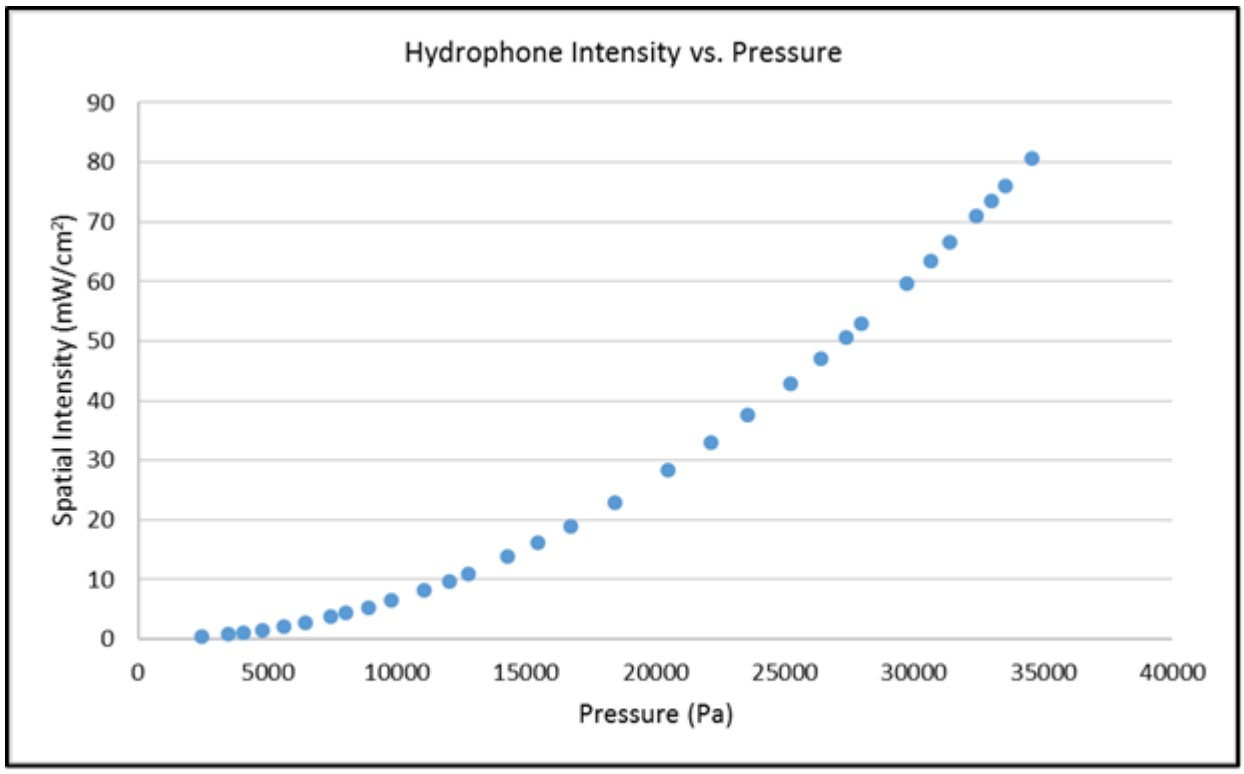


**Figure 27. The mathematically derived relationship between spatial intensity and recorded hydrophone pressure.**

The mathematically derived relationship between spatial intensity and pressure can be seen in figure 27.[293] Although self-evident based on Equation 3, it was important to establish and plot the positive proportionality between spatial intensity and pressure when using the high-resolution hydrophone. As hypothesized, with an increase in amplitude on the waveform generator, the resultant force increased as well as can be seen in figure 28. Intuitively,

amplitude was proportional to force generated. Additionally, as duty cycle increased, so did the force at the same particular amplitude. With a higher duty cycle, the waveform is generated for a longer time period (or greater percentage of time), resulting in generating a greater mechanical response through the transducer, hence manifested a greater force. Force was directly related to the designated amplitude and duty cycle.

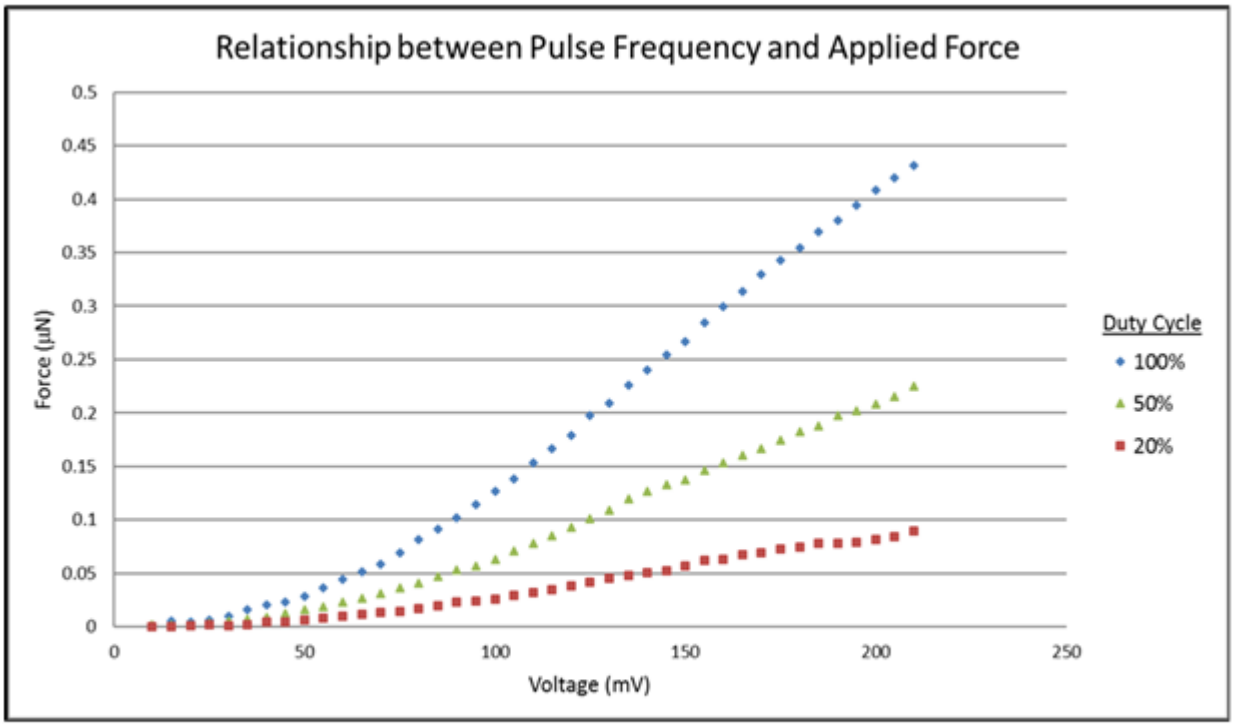


**Figure 28. Amplitude sweep with varying duty cycles (20, 50, and 100%) with calculated force output.**

Next, with a simple mathematical equation noted earlier (Equation 3), spatial intensity is proportional to force; hence as amplitude or duty cycle increased and created a greater force or pressure (force per unit area), the calculated spatial intensity increased as seen in figure 29. To reiterate, spatial intensity is the power per unit area (for our purposes measured in $mW/cm^2$) and is perhaps the most important clinical parameter.

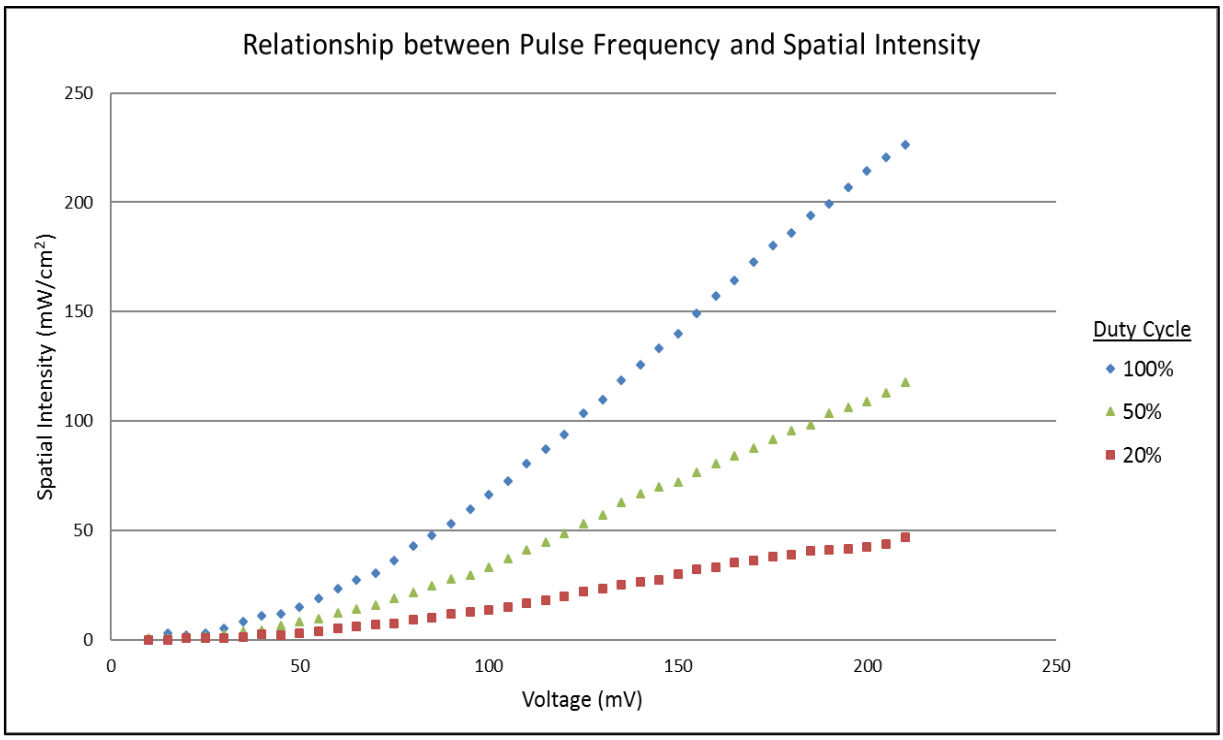


**Figure 27. Amplitude sweep with varying duty cycles with calculated special intensity output.**

To show the relative forces that a given duty cycle produces compared to a continuous signal (or 100% duty cycle), the correlation between the amplitude sweeps of the 20% and 50% duty cycles, or 200µs and 500µs pulses respectively, when using a 1,000µs pulse repetition frequency, was plotted by the percentage mass at each amplitude in comparison to the continuous waveform (figure 30). With the exception of very low amplitudes, the theoretical values matched up very closely to the experimental values. The 20% and 50% duty cycles each produced about 20% and 50% of the mass (or force) that the 100% duty cycle, or continuous, waveform generated.

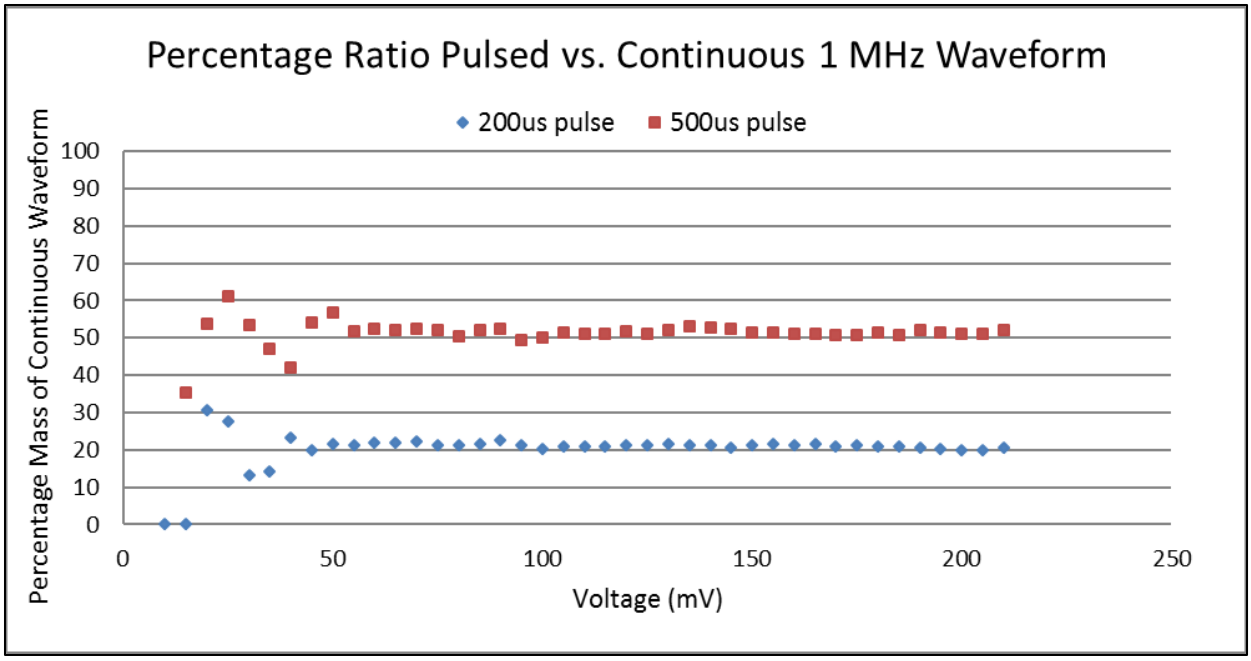


**Figure 28. Amplitude sweep with varying duty cycles compared as percentages of the continuous waveform in mass.**

Figure 31 shows the amplitude sweeps and correlated spatial intensities using the hydrophone setup with two different amplifiers that were purchased so that more than one ultrasound setup could be used for *in vitro* or *in vivo* experiments at once. We had to be conscious of the particular amplifier and amplitude chosen so that the desired output was always as expected from extrapolated values from the data set. As the two amplifiers had slightly different gains, one amplifier would output a different voltage than the other for a given amplitude. In order to keep consistency for output for both setups, we had to be conscious at all times of which amplifier was being used so that proper input values would correlate with consistent and exact outputs for both ultrasound setups. Also plotted is the spatial intensity for the cone and balance setup previously used in the preliminary data section. The spatial intensity values for the cone and balance setup provided a second verification to

validate that hydrophone was outputting appropriate data. Additionally, both calculated best fit lines closely correlated with the amplitude sweeps for each ultrasound setup with both values of $R^2 > 0.99$.

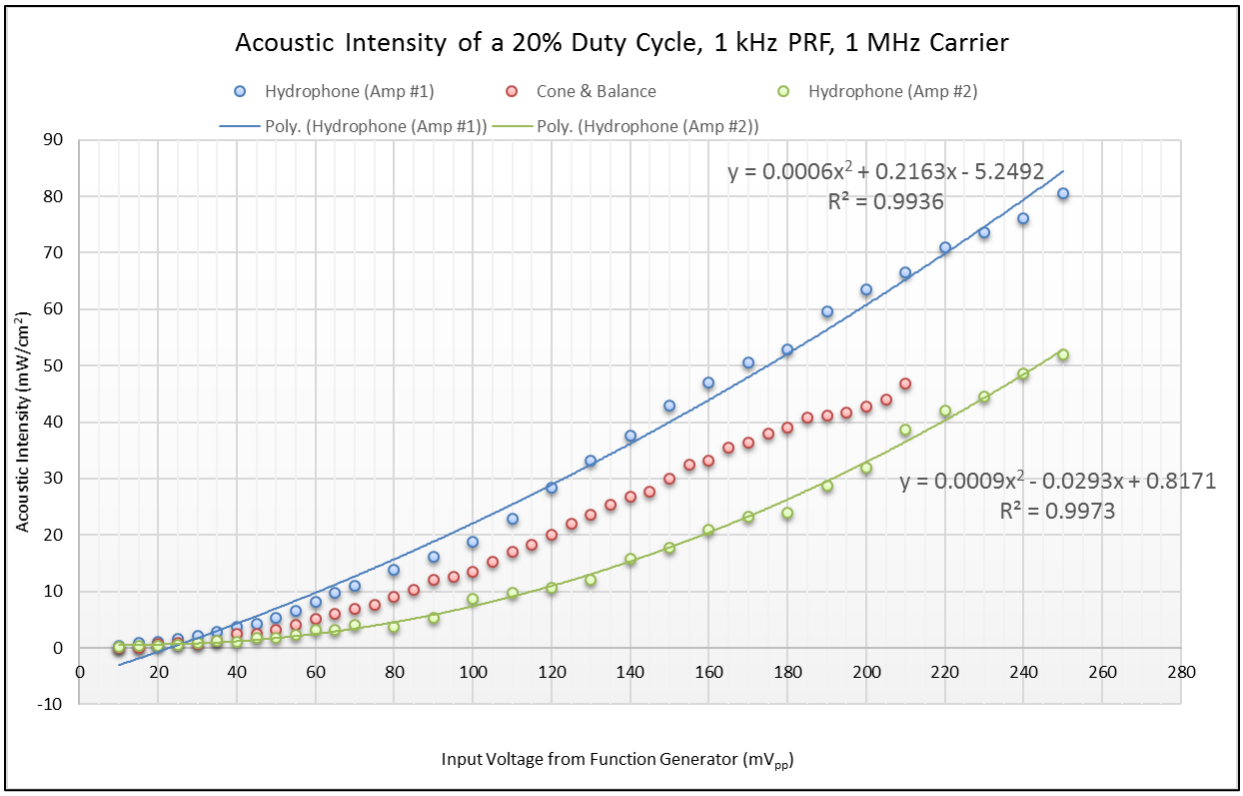


**Figure 29. Amplitude sweep with varying duty cycles with calculated special intensity output.**

### 3.3.2. Collagen Hydrogel Characterization via Rheology and SEM

As hypothesized, the relationship between the collagen concentration within the fabricated hydrogels and the storage and loss moduli was directly proportional (figure 32). More collagen within a hydrogel provided a more rigid, yet resilient scaffold which in turn could be useful when designing scaffolds for particular tissue engineering applications. However, at the highest collagen concentration, 5 mg/mL, the viscosity of the hydrogel was rather high and may make it difficult for cellular proliferation, migration, communication, and waste transport, which may need to be investigated further. The data provided evidence of the viscoelastic nature of the collagen hydrogels given that their response is not purely elastic as expressed from the loss moduli plotted.

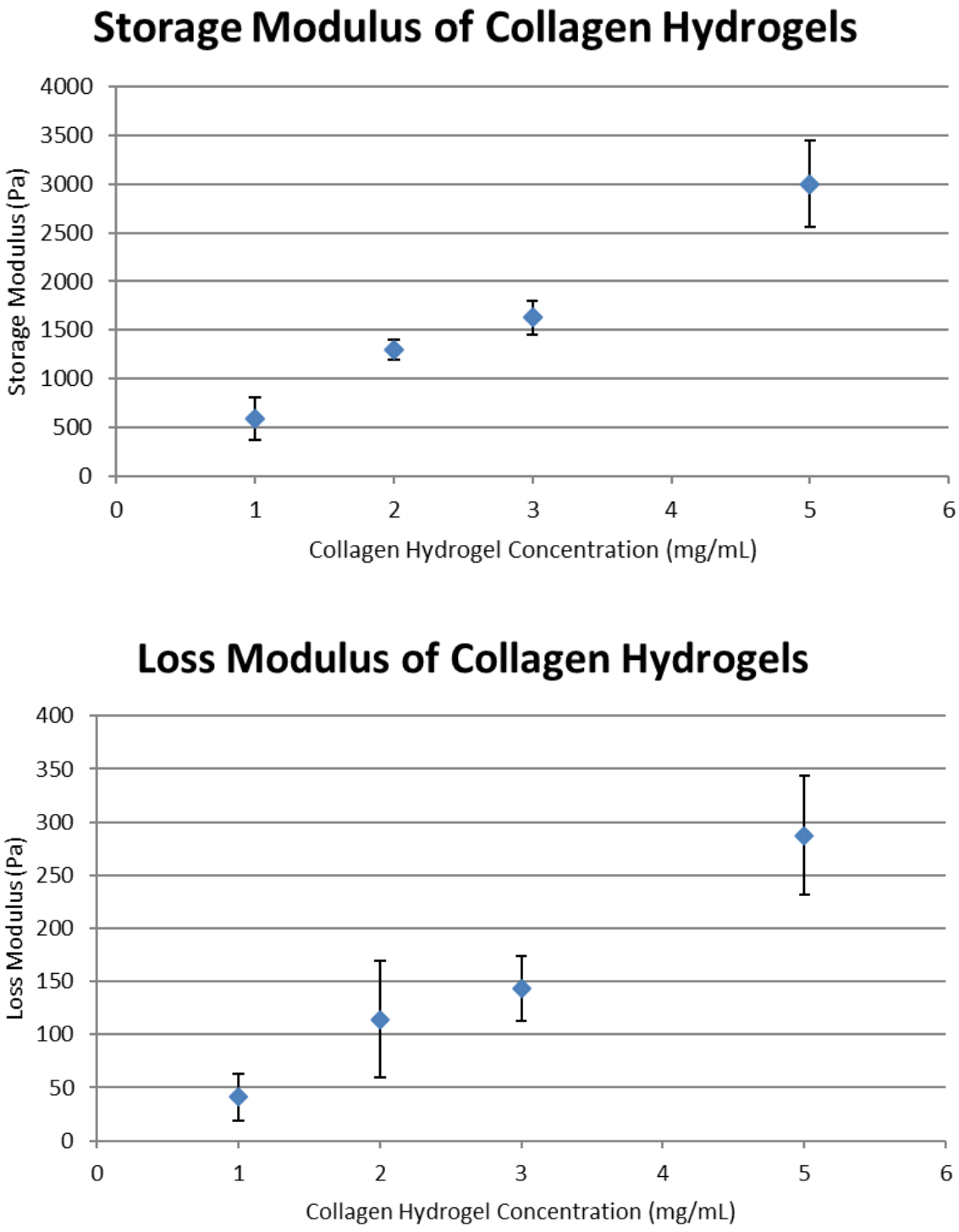


**Figure 30. Storage moduli (top) and loss moduli (bottom) of collagen hydrogels.**

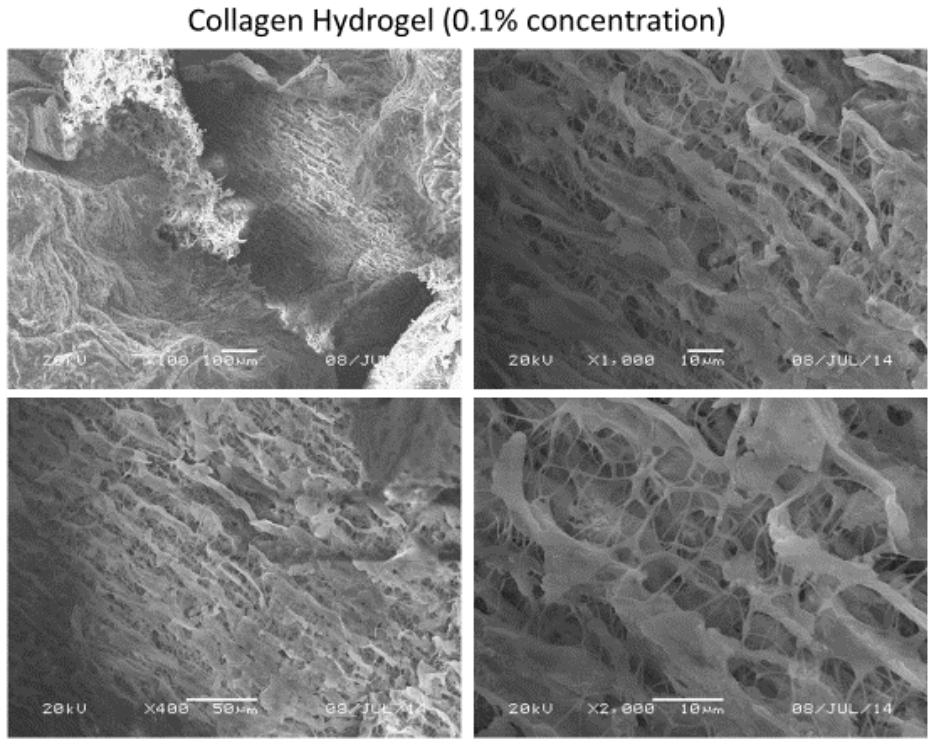


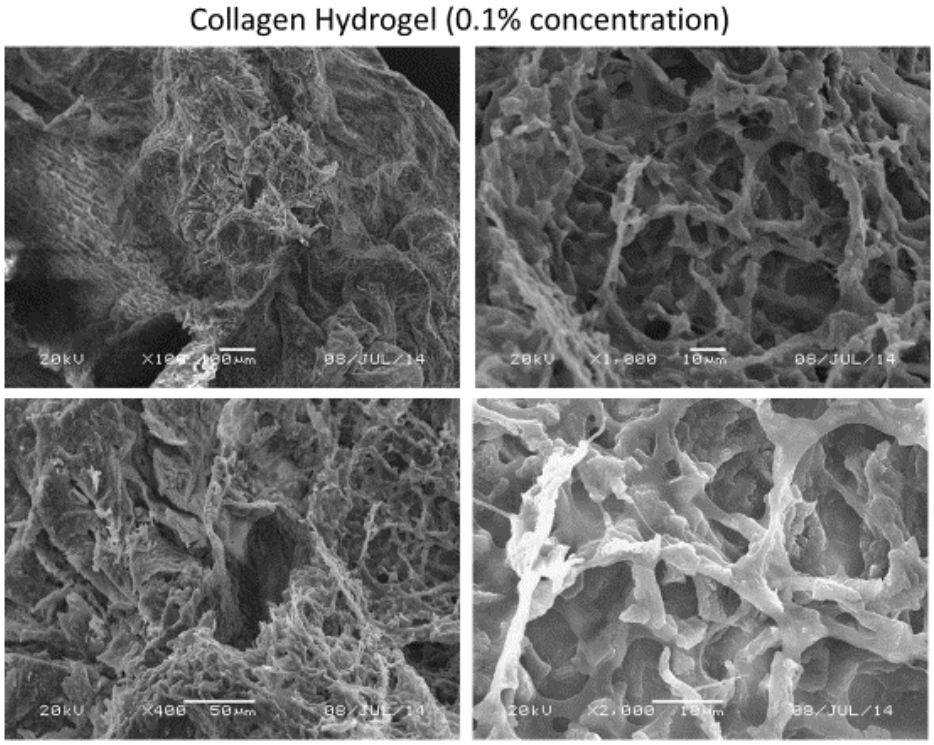


**Figure 31. SEM images of 0.1% collagen hydrogels at 100, 400, 1,000, and 2,000X.**

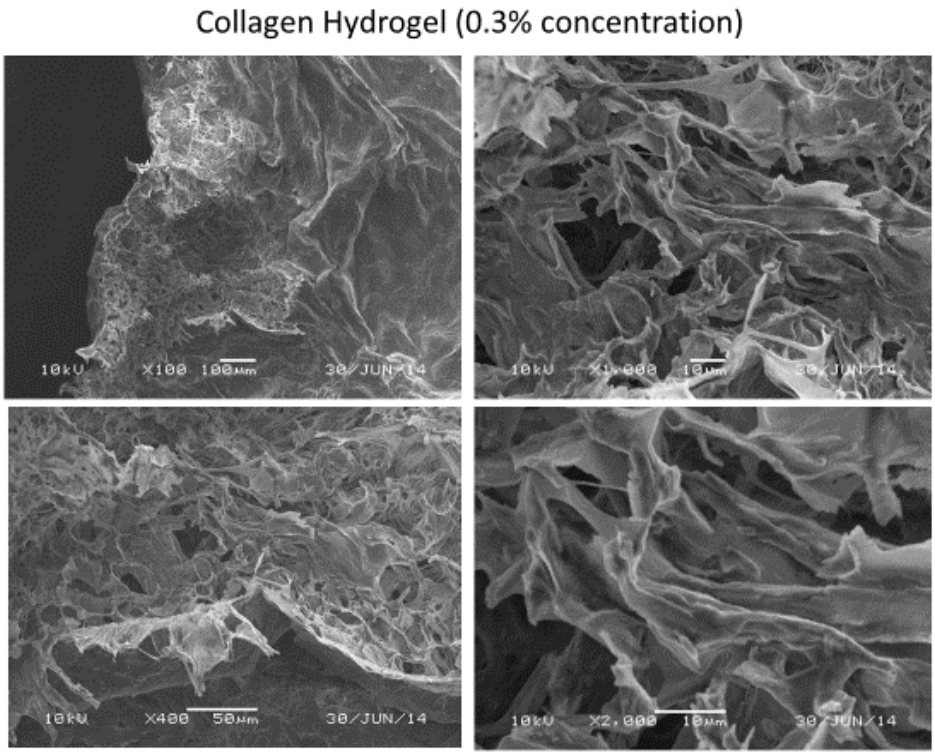


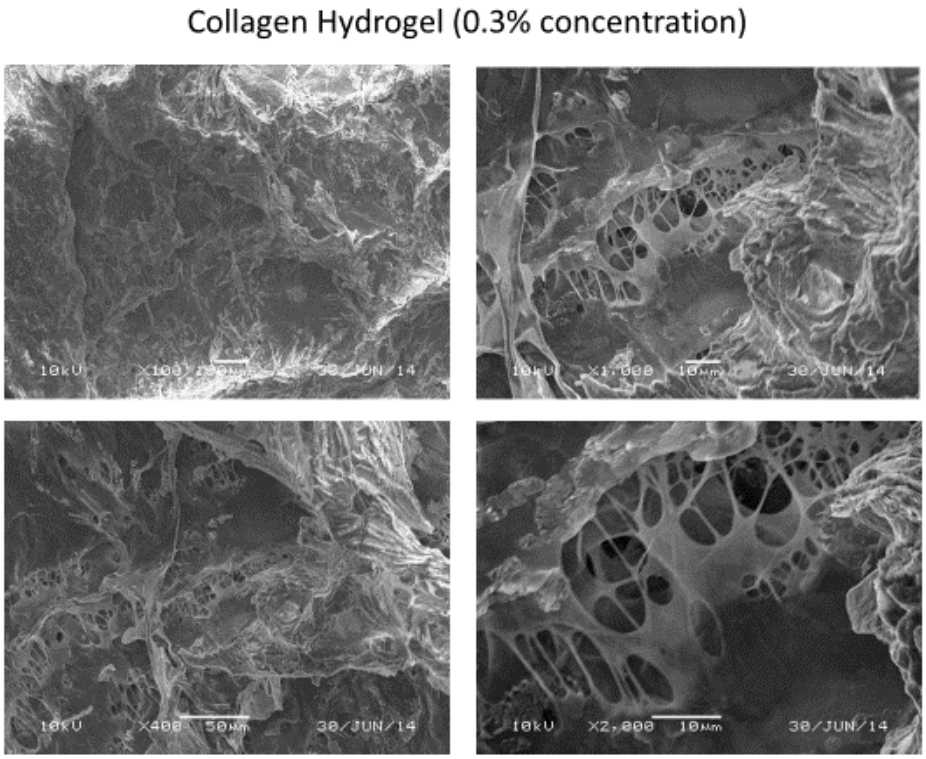


**Figure 32. SEM images of 0.3% collagen hydrogels at 100, 400, 1,000, and 2,000X.**

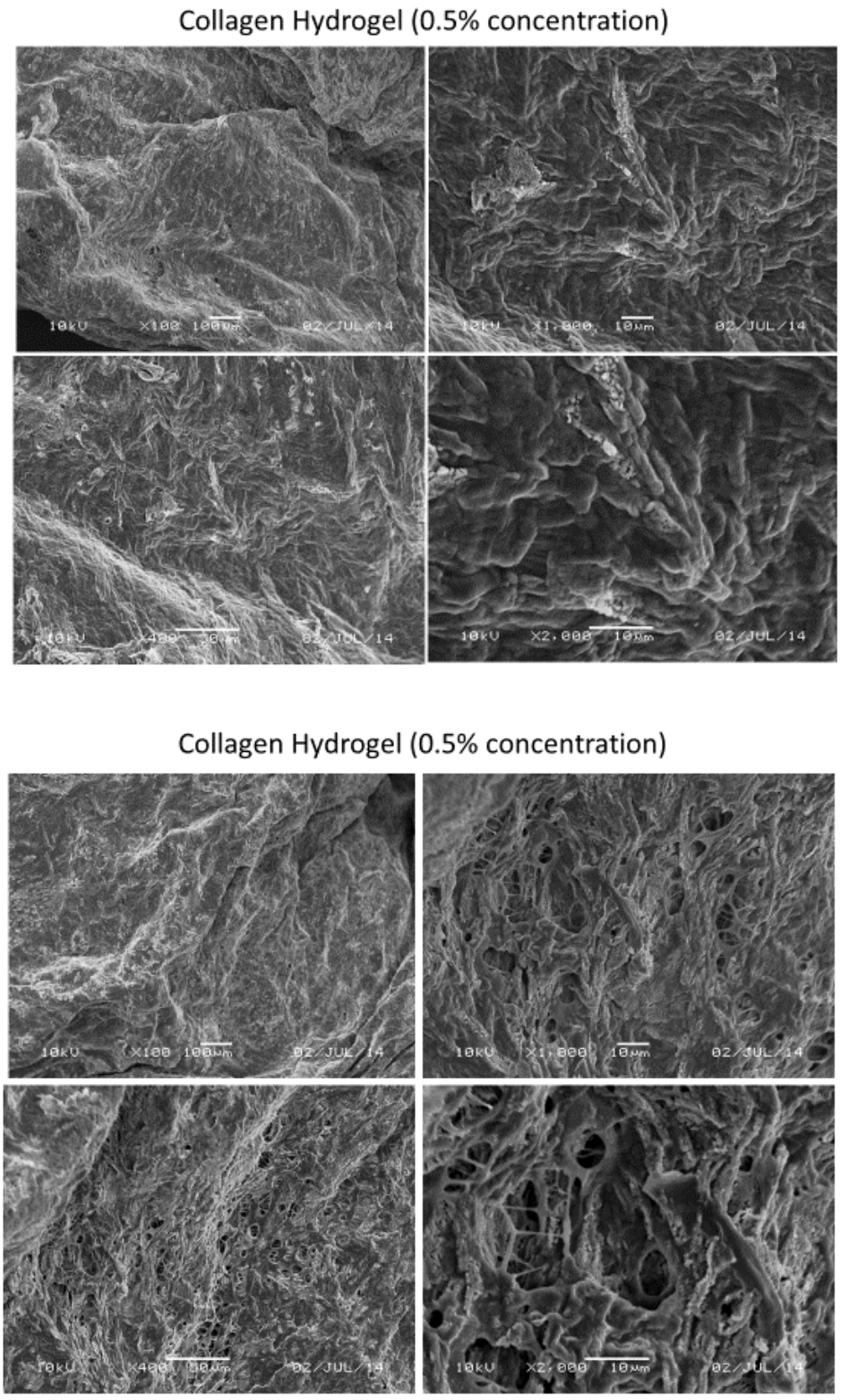


**Figure 33. SEM images of 0.5% collagen hydrogels at 100, 400, 1,000, and 2,000X.**

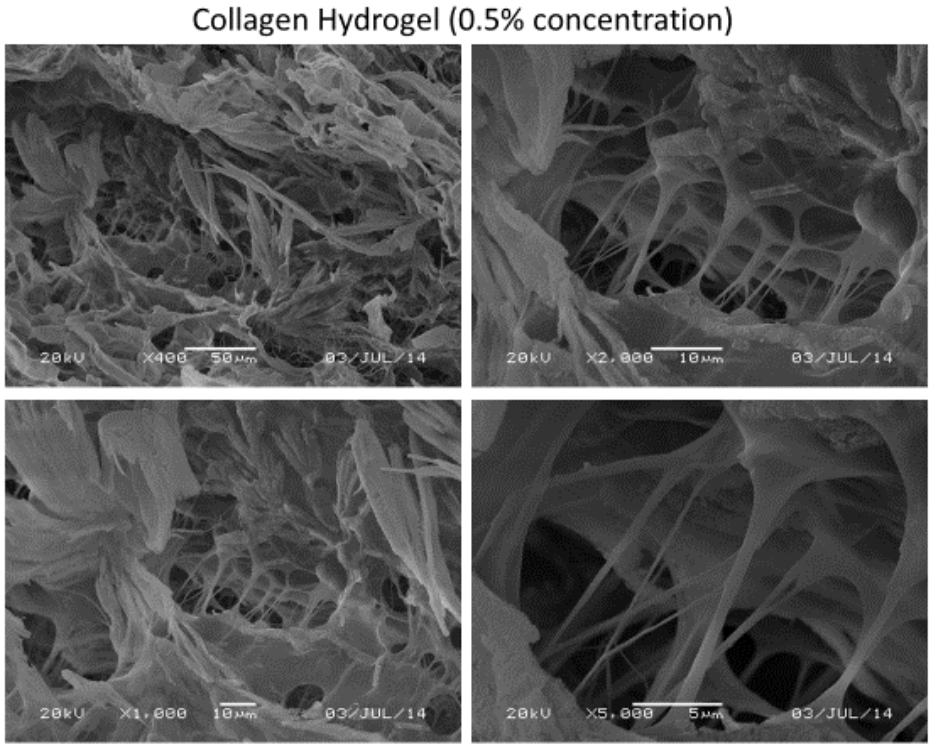


**Figure 34. SEM images of 0.5% collagen hydrogels at 400, 1,000, 2,000, and 5,000X.**

SEM imaging of three different concentrations of collagen hydrogels after freeze fracturing, lyophilizing, and sputter coating showed different morphology and porosity as concentration changed from 0.1% collagen in figure 33, 0.3% collagen in figure 34, and 0.5% collagen in figure 35. Figure 36 has additional images of the 0.5% collagen hydrogel at higher magnifications: 400, 1,000, 2,000, and 5,000X. The lowest hydrogel concentrations appeared to have the largest pores and were the least dense in terms of matrix. As higher collagen concentrations have a higher ratio of solid mass compared to water, intuitively the scaffolds were noticeably denser in matrix composition. It appears that a ~10µm cell would be able to infiltrate the collagen fiber network of a 0.1% collagen hydrogel but may be difficult to migrate through a 0.5% collagen hydrogel. However, based on the flexibility and elasticity of the

higher concentration collagen hydrogels investigated, encapsulated cells may be able to attach and displace collagen fibers and receive nutrients or growth factors via fluid exchange through the scaffold.

### 3.3.3. Mechanical loading of hydrogels via ultrasound and quantification of deformation via fluorescent imaging

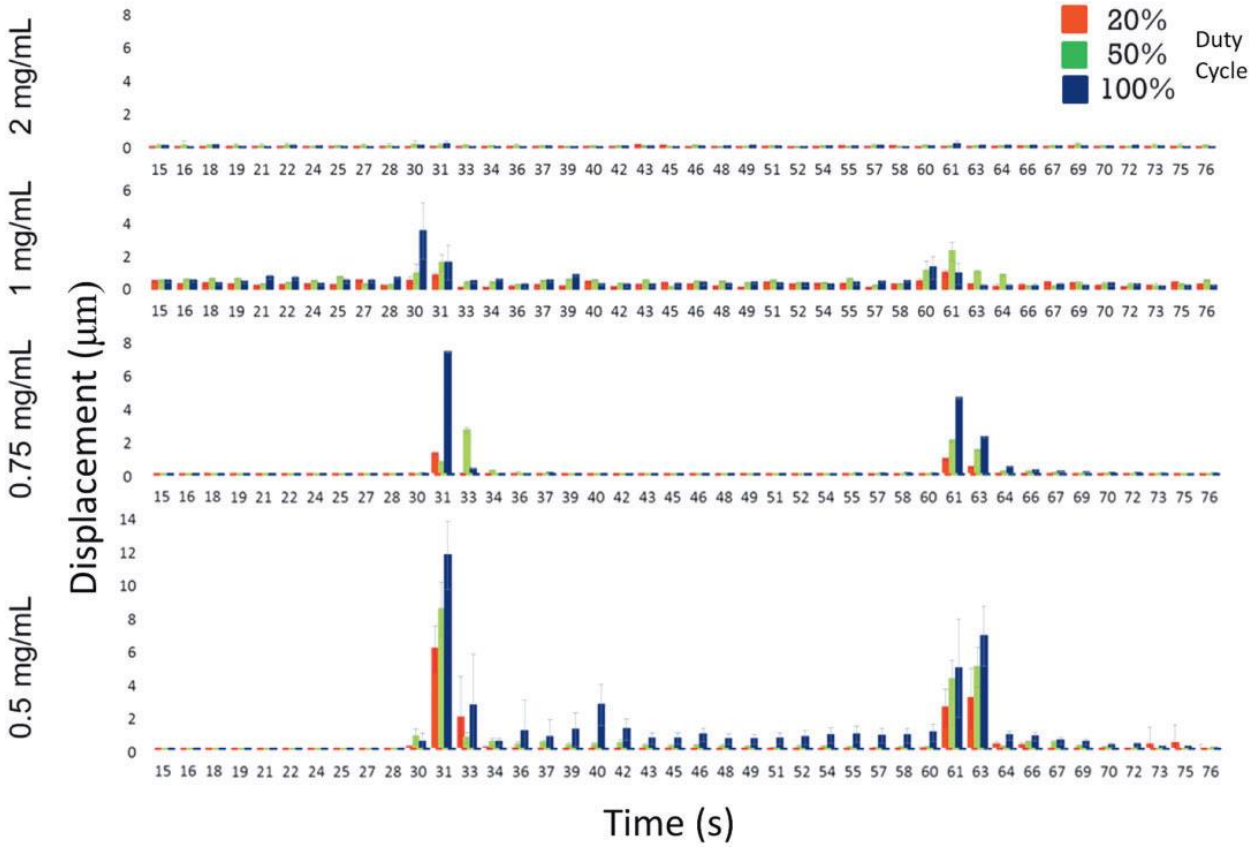


**Figure 35. Mean displacement of fluorescent beads every 1.5 seconds in four different collagen hydrogel concentrations from LIPUS treatments of 20, 50 and 100% duty cycles.**

The fluorescent beads encapsulated within the collagen hydrogels showed displacement from both the onset and cessation of ultrasound, suggesting that the hydrogel deformation occurred when exposed to ultrasound treatment, and subsequent recovery occurred at treatment cessation. While fluorescent microscopy imaging was performed using Volocity analysis software, the mean bead displacements (absolute value) in each of four different hydrogel

concentrations (0.5, 0.75, 1, and 2 mg/mL) were plotted every 1.5 seconds as shown in figure 37. LIPUS was turned on at 30 seconds and turned off at 60 seconds, and beads were tracked for a total of 90 seconds. Given that the encapsulated beads were randomly distributed throughout the hydrogel, the mean displacement of beads was assumed to be indicative of the general deformation the hydrogel experienced. This assumption was made in part due to the fact that the fluorescent beacons were composed of polystyrene, a synthetic aromatic polymer similar in density (1.04 $g/cm^3$) to that of water, hence physical movements should not have differed significantly from the surrounding hydrogel substrate given its similar nature.[294]

The greatest deformation of the hydrogels occurred with the lowest collagen concentration and hence the lowest storage modulus. Hydrogel deformation was therefore indirectly proportional to collagen concentration. Hence as collagen concentration increased and storage modulus increased, mean bead displacement decreased. The majority of the gel deformation occurred as LIPUS was turned on, or acoustic radiation force was applied. Bead displacement spiked during the two or three 1.5 second intervals when the acoustic radiation force was applied. After the initial deformation, there was little bead displacement until 60 seconds when LIPUS was turned off and the acoustic radiation force was no longer applied. The second increase in displacement occurred around the 60 second time intervals, but was slightly lower than the initial bead displacement within that hydrogel when LIPUS was applied at 30 seconds. Since the mean bead displacements plotted in figure 37 are absolute values, it is apparent that the hydrogels were likely deformed in one direction to a particular point of equilibrium between the acoustic radiation force and the elasticity of the collagen hydrogel applying an equal and opposite force and then recovered in the other direction. Once LIPUS was turned off, the hydrogels relaxed and returned back near their original positions. Given

the viscoelastic properties of the hydrogels indicated by the rheology testing, it is intuitive that the hydrogels experienced a higher degree of bead displacement at the initial application of LIPUS compared to their recovery displacement when LIPUS was stopped. The hydrogels did not fully recover to their exact initial positions due to the loss in energy from the viscous portion of the hydrogel.

In addition to collagen concentration being a factor in mean bead displacement, as we would expect the greater the duty cycle, the greater the beads were displaced as a greater force was applied. The bead displacement that occurred right at 30 seconds when LIPUS was turned on for about two or three 1.5 second intervals was greatest with the 100% duty cycle, slightly less with the 50% duty cycle, and the least with the 20% duty cycle. As mentioned before, the lowest concentration hydrogel experienced the greatest deformation and each gel experienced slightly less deformation as their collagen concentration increased. However, at the 2 mg/mL hydrogel, little to no deformation was accounted for, indicating that the particular collagen concentration was the upper limit for the particular loads being applied considering amplitude was held constant for all three duty cycles and the 20% duty cycle expressed the clinical intensity of 30 $mW/cm^2$. To verify that the 2 mg/mL collagen hydrogel was simply at the study's limit in terms of applied force and no deformation being present, we increased the amplitude of our signal which immediately resulted in noticeable bead displacement again.

Rather than looking at bead movement at short intervals, the total mean path length was calculated for each of the gels and duty cycles as seen in figure 38. Once again, as collagen concentration increased, gel deformation was assumed to have decreased as mean path length decreased in all but one group, the 0.1% collagen gel, which appeared to be an outlier. Additionally, as duty cycle increased, so did the mean path length as would be assumed since

a greater force was being applied. As shown in figure 39, mean path lengths were split up into separate time intervals, displaying that the beads traveled the most during LIPUS treatment and usually more with higher duty cycles. Mean path length was the least before ultrasound was applied fairly consistently throughout the groups and simply represents noise and Brownian motion. The mean path length was the second greatest during the post ultrasound phase when the hydrogels were recovering. Additionally, mean path lengths were separated into total mean path length (meaning in any direction), and then represented in the x, y, and z coordinates individually. The acoustic radiation force was applied to the hydrogels directly on top by submerging the transducer in the media. The transducer was uniaxially aligned with the z axis; however, the majority of the bead deformation did not occur in the z-direction. Most of the bead displacement was actually in the x,y plane.

| Mean Path Length (µm) Traveled over the Entire 90 Seconds in all Directions | | | | | | | | |
|---|---|---|---|---|---|---|---|---|
| | 0.05% Collagen | | 0.075% Collagen | | 0.1% Collagen | | 0.2% Collagen | |
| Duty Cycle | Mean Path Length (µm) | STDEV | Mean Path Length (µm) | STDEV | Mean Path Length (µm) | STDEV | Mean Path Length (µm) | STDEV |
| 20% | 36.63 | 18.36 | 13.01 | 6.34 | 19.59 | 3.15 | 6.39 | 5.07 |
| 50% | 35.95 | 9.14 | 15.68 | 2.10 | 26.49 | 3.84 | 6.15 | 2.25 |
| 100% | 58.88 | 19.67 | 29.86 | 1.72 | 31.57 | 9.49 | 8.62 | 3.54 |

**Figure 36. Mean path length of beads traveled during the entire 90 seconds.**

| Mean Path Length (µm)Traveled within the Separate Time Frames (XYZ): | | | | | | | | | | | | | | | | | | |
|---|---|---|---|---|---|---|---|---|---|---|---|---|---|---|---|---|---|---|
| | 20% | | | | | | 50% | | | | | | 100% | | | | | |
| | Pre | | During | | Post | | Pre | | During | | Post | | Pre | | During | | Post | |
| % Col | AVG | STDEV | AVG | STDEV | AVG | STDEV | AVG | STDEV | AVG | STDEV | AVG | STDEV | AVG | STDEV | AVG | STDEV | AVG | STDEV |
| 0.05% | 2.72 | 1.99 | 28.51 | 8.62 | 6.87 | 11.58 | 2.24 | 1.29 | 32.11 | 7.92 | 1.60 | 0.41 | 3.16 | 1.46 | 55.38 | 19.46 | 2.11 | 0.50 |
| 0.075% | 2.49 | 1.43 | 7.35 | 1.48 | 2.90 | 3.73 | 2.16 | 0.99 | 11.48 | 0.85 | 1.93 | 0.83 | 1.81 | 0.41 | 26.00 | 0.60 | 1.91 | 0.80 |
| 0.1% | 5.56 | 0.59 | 7.36 | 0.34 | 4.10 | 0.50 | 9.56 | 1.07 | 14.35 | 0.66 | 4.46 | 0.60 | 12.96 | 1.75 | 15.02 | 1.91 | 4.48 | 0.81 |
| 0.2% | 2.41 | 2.56 | 2.33 | 1.37 | 1.64 | 1.20 | 1.89 | 0.76 | 2.46 | 0.90 | 1.80 | 0.68 | 3.02 | 1.11 | 3.45 | 1.53 | 2.15 | 0.98 |

| Mean Path Length (µm)Traveled within the Separate Time Frames (X): | | | | | | | | | | | | | | | | | | |
|---|---|---|---|---|---|---|---|---|---|---|---|---|---|---|---|---|---|---|
| | 20% | | | | | | 50% | | | | | | 100% | | | | | |
| | Pre | | During | | Post | | Pre | | During | | Post | | Pre | | During | | Post | |
| % Col | AVG | STDEV | AVG | STDEV | AVG | STDEV | AVG | STDEV | AVG | STDEV | AVG | STDEV | AVG | STDEV | AVG | STDEV | AVG | STDEV |
| 0.05% | 0.53 | 0.33 | 10.96 | 1.89 | 0.94 | 0.31 | 0.41 | 0.15 | 14.91 | 1.58 | 1.18 | 0.20 | 1.13 | 0.24 | 21.19 | 3.91 | 1.73 | 0.47 |
| 0.075% | 1.46 | 0.20 | 3.79 | 0.18 | 1.52 | 0.52 | 1.28 | 0.24 | 7.41 | 1.03 | 1.52 | 0.27 | 2.01 | 0.06 | 14.11 | 0.13 | 2.69 | 0.08 |
| 0.1% | 4.16 | 0.45 | 5.85 | 0.17 | 3.03 | 0.15 | 6.82 | 0.24 | 12.54 | 0.38 | 3.45 | 0.13 | 10.14 | 2.07 | 12.56 | 1.15 | 3.06 | 0.21 |
| 0.2% | 0.39 | 0.11 | 0.43 | 0.19 | 0.29 | 0.13 | 0.85 | 1.29 | 0.69 | 0.74 | 0.59 | 0.84 | 0.67 | 0.15 | 0.95 | 0.35 | 0.35 | 0.17 |

| Mean Path Length (µm)Traveled within the Separate Time Frames (Y): | | | | | | | | | | | | | | | | | | |
|---|---|---|---|---|---|---|---|---|---|---|---|---|---|---|---|---|---|---|
| | 20% | | | | | | 50% | | | | | | 100% | | | | | |
| | Pre | | During | | Post | | Pre | | During | | Post | | Pre | | During | | Post | |
| % Col | AVG | STDEV | AVG | STDEV | AVG | STDEV | AVG | STDEV | AVG | STDEV | AVG | STDEV | AVG | STDEV | AVG | STDEV | AVG | STDEV |
| 0.05% | 0.67 | 0.27 | 5.51 | 2.29 | 0.83 | 0.32 | 0.47 | 0.12 | 19.10 | 4.45 | 2.97 | 0.80 | 0.86 | 0.32 | 33.00 | 11.86 | 4.78 | 1.36 |
| 0.075% | 0.70 | 0.18 | 2.58 | 0.36 | 1.18 | 1.64 | 0.59 | 0.16 | 5.35 | 0.84 | 1.19 | 0.54 | 0.75 | 0.09 | 10.71 | 0.10 | 1.25 | 0.17 |
| 0.1% | 6.59 | 0.82 | 8.72 | 1.43 | 4.28 | 1.33 | 8.55 | 2.22 | 12.38 | 2.20 | 5.56 | 1.37 | 7.57 | 1.72 | 18.46 | 6.61 | 5.40 | 1.79 |
| 0.2% | 0.38 | 0.18 | 0.42 | 0.11 | 0.31 | 0.15 | 0.67 | 0.85 | 0.95 | 0.63 | 0.54 | 0.70 | 1.54 | 0.39 | 0.73 | 0.34 | 0.44 | 0.20 |

| Mean Path Length (µm)Traveled within the Separate Time Frames (Z): | | | | | | | | | | | | | | | | | | |
|---|---|---|---|---|---|---|---|---|---|---|---|---|---|---|---|---|---|---|
| | 20% | | | | | | 50% | | | | | | 100% | | | | | |
| | Pre | | During | | Post | | Pre | | During | | Post | | Pre | | During | | Post | |
| % Col | AVG | STDEV | AVG | STDEV | AVG | STDEV | AVG | STDEV | AVG | STDEV | AVG | STDEV | AVG | STDEV | AVG | STDEV | AVG | STDEV |
| 0.05% | 1.52 | 1.25 | 7.82 | 6.19 | 3.04 | 5.88 | 1.26 | 0.97 | 4.98 | 5.34 | 0.70 | 0.29 | 1.67 | 0.76 | 10.93 | 9.53 | 1.20 | 0.67 |
| 0.075% | 0.86 | 0.70 | 1.12 | 0.73 | 0.78 | 0.74 | 0.73 | 0.50 | 1.08 | 0.72 | 0.73 | 0.40 | 0.49 | 0.19 | 0.93 | 0.30 | 0.71 | 0.32 |
| 0.1% | 1.52 | 0.75 | 1.43 | 0.82 | 1.08 | 0.66 | 2.31 | 1.45 | 1.53 | 0.92 | 0.98 | 0.74 | 1.93 | 0.69 | 1.98 | 1.28 | 1.29 | 0.80 |
| 0.2% | 1.56 | 2.22 | 1.06 | 0.73 | 0.78 | 0.69 | 1.71 | 2.20 | 1.50 | 1.23 | 1.20 | 1.08 | 1.34 | 0.75 | 1.34 | 0.68 | 0.99 | 0.46 |

**Figure 37. Mean path length of beads traveled within separate time frames: before; during; and after LIPUS.**

### 3.4. Discussion

The highly tunable ultrasound system developed has allowed us to control the output of force, pressure, spatial intensity, etc. by the use of the calibration curves which were developed from amplitude sweeps and hydrophone output. By selecting a particular amplitude, we can control any particular output desired for a study. Additionally, by selection of the amplitude and/or duty cycle, we can control hydrogel deformation (in this case collagen hydrogels) through the known amount of load being applied manifested at those particular settings. A hydrogel of a particular concentration can be chosen as well for an application that desires a particular stiffness, or storage modulus. The hydrophone allowed for real time acquisition of pressures developed from the mechanical vibration expelled from the ultrasound transducer. Where high intensity focused ultrasound (HIFU) can be used in acoustic radiation force imaging[295] in a technique known as elastography,[296] where the acoustic wave generated can physically displace the tissue it propagates through, ultimately allowing for the characterization of the tissue's mechanical properties,[297] we wanted to investigate if LIPUS in fact produced a measurable acoustic radiation force and if this force was great enough for hydrogel deformation and *in vitro* and *in vivo* responses.

From our work, we also now know more about the behavior and integrity of the collagen hydrogels. When acoustic radiation force was applied to the four collagen hydrogels of varying stiffness, a fairly immediate and uniform deformation was experienced which was concluded by the mean of ten bead displacements at every 1.5 second time interval. Through Wolff's law, we know that bone responds positively through physical force and is remodeled based on

where forces are greater or lesser. The signal used in LIPUS therapy for fracture healing has a pulse repetition frequency of 1 kHz with a carrier frequency of 1 or 1.5 MHz. That means that the 1 or 1.5 MHz signal is pulsed or turned on 1,000 times per second and given that a 20% duty cycle is used that means that the signal is only on for 20% of that particular interval during the pulse. Biologically speaking, a cell likely cannot distinguish a force applied 1,000 times per second any different than if the force was applied 500 times per second or 2,000 times per second. From the hydrogels response, it was evident that the load was felt as one continuous load, hence why the hydrogels deformation took place in about three seconds and then did not change until the load was removed (LIPUS was turned off) where the hydrogel experienced almost full recovery evidenced from the mean bead displacement peaking slightly less than its peak when the load was applied. The graphs show about an 80% recovery after the acoustic radiation force is stopped.

We verified that hydrogels are in fact deforming in one direction under LIPUS and returning back in the other direction during recovery by looking at the mean displacements in all three individual coordinates in x, y, and z and not taking the absolute value. From this it is evident that the hydrogels are deformed in one direction when loaded and recover back in the other direction when unloaded. Additionally, the majority of the deformation did not occur in the z-direction which is uniaxial to the acoustic radiation force. Typically the deformation would occur in the direction of the load; however, with our setup and limitations with the microscope, it was only possible to image a z-stack (an x,y slice) up to about 100µm in the z-direction away from the surface of the coverslip. Based on the laws of laminar flow, molecules of a fluid move the least close to the surface of the pipe or structure they reside in. Similarly, given that the z-stacks we acquired were only at maximum 100µm away from the coverslip,

any movement of the beads bringing them closer to the surface of the coverslip would hinder their further movement in theory. So despite the acoustic radiation force being applied in the z-direction and based on how close the imaged beads were to the surface of the cover slip, the beads ultimately moved in the x,y plane more than they did in the z-direction. The hydrogels are over 99% water as well, and given that water is an incompressible fluid, the hydrogel could not deform into a space that is smaller than it started with. When the acoustic radiation force was applied in the z-direction, the beads had to move with fluids as they go from high pressure to lower pressure areas. The greatest pressure would be closest to the coverslip so the beads moved perpendicular to the acoustic radiation force in the x,y plane where pressure would become less as they being to move out of the ultrasound beam. And based on laminar flow, if the beads stayed higher in the z-direction, or avoided moving closer to the coverslip, then they would experience less friction and be able to displace further in the x,y plane.

Also, mentioned before was the notion of the pulse repetition frequency of the typical LIPUS signal in fracture healing. It was evidenced that the hydrogels only deformed that one time at the instant the acoustic radiation force was applied. The only time the beads moved again (besides Brownian motion) was when LIPUS was stopped. This is similar to stepping on a scale to weigh yourself and stepping off. Since bone responds to physical loads positively as expressed by Wolff's law, perhaps there would be more benefit to not have a pulse repetition frequency of 1 kHz where the carrier signal is applied 1,000 times per second. Subsequently, the scaffolds and likely cells as well cannot distinguish the rate of that repetition frequency and simply deform to a point of equilibrium for the duration of LIPUS treatment, which is 20 minutes per day clinically. Perhaps bone cells would respond better to a repeated loading and unloading as described by Wolff's law, meaning that a pulse repetition frequency around 1 Hz

may be of greater benefit. With that parameter, the cells would be loaded and unloaded every one second for the 20 minute treatment. The characterization of the ultrasound system allows for the possibility to run many different studies and investigate many different parameters in hopes to first optimize the LIPUS therapy and secondly discover the underlying mechanism of action of its efficacy.

# 4. SPECIFIC AIM II: EFFECT OF ULTRASOUND IN VITRO: CELLS AND ENCAPSULATED CELL-HYDROGEL CONSTRUCTS

## 4.1. Introduction

With the development of a highly tunable ultrasound system, we have demonstrated via the characterization with a needle hydrophone, the presence of a measurable acoustic radiation force (ARF) even at low intensities such as what is used in low intensity pulsed ultrasound (LIPUS) where clinical effectiveness has been shown for years by the transdermal treatment for fracture healing and non-union defect repair.[272,279] Where ARF is traditionally recognized in higher intensity medical ultrasound modalities such as diagnostics and imaging techniques,[230,289] we have now shown that LIPUS also produces a measurable ARF which may be a driving factor in the long unidentified and underlying mechanism for the benefits of LIPUS in orthopedic healing, which we hypothesized holds a positive correlation. Other groups have suggested that the efficacy of LIPUS may be derived from local heating effects, which could lead to enhanced local blood flow.[298,299] However, with the designated limit in local heating effects set by the FDA, long duration therapeutic ultrasound devices are not to exceed 1°C in temperature increase.[300] One may question if LIPUS devices with a spatial intensity limited by such a small temperature increase may be negligible to the benefits in local tissue response. Additionally, blood flow and other fluid exchange may potentially and quickly flush out any notable temperature changes in the area.

As mentioned earlier in *Bioeffects of Ultrasound*, there are three main mechanisms of action with ultrasound: acoustic radiation force; acoustic torque; or acoustic streaming. As there has been much *in vitro* work done investigating cellular responses to LIPUS, to our

knowledge our work was the first to investigate the acoustic radiation force with deformable scaffolds to not only osteogenic cellular markers, but particularly markers indicative of mechanical stress. Beyond this work being done *in vitro* with pre-osteoblasts on tissue culture polystyrene (TCP), importantly we extended our work to a more accurate cellular environment to that which more closely exists *in vivo* via tissue mimetics and the collagen hydrogel three-dimensional scaffolds. Where our *in vitro* work exposed our cells to acoustic radiation force via the application of LIPUS from submerged ultrasound transducers in culture media, encapsulated cell/hydrogel constructs were subjected to acoustic radiation force as well as acoustic streaming, or fluid flow. Fluid flow is present in bone channels known as canaliculi and manifests itself as a shear force as is well documented in literature specifically in the field of mechanotransduction as previously discussed.[237,301,302]

To note, we demonstrated that LIPUS produces an acoustic radiation force during both *in vitro* experiments as well as *in vivo*. Additionally, for the feasibility of the manifestation of acoustic radiation force in translational research for the clinical realm, we verified that acoustic radiation force does indeed pass through rat skin with about only a 10% attenuation (figure 40). Briefly, we validated this by using our acoustic radiation force cone and balance setup as previously described; however, we coupled a layer of freshly harvested rat skin directly adjacent to the ultrasound transducer to mimic the clinical transcutaneous treatment of LIPUS. We performed an amplitude sweep with the ultrasound system and plotted the measured mass from the balance for runs with and without the rat skin, holding all other parameters constant. By calculation, the difference between the two measured forces for LIPUS treatment with and without the layer of rat skin demonstrated only roughly 10% attenuation of the signal. It was apparent that the phenomenon of acoustic radiation force is capable of propagating through

biological tissues; hence this allowed us to make assumptions beyond our *in vitro* experiments that acoustic radiation force effects should be evaluated *in vivo*. Also, fluid flow is manifested by LIPUS application *in vitro* as evidenced from data not shown; however, it was demonstrated in preliminary studies where dye was dropped in a fish tank in front of the ultrasound transducer resulting in the dye being propelled forward. However, evidence of proof of fluid flow *in vivo* has yet to be confirmed, yet is a likely possibility taking all factors into account.

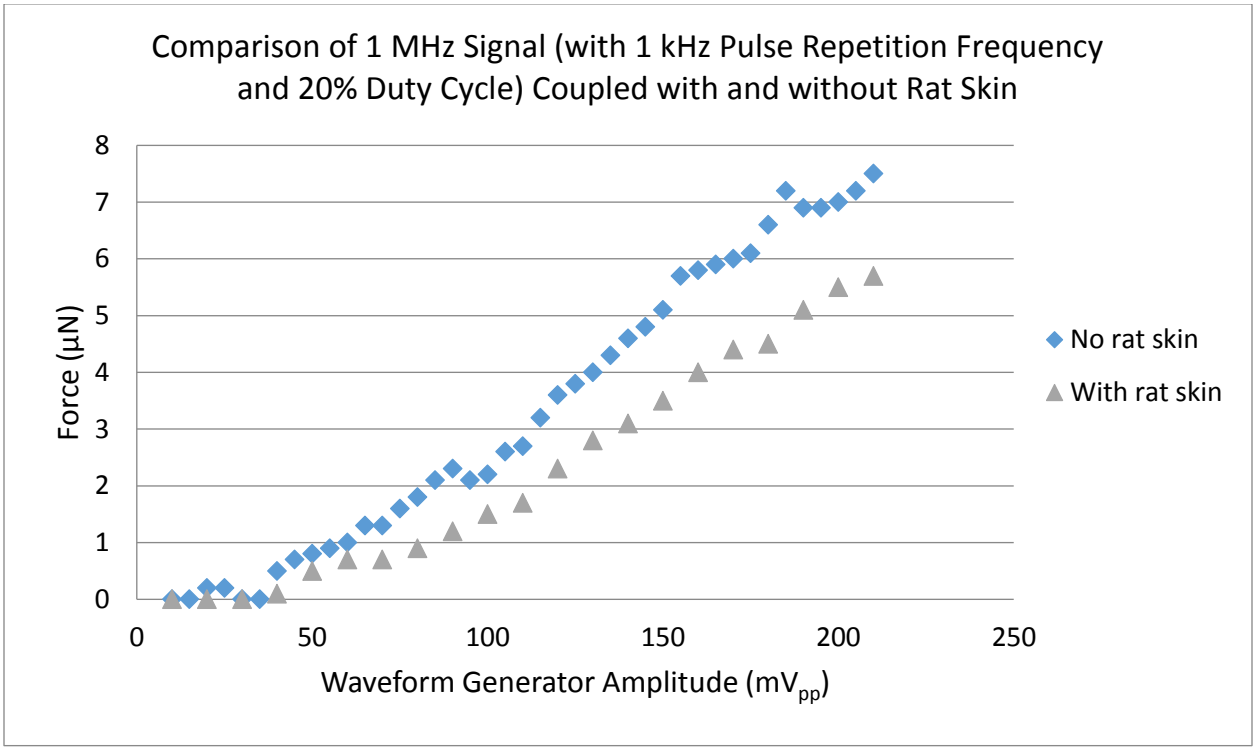


**Figure 38. Relationship between generated acoustic radiation force with a LIPUS setup coupled with and without rat skin.**

## 4.2. Materials and Methods

Next, in order to evaluate the effect of LIPUS on cells alone (on TCP) and cells encapsulated in collagen type I hydrogels, MC3T3-E1 cells, a well-documented preosteoblast cell line derived from mouse calvaria,[303–306] were used for each of the studies, and qRT-PCR was performed for common osteogenic markers. In both studies (on TCP and hydrogel encapsulation), cells were cultured in alpha-MEM media supplemented with 10% FBS and 1% Penicillin/Streptomycin purchased from Gibco (Grand Island, NY). For the TCP study, cells were seeded at a density of 50,000 cells per well in a 6-well plate using the clinical intensity of LIPUS (30 $mW/cm^2$) (experimental group) over 3, 7, 14, and 21 day time points compared to the group receiving no treatment (control group). RNA was extracted and isolated using the Qiagen RNeasy kit (Valencia, CA) and converted to cDNA using Clontech's EcoDry Premix (Mountain View, CA) both based on the manufacturer's protocols. qRT-PCR analysis was performed using Taqman primers (Thermo Fisher Scientific, Rockford, IL) normalizing the genes to housekeeping gene GAPDH and analyzing the response of the following markers: alkaline phosphatase, osteocalcin, osteopontin, collagen 1a1, and RUNX-2.

The same analysis was performed for the cells encapsulated in rat tail Collagen Type I (BD Biosciences, Franklin Lakes, NJ) hydrogels (1, 2, and 3 mg/mL). The cells were added at a density of 250,000 per 3 mL per 6-well plate at the last step of the collagen solution preparation on ice, mixed thoroughly, and immediately placed in a 37°C incubator where they were allowed to gelate. After gelation, 2 mL of media was placed on top of each hydrogel construct and replaced every 48 hours. To verify viability, MC3T3 cells were immunostained with a live/dead assay (Invitrogen, Carlsbad, CA) and imaged with a LSM 510

META/ConfoCor 2 system (Zeiss, Oberkochen, Germany) before, during, and after LIPUS treatment to verify that cells remained viable and alive.

Additionally, to evaluate whether LIPUS impacted cell proliferation in hydrogels, MC3T3 cells were encapsulated in 3 mL of 1 mg/mL (0.1%) collagen type I hydrogel concentration in six-well plates in alpha-MEM media supplemented with 10% FBS and 1% P/S. Cells encapsulated in collagen were maintained in 37°C and 5% $CO_2$ and medium was changed every two days. Cell cultures were treated each day with the clinical intensity of LIPUS (30 mW/cm$^2$) for 20 min/day (experimental group) and no LIPUS (control group) over 1, 3, and 7 day time points. At each time point, cells were isolated by digesting the collagen hydrogel with enzyme collagenase (Thermo Fisher Scientific, Waltham, MA) and centrifuged to form a cell pellet. The cell pellet was re-suspended in 400 mL of PBS and 2% FBS from Gibco (Grand Island, NY). Propidium iodide (1 mL/400 mL) was added to each sample (1uL/400uL for each group) to fluorescently tag the dead cells, and the total number of viable cell count was measured by magnetic-activated cell sorting (Miltenyl Biotec, Germany). One-way analysis of variance (ANOVA) statistical analysis was used to determine statistical significance between each group ($p<0.05$). Additionally, LIPUS treatment and no treatment was compared with MC3T3s both on TCP and in the same viscosity hydrogels as listed above with the confocal microscope; however, an Actin stain (Molecular Probes, Eugene, OR) was used with a z-stack acquisition and rendering (Zeiss software suite) in the hydrogels to visualize cell morphology differences between LIPUS and control groups as well as actin filament alignment and polymerization.

To investigate osteogenic response or expression, the cell-encapsulated hydrogels were exposed to the clinical intensity of LIPUS (30 mW/cm$^2$) for 1, 3, and 7 days for 20 minutes

per day (experimental group) and no LIPUS treatment (control group). At each time point, media was aspirated from each hydrogel and then rinsed with HBSS (Gibco, Grand Island, NY). Additionally, in order to digest the collagen scaffolds, collagenase (Gibco, Grand Island, NY) was used according to protocol. Each digested well with cells was placed into a 15 mL centrifuge tube and spun down. After this point, the qRT-PCR process was the same as with the TCP protocol above; the cell pellet was resuspended with the first solution of the Qiagen RNeasy kit (Valencia, CA) and extracted to proceed as described by the protocol. However, an additional marker of interest was added for qRT-PCR analysis, cyclooxygenase-2 (COX-2), officially known as prostaglandin-endoperoxide synthase 2 (PTGS2), which has shown upregulation in osteoblasts from mechanical stimuli both *in vitro*[307,308] and *in vivo*.[309] This study was repeated by the same parameters listed above except for the time points. As COX-2 is expressed very quickly after mechanical stimulus, the experimental group was administered ultrasound for 20 minutes and samples were collected immediately after treatment and 30 minutes after. Additionally, based on results, varying LIPUS intensities were applied to the MC3T3 cells: particularly 30, 150 and 30 $mW/cm^2$. We hypothesized that the acoustic radiation force from ultrasound treatment would provide a similar mechanical stimulus hence resulting in a positive correlation between COX-2 expression and LIPUS treatment and also intensity.

### 4.3. Results

The *in vitro* results with MC3T3-E1 cells from our studies are discussed in this section. Figure 39 shows a light microscopy image of MC3T3-E1 cells' growth and morphology in a three-dimensional environment, a 0.1% collagen hydrogel, after seven days (figure 41A) compared to a phase-contrast image of MC3T3-E1 cells grown on TCP (figure 41B). The cells had a different morphology compared to ones grown on TCP that acquired a more quilted and patterned look. In three-space, cells were able to migrate and grow in any direction by extending processes from the center of the cell body.

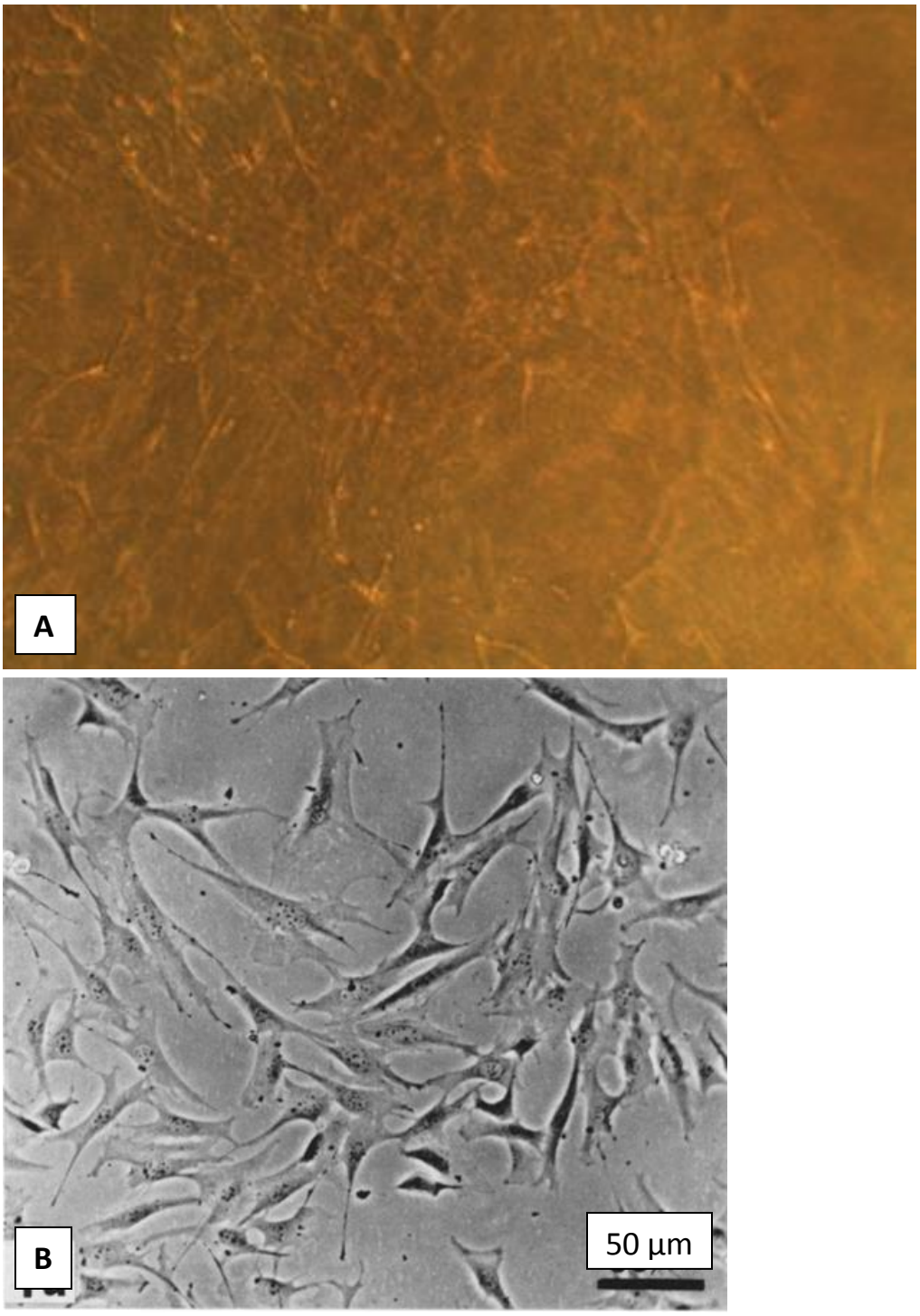


**Figure 39. Light microscopy image of MC3T3 cells encapsulated in a 0.1% collagen hydrogel (3-dimensional matrix) and cultured for 7 days (A) [mag]. Phase-contrast microscopic appearance of MC3T3-E1 cells in day-2 cultures (2-dimensional substrate, TCP), mag = 250X (B). Morphological differences can be seen between both growth environments.**

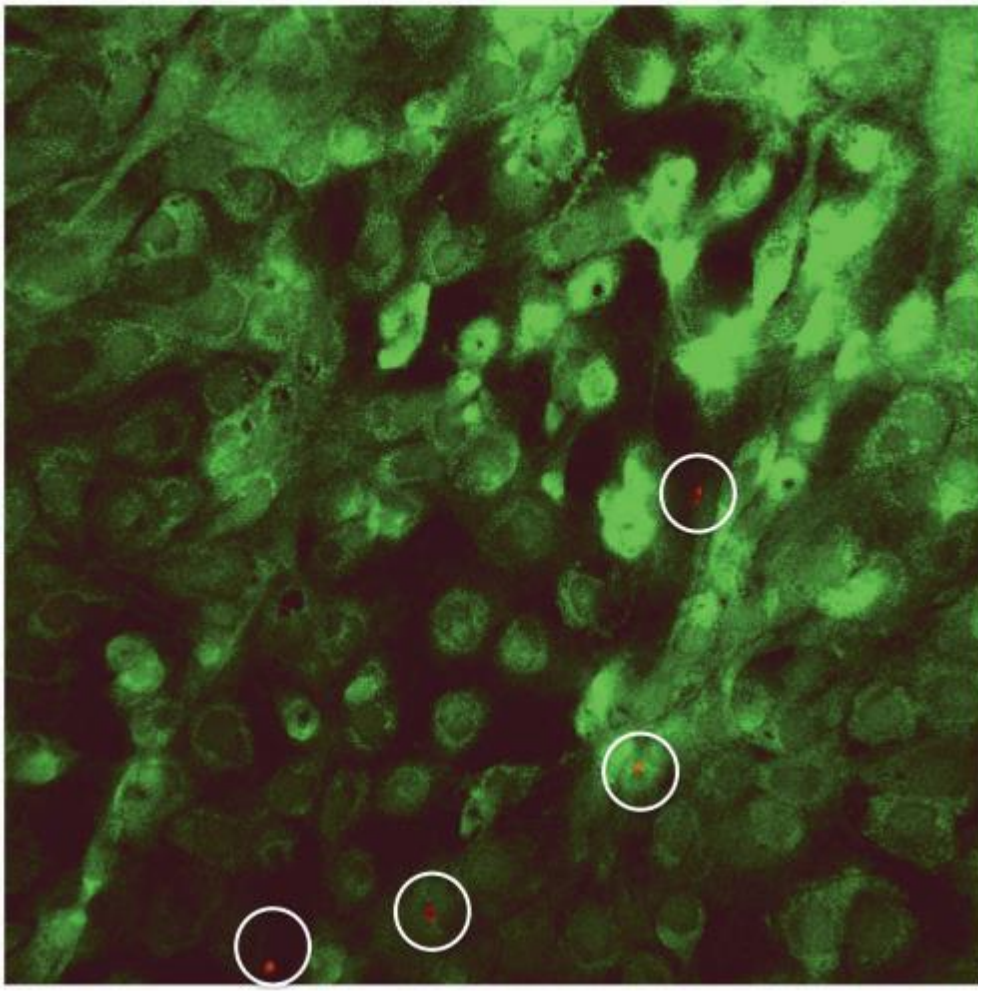

**Figure 40. Confocal microscopy image of a LIVE/Dead assay indicating abundant MC3T3 viability of encapsulated cells in a 0.1% collagen hydrogel within 24 hours of culture. Viable cells appear green while dead cells appear red (circled in white) (mag = 10X).**

Figure 42 shows a confocal microscopy image of MC3T3 cells treated with the live/dead assay. Live cells are shown in green after 24 hours of culture in a 0.1% collagen hydrogel, while the dead cells are shown in red. It is clear from the image that there was abundant cell viability when cells were cultured for 24 hours given that the image shows mostly green (live) cells and a very limited number of red (dead) cells which are circled in white for

ease of visibility. Cells were able to proliferate, migrate, and remain viable within their growth environment of collage type I hydrogel.

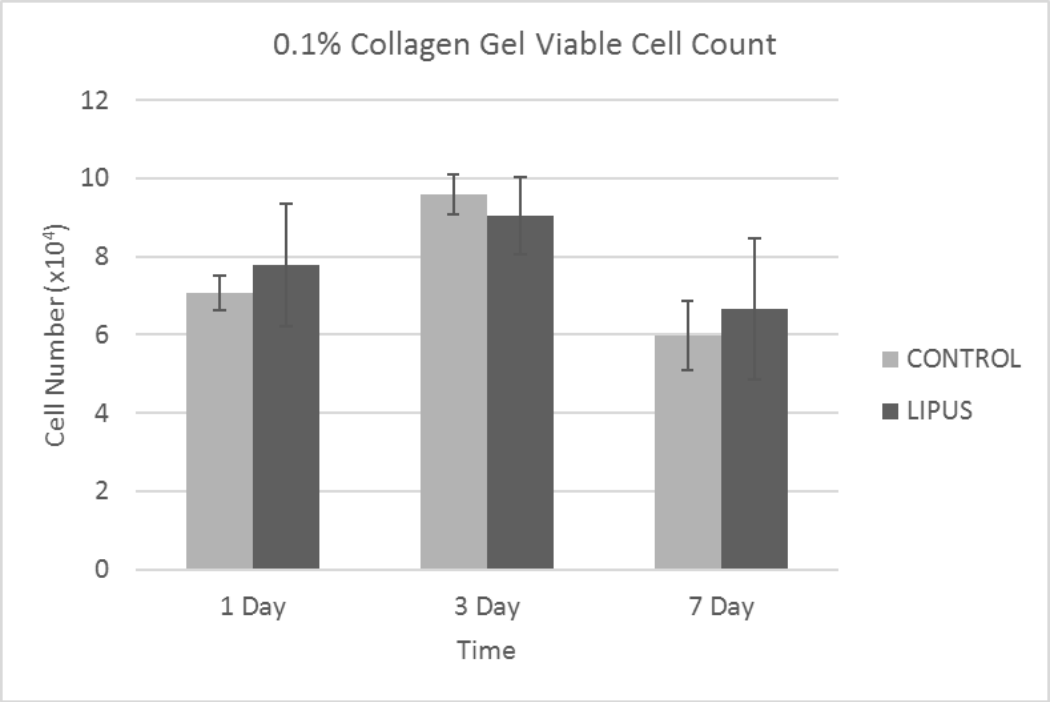


**Figure 41. Proliferation study of MC3T3 cells encapsulated within a 0.1% collagen hydrogel with (experimental) and without (control) ultrasound treatment**

The MACs system with flow cytometry demonstrated no statistically significant difference in viable cell count in terms of LIPUS treated versus untreated cells in 0.1% collagen hydrogels (figure 43) as well as LIPUS treated versus untreated cells on TCP (figure 44). Viable cell count increased in both LIPUS treated and untreated groups over three days; however, at the 7 day time point viable cell count dropped off by about 30%. From numerous

studies and trials, the collagen hydrogels seemed to have an upper limit on workability at around one week where the hydrogels would begin to detach from the cell culture dish, or degrade, or shrink. This resulted in difficulty in consistency of experimental parameters for desired studies beyond a one week timeframe. Therefore, for feasibility reasons, we did not extend our collagen hydrogel studies beyond 7 days.

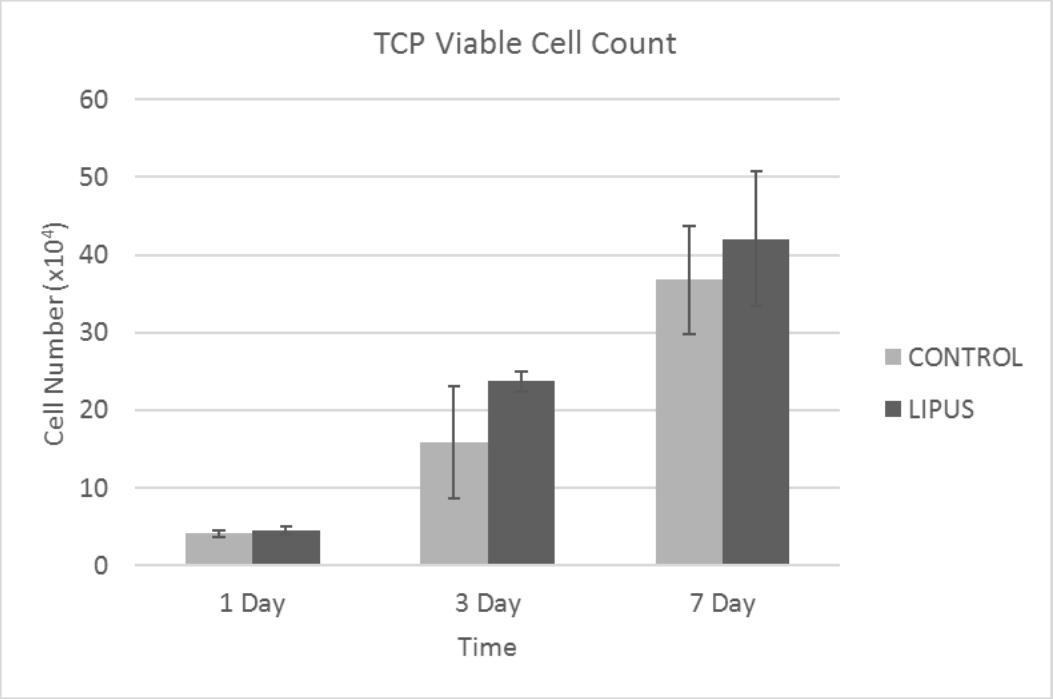


**Figure 42. Proliferation study of MC3T3 cells cultured on TCP with (experimental) and without (control) ultrasound treatment.**

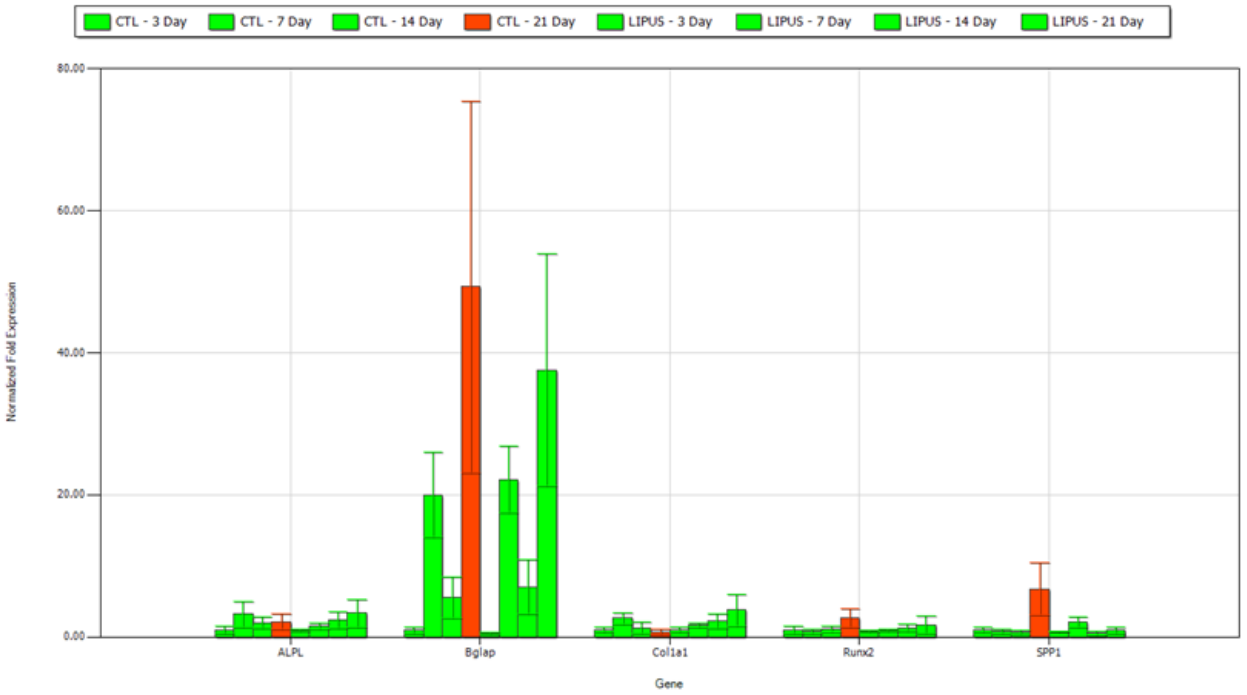


**Figure 43. Gene expression of MC3T3-E1 cells cultured on TCP of five different osteogenic markers with (experimental) and without (control) ultrasound treatment over 3, 7, 14, and 21 days.**

A 3, 7, 14, and 21 day study of LIPUS treated and untreated MC3T3 cells on TCP showed a positive correlation between LIPUS treatment and alkaline phosphatase (ALP) and collagen 1a1 (COL1a1) expression (figure 43). ALP and COL1A1 expressions both peaked in the untreated groups at day 7 and subsequently decreased over 14 and 21 days. The groups treated with LIPUS gradually and sustainably increased from the first measured expression level at day 3 all the way until day 21.

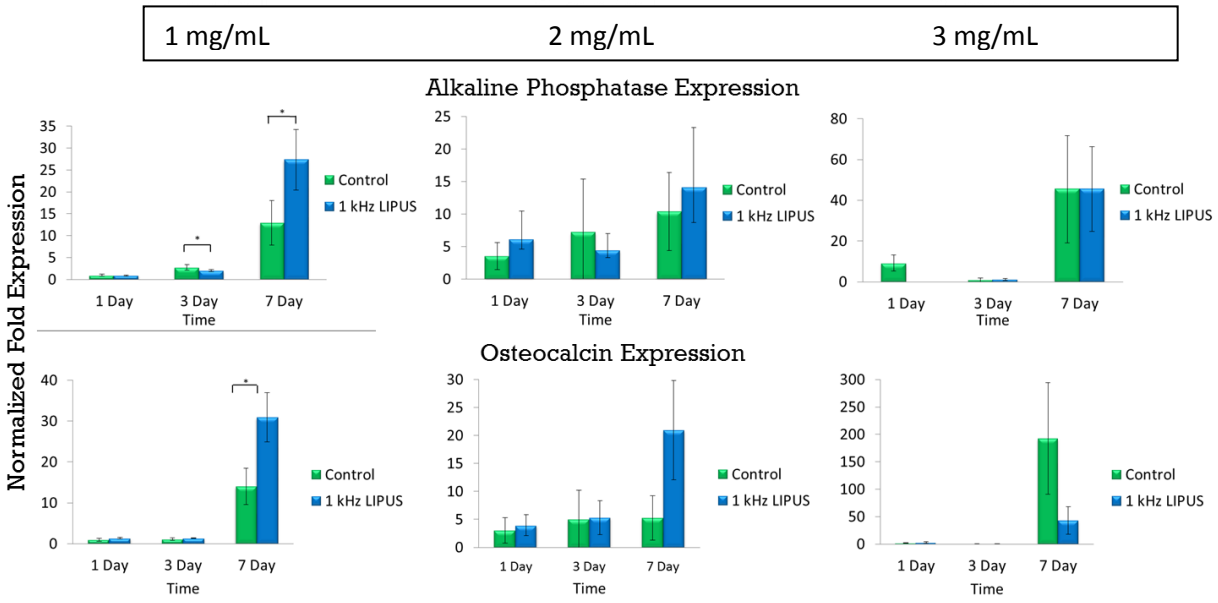


**Figure 44. Proliferation study of MC3T3 cells encapsulated within at 0.1% collagen hydrogel with and without ultrasound treatment**

In a 1, 3, and 7 day study in 0.1, 0.2 and 0.3% collagen hydrogels with 20 minute daily treatments of LIPUS, the 0.1% collagen hydrogels treated with LIPUS demonstrated a statisticaly significant ($P < 0.05$) upregulation in alkaline phosphatase (ALP) and osteocalcin (OCN) expression, two markers of osteogenic differentiation, at the 7 day time point (figure 46). As collagen concentration increased, as in the 0.2% collagen hydrogel study, the expression of ALP and OCN was not statistically greater in the LIPUS treated group in comparison to the untreated group during any of the 1, 3, and 7 day time points. The 0.3% collagen hydrogel study showed the most irregularity and variability in data with no groups expressing statistically different expression levels; however, at the 7 day time point, expression levels of ALP was similar between LIPUS treated and untreated groups, and OCN expression

level was decreased for the LIPUS treated group in comparison to the untreated group, possibly suggeseting a reversal of the trend seen in the 0.1% hydrogels.

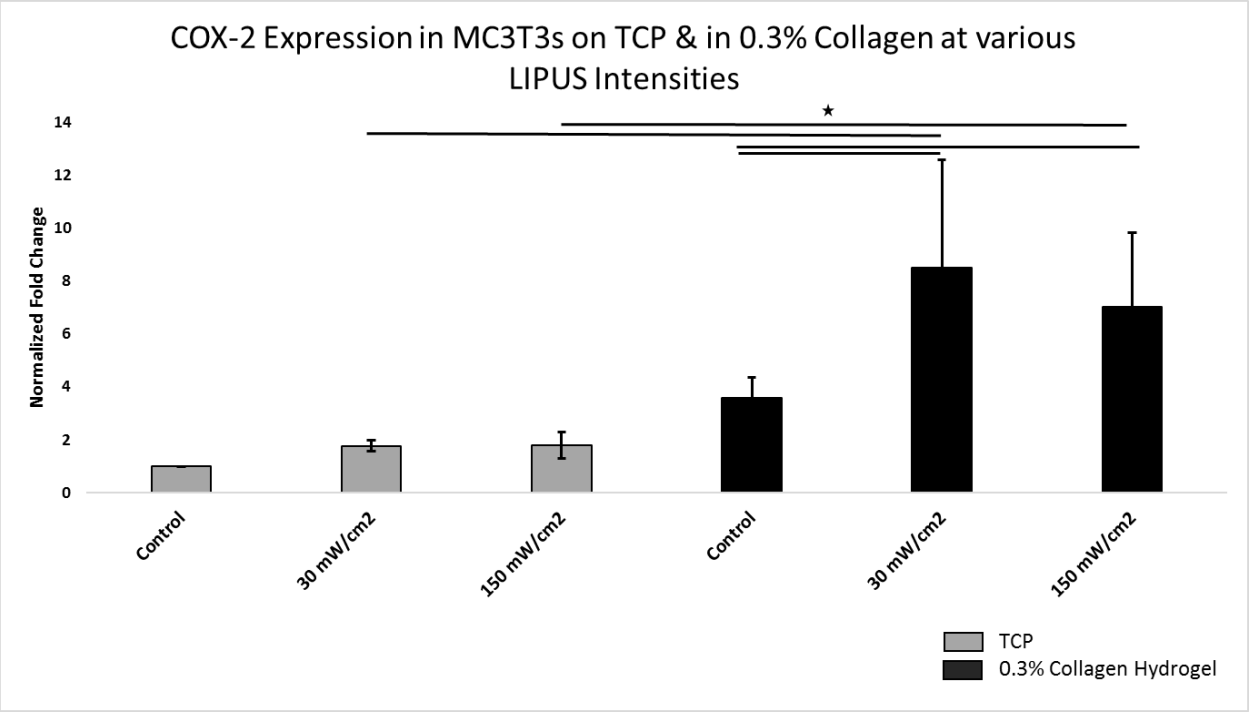


**Figure 45. COX-2 expression levels after 30 minutes of MC3T3-E1 cells cultured on TCP and encapsulated in 0.3% collagen hydrogels both treated (experimental) and untreated (control) with LIPUS.**

COX-2, an indicator of mechanical stress, showed upregulation in MC3T3-E1s in groups treated with LIPUS in 0.3% collagen hydrogels in comparison to the same groups left untreated on TCP (figure 45). Additionally, within the collagen hydrogels, both LIPUS groups (30 and 150 mW/cm$^2$) showed a statistically significant ($P < 0.5$) upregulation in comparison to the control hydrogel. Even the control hydrogel seemed to have an increase in expression simply due to cellular culture in the hydrogel in comparison to the TCP control; however, the increase was not statistically significant with a sample size of n=3.

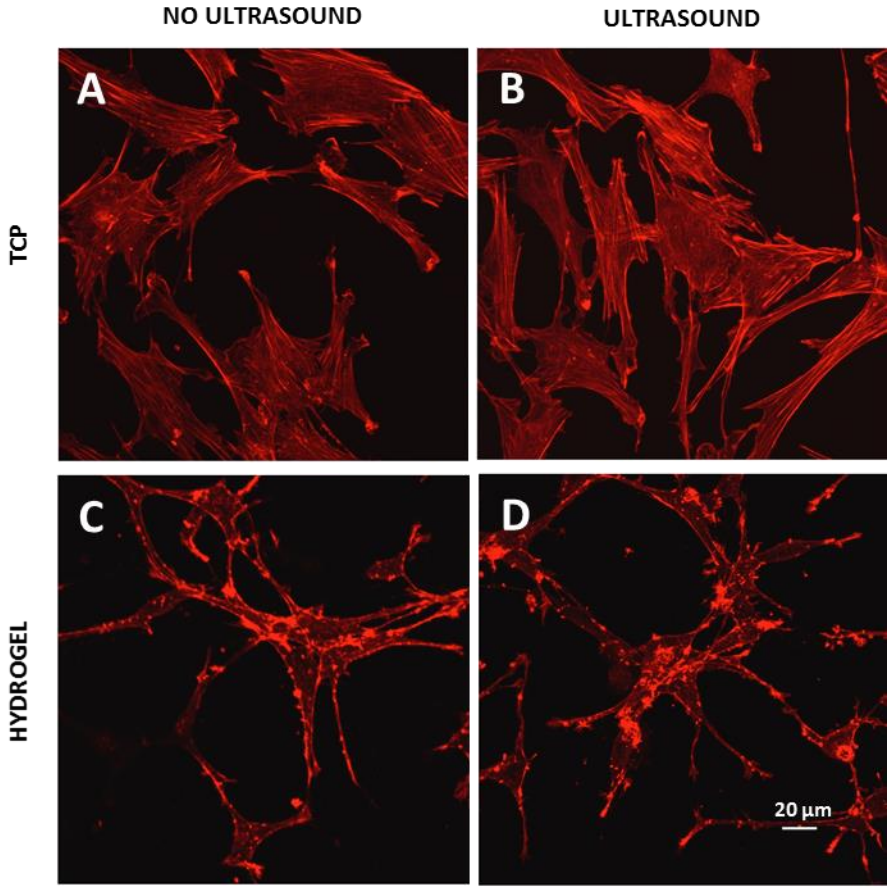


**Figure 46. Confocal image of f-actin immunostained MC3T3-E1 cells cultured on TCP and in a 0.3% collagen hydrogel with and without ultrasound treatment.**

Confocal images of MC3T3 cells immunostained with f-actin show filaments are highly polymerized and organized with the cells seeded on TCP both without (A) and with (B) acoustic radiation force (figure 48). With the cells cultured in the 0.3% collagen hydrogels, actin is disorganized and lacks actin fiber alignment both without (C) and with (D) acoustic radiation force.

## 4.4. Discussion

Results showed positive feasibility of growing or encapsulating pre-osteoblasts (MC3T3-E1 cells) in collagen hydrogels. Further, the osteogenic marker expression showed statistically significant differences between MC3T3 cells treated with acoustic radiation force compared to cells that did not receive treatment in various markers depending on the substrate (TCP or collagen hydrogel) that they were grown on. Acoustic radiation force appears to be a driving factor in the response of MC3T3s not only with osteogenic markers alkaline phosphatase and osteocalcin, but also the mechanosensory marker COX-2. While researchers remain unclear on the exact bioeffects of LIPUS in terms of fracture healing, our hypothesis linking acoustic radiation force to mechanotransduction as a driving force seems feasible considering the upregulation of COX-2 expression from LIPUS treatment.

Fluid shear stress has been shown to promote COX-2 and prostaglandin E2 (PGE-2) release in MC3T3-E1 cells by the formation of focal adhesions on fibronectin.[310] PGE-2 is downstream of COX-2 and is a potent activator of the Wnt signaling pathway. Both PGE-2 and COX-2 are considered principle mediators of inflammation in diseases such as rheumatoid arthritis and osteoarthritis. Nonsteroidal anti-inflammatory medications (NSAIDs) and selective cyclooxygenase-2 (COX-2) inhibitors such as Celebrex™ (celecoxib) are commonly clinically prescribed in orthopedics to reduce PGE-2 production to diminish the inflammation seen in these diseases, but present risks from continued use that may include both gastrointestinal bleeding and prothrombotic tendencies.[311] Additionally, PGE-2 has been implicated in regulating the developmental specification and regeneration of hematopoietic stem cells through cAMP/PKA activity.[312] While over expression of inflammatory signals can

be clinically bothersome, appropriate expression is certain instances can also be beneficial such as in mechanotransduction in bone. Considering the current knowledge of the mechanosensory expression of COX-2 and our demonstration of acoustic radiation force in addition to the acoustic streaming phenomenon demonstrated during our dye experiment in a fish tank, we suggest that the *in vitro* upregulation of COX-2 in response to ultrasound treatment comes from either the stimulus of acoustic radiation force, acoustic streaming, or perhaps a combination of both.

As acoustic radiation force did not show any negative signs of treatment in terms of proliferation and cell viability on TCP and in collagen hydrogels, we were successfully able to proceed with further studies investigating the effects of mechanical stimulus *in vitro*. Actin is the most abundant protein in most eukaryotic cells. Actin filaments (F-actin) are linear polymers of globular actin (G-actin) subunits and exist as microfilaments in the cytoskeleton. Both F-actin and G-actin are essential for important cellular functions such as the mobility and contraction of cells during cell division.[313] Effects of substrate stiffness on cell morphology, cytoskeletal structure, and adhesion have been well documented in literature.[314] F-actin polymerization is affected by mechanical stimuli and has been studied in mechanobiology pathways[315] and is of interest to its translation in bone mechanotransduction. MC3T3-E1 cells immunostained for f-actin showed that softer substrates such as the collagen hydrogel, did not possess highly organized or polymerized F-actin independent of whether receiving LIPUS treatment. Additionally, the MC3T3-E1 cells grown on TCP, a hard surface, showed a high level of F-actin polymerization both with and without LIPUS treatment. As F-actin plays a significant role in cell attachment and mobility, it is likely that the softer substrate collagen hydrogels opposed to the rigid substrate TCP did not provide a sufficient amount of mechanical

stability, leading to less F-actin production and polymerization which has been a similar them with other matrices of lower mechanical stability.[316,317] While lower F-actin polymerization may indicate decreased cellular attachment and migration in the collagen hydrogels studied, the *in vitro* collagen hydrogel model may not necessarily translate to *in vivo* results. TCP has been widely used for *in vitro* cell studies as it has been optimized for cellular attachment. As such, drawing early conclusions by comparing the results on the two substrates may be lead premature and incorrect assumptions. Additionally, in this *in vitro* collagen hydrogel system, the MC3T3-E1 pre-osteoblast cells were analyzed in an environment early in their maturation process, where native bone tissue, as a naturally occurring composite material, proximally exhibits the rigidity of the calcium phosphate matrix. With this in mind, *in vivo* response of F-actin polymerization under the mechanical stimulus of acoustic radiation force through LIPUS may be significantly different in comparison to results seen *in vitro*, particularly with other local environmental nutrient exchange and biochemical signaling.

The fabrication of collagen hydrogels and the length of time for an appropriate level of workability depends on the collagen concentration, but in general most collagen hydrogels start degrading at around one week. Future studies as well as possible use in a clinical setting will require a more consistent methodology and confidence in a more prolonged collagen hydrogel matrix sustainability to ensure encapsulated cells stay localized within the hydrogel which is desired for successful defect repair. Furthermore, we have successfully developed a methodology to encapsulate MC3T3-E1 pre-osteoblasts in collagen hydrogels of a desired mechanical stiffness, or storage modulus, based on the collagen concentration used during scaffold fabrication. Importantly, the developed cell encapsulation protocol will likely support other cells and be a feasible solution to inject patient-specific cells such as mesenchymal stem

cells into the defect site where they will likely remain localized and be held in place long enough to establish their own extracellular matrix. A common hurdle to overcome with cell and drug-based therapies for tissue engineering applications is the successful delivery of the cells or drug(s) in the immediate location of the defect, prevention of the cells or drug(s) leaving the vicinity, and their sustainability. Since the collagen hydrogel gelates once it is neutralized with a base and heated to 37°C, it is a possibly feasible delivery solution to localize and maintain the cells in the defect. Some investigation of length of time for degradation to occur *in vivo* would be useful considering the time in a culture dish with little disturbance or fluid exchange still degrades the hydrogel after about only a week. It is likely that degradation would occur much quicker in vivo which could be a potential pitfall. Ultimately what is important is if the collagen hydrogel has enough time to deliver the cells to the defect because the primary use of the hydrogels are delivery vehicles for cells and potentially growth factors as well. Early termination of the hydrogels functionality to deliver cells and not be harmful to local cells and tissue may need further investigation. Additionally, in terms of LIPUS treatment, clinical use could go on for 4-8 weeks until the defect is fully healed hence is the second reason why the hydrogels need to hold their integrity – so that they can serve as a deformable and loadable matrix.

Importantly, with acoustic radiation force, we can remotely and non-invasively load the cells to further enhance and accelerate bone healing beyond the use of LIPUS alone and to potentially avoid the need for invasive surgical intervention where complications and problems may occur. Additionally, with high medical costs and the patient's decision to undergo surgery where there will be significant post-operative pain as well as a lengthy healing time, a more feasible and effective option is to load the patient's own mesenchymal stem cells using acoustic

radiation force by injecting the solution of the patient's cells and collagen hydrogel into the defect site to form the cell-encapsulated collagen hydrogel scaffold. With the cells held in place and feeling the physical load of daily applied acoustic radiation force treatments, the cells will likely differentiate down the bone lineage and provide new and remodeled bone formation. Before clinical implementation of this treatment can be pursued, other in vivo studies may provide insight into how loaded cells respond to acoustic radiation force which leads us to the final specific aim and study with a mouse calvarial defect model.

# 5. SPECIFIC AIM III: ANALYSIS OF ULTRASOUND TREATMENT IN VIVO: MOUSE CALVARIAL DEFECT WITH COLLAGEN HYDROGELS

## 5.1. Introduction

Non-invasive, transcutaneous LIPUS therapy has shown clinical efficacy in bone healing for over two decades. Studies have shown that LIPUS therapy is capable of reducing fracture healing time by 38% in addition to healing non-union defects at an 85% success rate.[269] As mentioned earlier, commercially available clinical units for orthopedics do not deviate from a particular set of parameters likely in part due to the fact that the underlying biological mechanism responsible for the wearable device's efficacy still remains largely unknown which is a major theme of this thesis. If a particular clinical treatment has proven efficacy and its mechanism of action remains unknown, then altering certain parameters will result in too many variables being changed and the chance of optimization will diminish. Additionally, a consistent method for measuring clinical efficacy is required in order to compare studies with various parameter differences in order for LIPUS optimization or discovery of mechanism(s) of action. Unfortunately, in the hundreds of LIPUS studies published, the measurement of clinical efficacy ranges from radiographical healing to various directly assessed functional end points such as time to return to regular daily activities or full weight bearing.[318]

While certain parameters may be limited to any degree of adjustment in the clinical setting due to regulatory and intellectual property factors such as the selection of a 30 mw/cm$^2$ spatial intensity by the FDA's approval in 1994 for the use of LIPUS in the treatment of fresh fractures and subsequent approval in 2000 for treatment of non-union defects, a parameter is not limited to change for *in vitro* investigations as well as in pre-clinical *in vivo* studies. Much

of the work of this thesis involved the analysis of LIPUS therapy to cells or their scaffolds or both by the use of a highly tunable ultrasound system developed and characterized in specific aim I. The final objective of this work is two-fold which will soon become apparent as indicated in the final specific aim of this thesis: first, the optimization of LIPUS therapy for bone regeneration, and second, the evaluation of LIPUS therapy by the physical force manifested by acoustic radiation force by hypothesizing that a physical force loading cells and their extracellular matrix is directly linked to the mechanism of action resulting in clinical efficacy. In terms of optimizing the use of LIPUS therapy, a hydrogel system such as the collagen hydrogel scaffold characterized earlier can serve as a carrier and deliver patient-specific cells to a particular defect and subsequently hold the cells in place so that LIPUS treatment can result in acoustic radiation force physically loading and deforming the cell-hydrogel constructs. As discussed earlier, bone responds positively to physical force via Wolff's law; however, during a typical fracture recovery, the physician immobilizes the fracture to avoid further damage or complications to the defect and surrounding tissues. In terms of bone regeneration, this concept sounds somewhat counter-intuitive. Therefore, if an immobilized defect site could somehow be physically loaded in a minimal way to not cause further damage or increased pain, the defect site may in theory respond positively to some physical forces.

A perfect way to achieve this concept is to use the previously characterized cell-encapsulated hydrogels to deliver patient-specific cells to the defect site through a syringe. Gelation of the collagen hydrogel would occur at body temperature which would localize and maintain the cells at the defect hopefully long enough for a series of daily LIPUS treatments to physically load and deform the cells and hydrogels to accelerate fracture healing. With the

method described, we could satisfy our goals to optimize or improve LIPUS therapy efficacy compared to the current clinical therapy in addition to using acoustic radiation force as a modality to physically load cell-hydrogel constructs. If a significant improvement occurs compared to control groups, with the data taken into consideration in the previous specific aims, combined results may ultimately provide evidence that the underlying mechanism of LIPUS efficacy in bone regeneration is indeed related to acoustic radiation force.

For our *in vivo* investigation, we hypothesized that results would reveal accelerated healing in defects filled with donor cell-loaded hydrogels of optimal viscosity to best transfer remotely applied acoustic radiation force to encapsulated cells. This would provide important proof-of-concept data to expand the exploration of loading bony defects with malleable constructs capable of being transcutaneously deflected to impart mechanical loading on both resident and neighboring cells. An animal model was developed and verified for its utility for such an application, hydrogel incorporation for bone repair. As previously discussed, we tested whether or not a physical force can be transmitted and measured on the other side of skin tissue it is coupled with in case the signal was not strong enough and would attenuate through a particular tissue. By evaluating the transmission of mechanical forces through a rat skin flap, we detected only minor attenuation of the impulse and therefore are confident that mechanical deflection of the implanted hydrogel would take place form the applied acoustic radiation force. As this study was the first *in vivo* ultrasound experiment in our lab, it was performed as a pilot study with a limited number of groups, but was performed to help lay the groundwork for future investigations.

## 5.2. Materials and Methods

A mouse calvarial defect model was chosen for performing an *in vivo* study to ultimately help tie concepts together as mentioned above by investigating *in vivo* bone healing response. Our *in vivo* analysis showed the efficacy of the combined treatment of LIPUS with an injectable BMSC-encapsulated type I collagen hydrogel over a healing time of 2 or 4 weeks in a mouse calvarial defect model. All procedures were done in accordance with approved

**Figure 47. Picture of the mouse calvarial defect hydrogel implantation wound closing (left) and post-surgery (right).**

Institutional Animal Care and Use Committee guidelines. The groups consisted of the hydrogels with encapsulated donor cells without LIPUS treatment (control) and hydrogels with cells and with LIPUS treatment (experimental). Briefly, samples were evaluated using x-ray

imaging, and histological analysis was performed on samples to evaluate the extent of donor cell survival, new bone formation, mineralization, and remodeling.

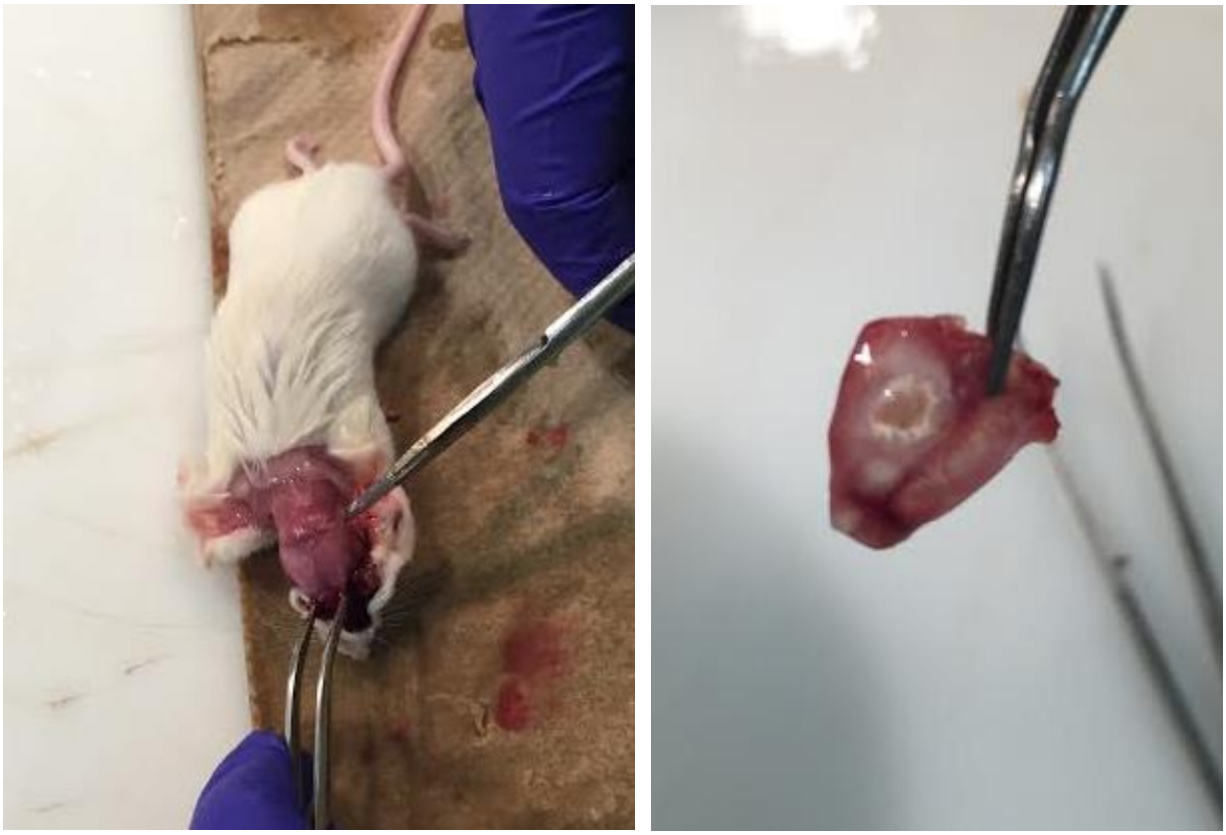

**Figure 48. Pictures of cranial tissue excision post-sacrifice (left) and excised cranial tissue sample for processing (right).**

BMSCs in recipient tissues were isolated from reporter mice. The skin at the surgical site was cleanly shaved and disinfected and a sagittal skin incision was made from the occipital to the frontal bone. The skin flap was then bluntly dissected and elevated. To minimize the regeneration potential from host osteoprogenitor cells residing in the periosteum we carefully dissected and removed the periosteum covering the entire defect. One 5 mm diameter full thickness defect was created on the left parietal bone with a 5-mm trephine bur under saline irrigation while preserving the underlying dura mater (figure 47). The space was filled with cell-loaded hydrogels (500,000 cells per gel) of the viscosity determined most effective in

Specific Aim 1, 3 mg/mL, and the skin flap sutured closed. Hydrogels without cells served as controls. Hydrogels were made according to protocol as previously discussed, except for the gelation process, where 200 μL of hydrogel was formed within a 1 mL syringe at 37°C for gelation into a suitable diameter (5 mm) and height for the defect site.

**Figure 49. *In vivo* setup showing LIPUS application while mouse is under anesthesia with the nose cone and stereotaxic device.**

Defects receiving acoustic radiation force had ultrasound gel coupled between the transducer and skin over the defect site were loaded for 20 minutes per day five of every seven days (five days on, two days off) throughout healing for 2 or 4 weeks. LIPUS was administered using 150 mW/cm$^2$ spatial intensity and the transducer was calibrated according to the protocol for ultrasound characterization as discussed in Specific Aim I. The mice were positioned on a

stereotaxic device (Stoelting) for LIPUS treatment over the defect site while under anesthesia (figure 48). The ultrasound transducer was positioned and held by a clamp with an adjustable base. Groups were given an IP injection of alizarin red complexone one day prior to sacrifice to identify actively mineralizing surfaces. After sacrifice, calvarial tissue was excised and processed (figure 49). Histology analysis was performed according to protocols for DIC, alkaline phosphatase, DAPI, GFP, alizarin red complexone, and TRAP staining. Representative samples were evaluated for the presence of encapsulated BMSC cells (GFP+ cells) to study the extent of donor cell survival and inflammatory cells. Defect loading with acoustic radiation force was compared to no loading, while presence of cells was compared to no cells. The osteogenic efficacy of loading and cell encapsulation was assessed based on the increase in mineralized bone volume. Microscopic evaluation of interface tissue morphometry provided high-resolution quantization of peripheral integration, discriminating whether or not the repair tissue has incorporated via a relatively seamless continuation of morphometry across the interface versus a remaining boundary requiring further remodeling.

## 5.3. Results

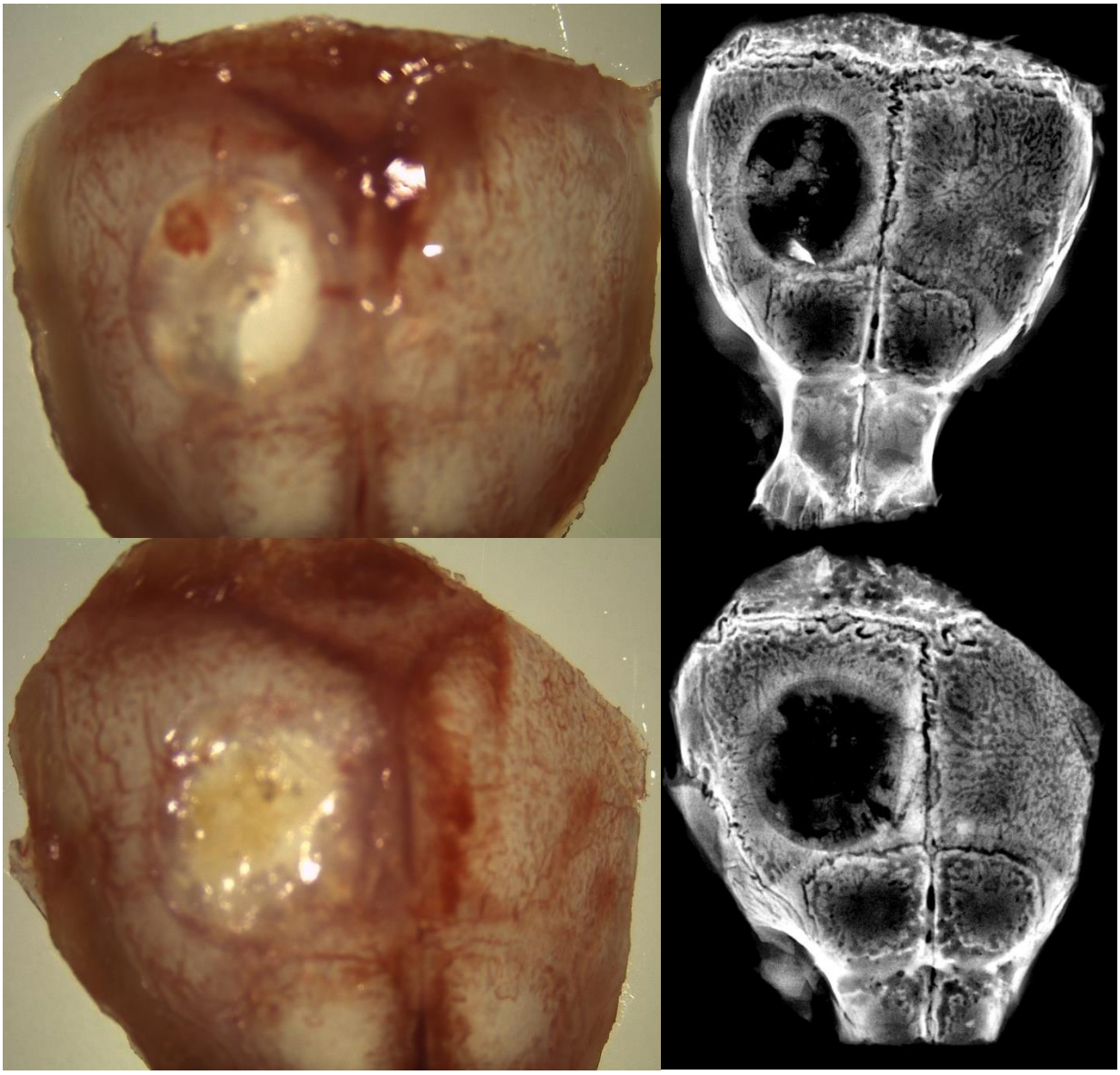

**Figure 50. Calvarial defect samples 2 weeks post-surgery. Pictures of samples were taken (left) and samples were imaged via x-rays (right). Sample on the top did not receive LIPUS treatment while the sample on the bottom received LIPUS treatment.**

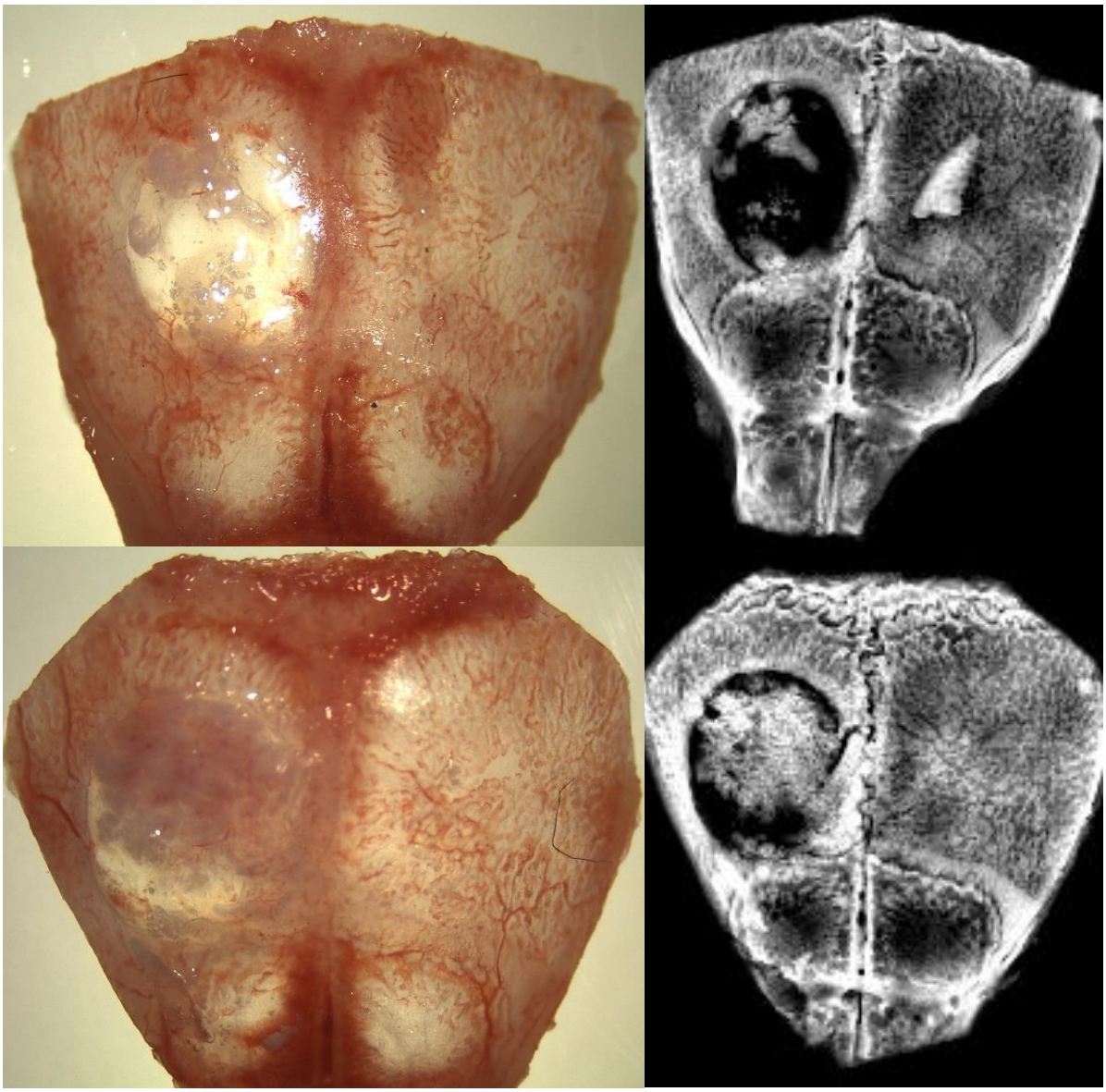

**Figure 51. Calvarial defect samples 4 weeks post-surgery. Pictures of samples were taken (left) and samples were imaged via x-rays (right). Sample on the top did not receive LIPUS treatment while the sample on the bottom received LIPUS treatment.**

LIPUS

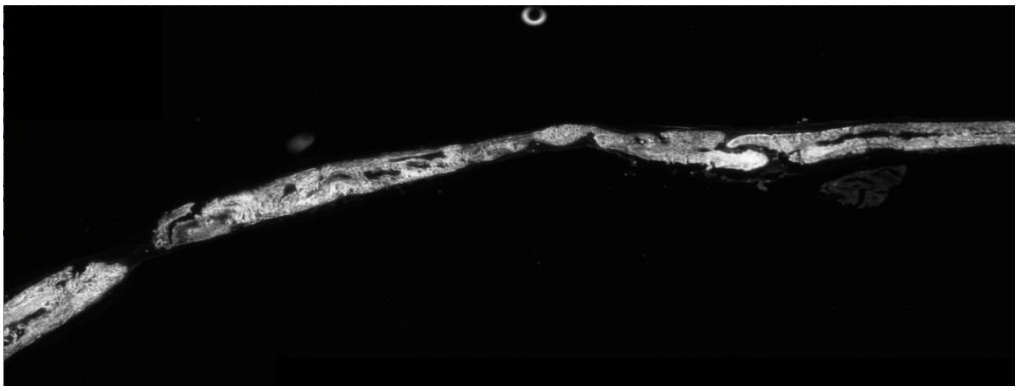

DIC

NO LIPUS

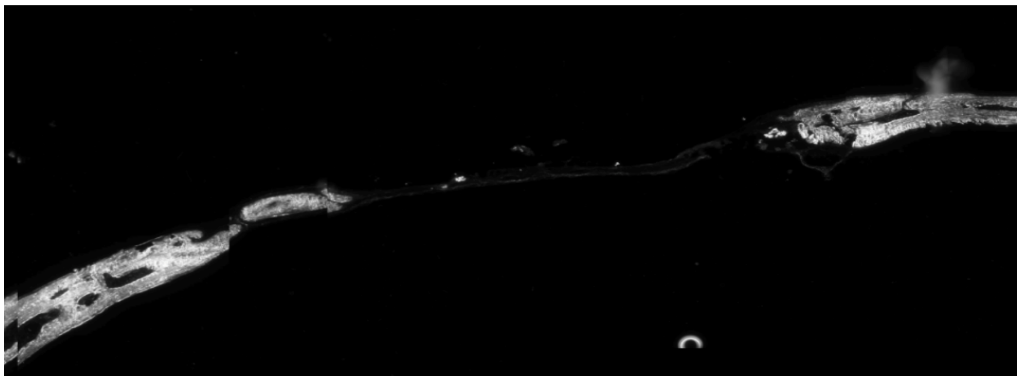

**Figure 52. DIC histology imaging of bone healing after 4 weeks showing effects of LIPUS treatment (top) and without LIPUS treatment (bottom).**

LIPUS

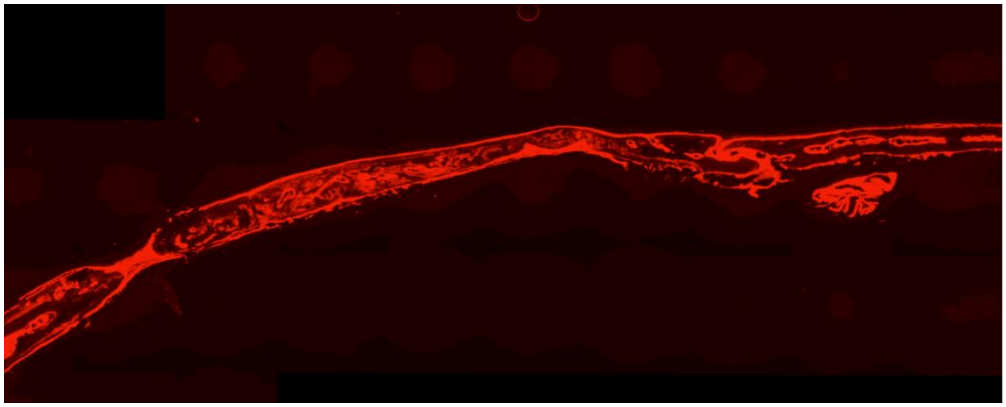

ALKALINE PHOSPHATASE

NO LIPUS

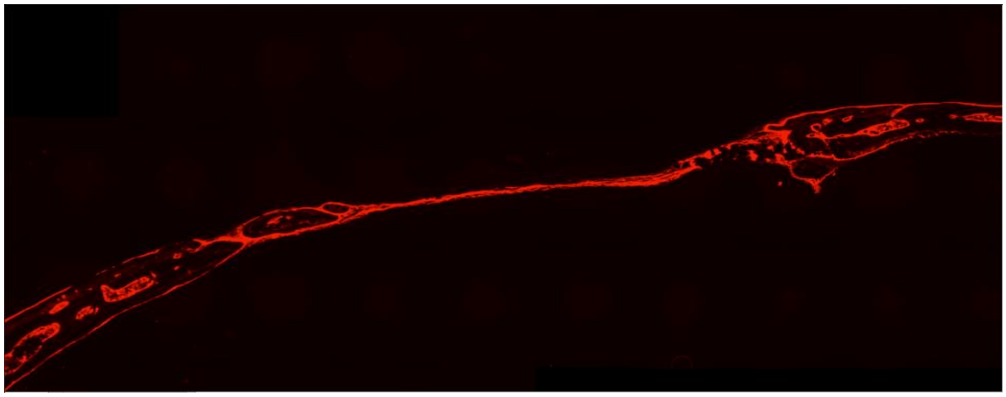

**Figure 53. Alkaline phosphatase histology imaging of bone healing after 4 weeks showing effects of LIPUS treatment (top) and without LIPUS treatment (bottom).**

LIPUS

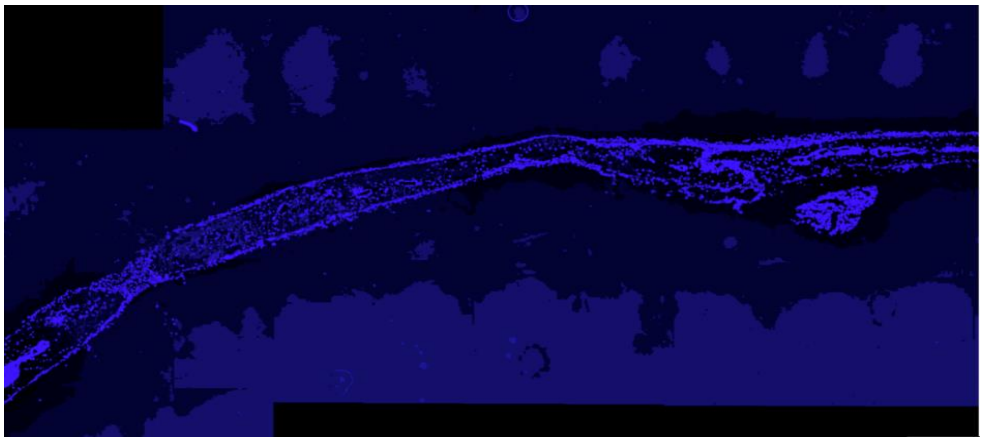

DAPI

NO LIPUS

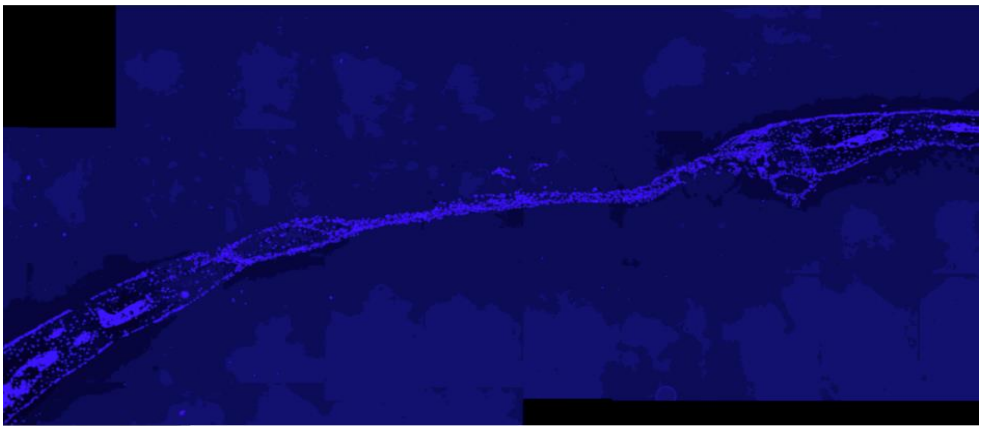

**Figure 54. DAPI histology imaging of bone healing after 4 weeks showing effects of LIPUS treatment (top) and without LIPUS treatment (bottom).**

LIPUS

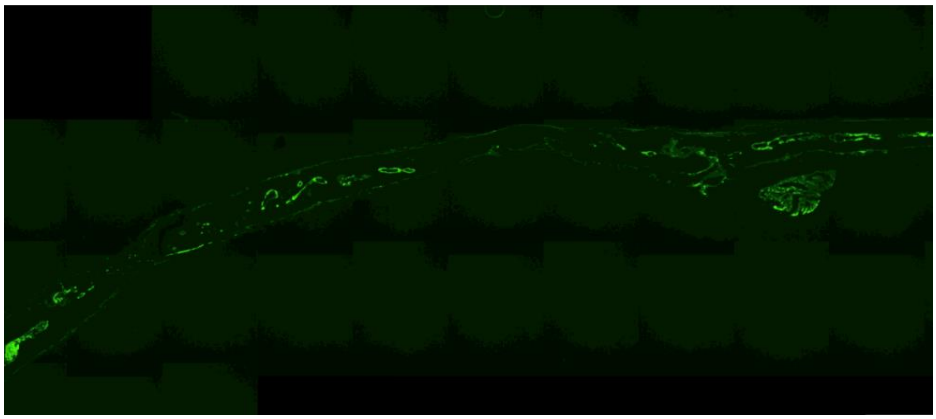

GFP (DONOR CELLS)

NO LIPUS

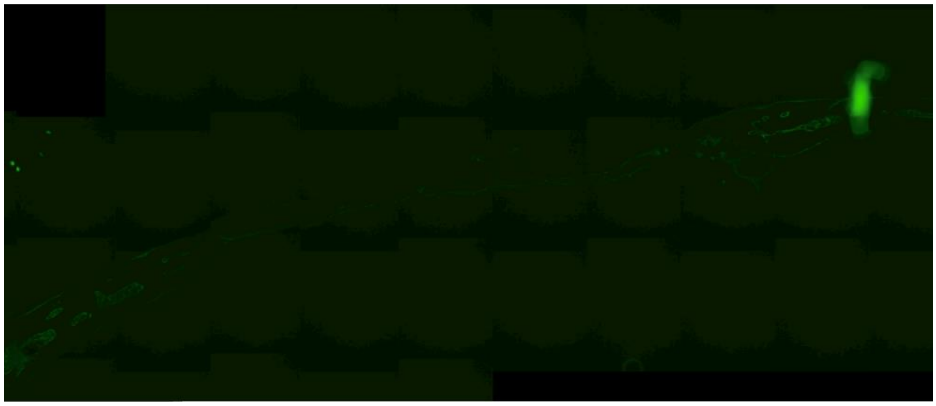

**Figure 55. GFP histology imaging of bone healing after 4 weeks showing effects of LIPUS treatment (top) and without LIPUS treatment (bottom).**

LIPUS

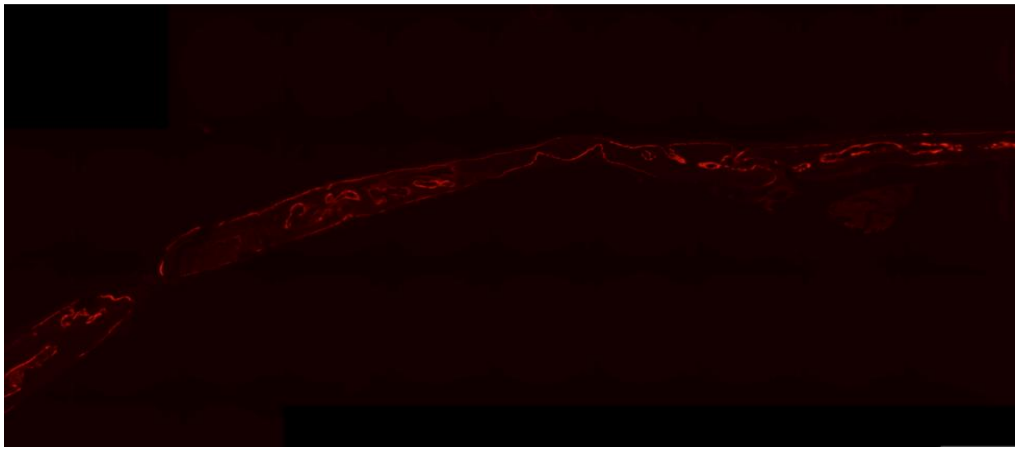

ALIZARIN COMPLEXONE (NEW BONE)

NO LIPUS

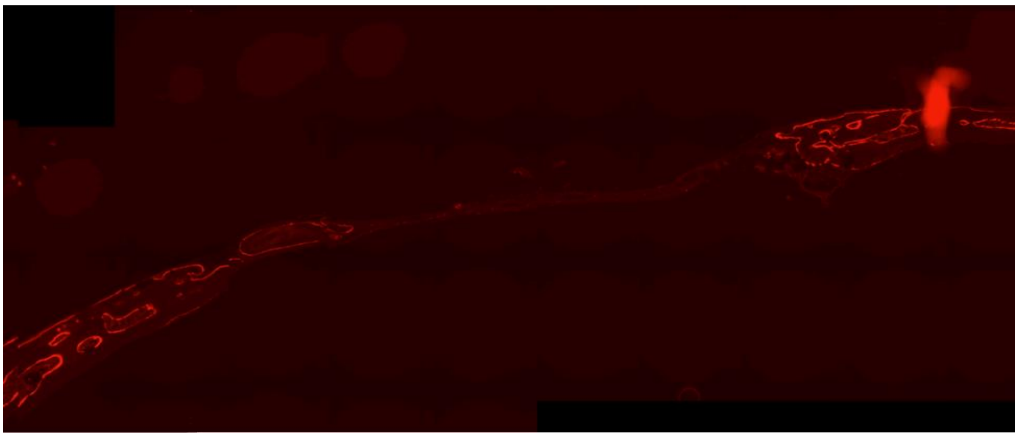

**Figure 56. Alizarin complexone histology imaging of bone healing after 4 weeks showing effects of LIPUS treatment (top) and without LIPUS treatment (bottom).**

LIPUS

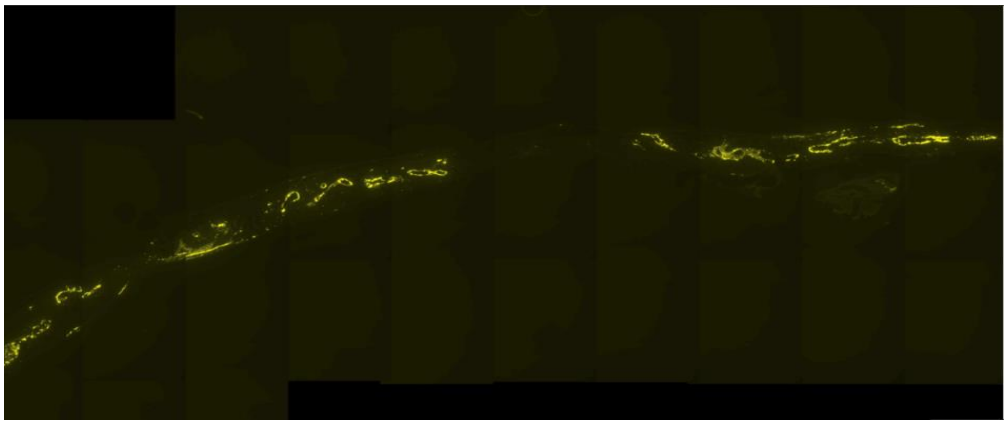

TRAP (OSTEOCLAST ACTIVITY)

NO LIPUS

**Figure 57. TRAP histology imaging of bone healing after 4 weeks showing effects of LIPUS treatment (top) and without LIPUS treatment (bottom).**

New bone formation was most evident in 4 week time points with LIPUS treated groups expressing greater evidence of bone healing compared to groups that did not received LIPUS treatment. As expected, less bone healing was seen at the 2 week time points; however, some LIPUS groups did indicate enhanced healing with LIPUS compared to the group left untreated. Two week samples are shown with photographic imaging and x-ray imaging (figure 50). The x-ray imaging indicated enhanced mineralization in the center and some of the edges of the

defect where LIPUS treatment was applied, while the group without treatment showed minimal and more randomized mineralization and less mineralization at the edges of the defect.

New bone formation was more evident in the four week time points (figures 51-57). Mineralization as shown by x-ray imaging was enhanced in the defect receiving LIPUS in comparison to the defect left untreated (figure 51). The defect receiving treatment showed well-disbursed mineralization throughout the defect site including at the edges of the defect; however, it was evident that mineralization and total healing was not complete at this time. Additionally, the photographic image of the calvarial defect tissue receiving LIPUS treatment showed enhanced tissue growth compared to the defect that did not receive treatment. Furthermore, x-ray imaging of the defect at 4 weeks without LIPUS treatment showed significantly less mineralization throughout the defect, particularly at the edges of the defect.

For comprehensiveness, further analysis for 4 week bone healing evidence was provided by histological analysis of the calvarial defect and host bone healing and integration by analyzing calvarial tissue cross-sections. DIC imaging showed enhanced healing clearly with high contrast in the LIPUS treated group in comparison to the group without treatment (figure 52). The tissue evidenced nearly complete continuity with a strong signal across the defect site and into the adjacent host bone while the defect site without LIPUS treatment evidence clear discontinuity and a large gap in bone tissue nearly spanning the entire site of the defect indicating minimal tissue regeneration occurred. Alkaline phosphatase staining, an indicator of bone mineralization, provided significant evidence of substantial bone healing in the 4 week defect site receiving LIPUS treatment shown by high signal expression indicating higher contents of mineralization and continuity across most of the defect site with appropriate integration into the local host bone tissue (figure 53). Signal for alkaline phosphatase was

evidenced on the exterior and interior of the defect bone formation, indicating high mineral deposition in the formation of cortical bone. The defect site that did not receive LIPUS treatment expressed significantly less alkaline phosphatase expression through lack of continuity across the defect site and lack of integration into the host bone.

DAPI histological expression, a stain for nuclei, was of significance as the imaging helped assess the level of active cells in the process of bone healing in comparison to alkaline phosphatase activity that expresses an extracellular deposit, which may remain in the local tissues independent of current cell viability. DAPI expressed high signal at 4 weeks for the defect site treated with LIPUS in comparison to the defect that did not receive treatment (figure 54). Additionally, again the defect that received LIPUS treatment expressed tissue growth and continuity across the defect site and into the host tissue. Greater signal was seen on the interiors and peripheries of the implant, indicating cellular activity and proliferation. While DAPI expression remained continuous in the defect site that did not receive LIPUS treatment, the signal did not evidence a formation of a periphery and interior tissue and cell formation.

GFP, a fluorescent stain for indicating the hydrogel implant's encapsulated donor cell survival, expressed less signal than the other stains after 4 weeks for both LIPUS treated and untreated groups (figure 55). However, signal was stronger in the defect receiving LIPUS treatment, although the expression was not continuous across the defect site and into the host tissue. Furthermore, the expression of GFP in the defect without LIPUS treated as significantly less and there was virtually no signal in the implant/defect site, while some signal was seen at the edges of the defect site where some donor cells appeared to survive.

Alizarin red complexone is an indicator of new bone formation and was expressed by evidence of slightly greater signal in the defect that received LIPUS treatment in comparison

to the defect without LIPUS treatment (figure 56). However, signal expression was not very high in either group. Slightly more continuity was seen in the LIPUS treated defect along with a thicker calvarial bone formation evidenced by a thicker band of signal. While the defect that did not receive treatment expressed a mostly continuous signal indicating bone formation across the majority of the implant, the thickness of bone formation was much thinner in comparison to the defect treated with LIPUS as the band of signal was thinner and less intense.

TRAP staining indicated the level of osteoclast activity in the defect bone healing process. The defect that received LIPUS expressed greater signal after 4 weeks than the defect that did not receive LIPUS (figure 57). However, both groups expressed a discontinuous signal indicating lack of continuity and formation or migration of osteoclasts across or throughout the defect sites. The defect that received LIPUS did express greater signal expression throughout the defect and at the defect-host tissue edges. The defect without LIPUS treatment expressed great discontinuity as there was nearly no signal except for that the host bone interfaces.

## 5.4. Discussion

Our *in vivo* investigation was conducted to provide important proof-of-concept data to expand the exploration of loading bony defects with malleable constructs capable of being transcutaneously deflected to impart mechanical loading on both resident and neighboring cells. We previously hypothesized that results would reveal accelerated healing in defects filled with donor cell-loaded hydrogels of optimal viscosity to best transfer remotely applied acoustic radiation force to encapsulated cells. Results at 4 weeks were more conclusive of bone regeneration and healing than the data demonstrated at 4 weeks; however, a 2 week period of bone healing is still premature in terms of the length of a typical fracture healing process, and there was still evidence of early bone healing in some groups.

As discussed previously, the mechanisms of action of LIPUS efficacy for fracture healing remain unknown; however, the data we presented may indicate the possibility between the mechanical stimulus of LIPUS being linked to mechanotransduction pathways. With the *in vitro* studies, alkaline phosphatase and osteocalcin expression was upregulated after 7 days of LIPUS treatment. Additionally, the marker indicative of mechanical stress, COX-2, was upregulated in association with acoustic radiation forces. Tying these concepts together along with other work through the research community, there is a likelihood that acoustic radiation force through LIPUS therapy for fracture healing may be effective in part through mechanical stimulation of cells at the fracture site resulting in mechanotransduction and enhanced bone regeneration in comparison to no treatment.

Significantly, our work demonstrated a few key findings for the use of implantable scaffolds as delivery vehicles for cell therapies in bony defects. Although evidence of bone healing at 2 weeks from LIPUS treatment did not greatly outweigh imaging results from the

groups without treatment, x-ray imaging of the defect treated with LIPUS did indicate greater signal at the edges of the defect where the defect without LIPUS treatment showed minimal to none, importantly indicating that LIPUS treatment resulted in early mineralization formation and seemingly initiated bone formation (figure 50). Furthermore at 4 weeks, the photographic images of the calvarial defect sites indicated a more continuous and consistent coloring in the regenerated tissue in the defect site in the group treated with LIPUS (figure 51). Intuitively, this more uniform consistency translated to significantly more mineralization in the LIPUS treated defect as evidenced by the signal in the x-ray imaging (figure 51) and translated to increased signal in the images stained for alkaline phosphatase, another indicator of mineralization (figure 53).

Investigation of cell activity and survival were important as one of our main objectives in addition to the remote mechanical stimulus of local tissue was the effective delivery and survival of cells to the defect through hydrogel implantation. Significantly, cell delivery and delivery and survival appeared successful as GFP imaging provided evidence of signal somewhat discontinuously across the defect site in the defects treated with LIPUS, but nevertheless, a positive presence of the encapsulated and implanted GFP-donor cells, indicating that they were successfully delivered and remained viable after 4 weeks (figure 54). While the signal for GFP in defects left untreated was significantly less and also discontinuous, some GFP-donor cells did still survive over the 4 week period independent of LIPUS treatment, expressing the utility of the hydrogel delivery system alone. On the other hand, the use of LIPUS treatment did significantly increase GFP-donor cell survival and viability compared to defects not receiving treatment, indicating that LIPUS directly played a role in cell survival, possibly through cellular nutrient maintenance and exchange. One theory behind LIPUS

efficacy suggests that LIPUS induces greater blood flow at the defect site and thus promotes better in vivo healing.[319] It is possible that the hydrogel scaffolds in the defects without LIPUS treatment were not able to exchange fluids as well for chemical and growth factor transport, receive oxygen, or discard toxins from cellular waste. Reasons for lack of fluid exchange could be lack of initiation of angiogenesis and vascularization or lack of integration of the hydrogel into host tissues at physical, chemical, and/or biological levels.

Further evidence of cell viability was expressed by DAPI imaging which provided conclusive evidence to greater cell presence by staining for cell nuclei in LIPUS treated defects compared to those left untreated (figure 55). These results suggest the LIPUS is playing a role in the regeneration of bone tissue and the proliferation of cells as significantly more are present across the defect site and on its edges both in continuity and in a two-level layer, where a strong signal was present on the periphery and interior of the scaffold. The defect left untreated importantly still expressed the presence of cells indicating the utility of our hydrogel system alone for the successfully delivery of cells to bony defect sites. However, the defect left untreated with LIPUS indicated significantly less signal and also a different arrangement and presence of stained nuclei. While signal was expressed in continuity across the defect site and at its edges, there was not an evidence of a two-level layer of bone tissue indicative of cortical bone formation for calvaria as indicated in the defect treated with LIPUS. This indicates that likely less tissue was regenerated in terms of calvarial thickness, which may lead to the conclusion that either LIPUS enhanced and/or accelerated bone regeneration in conjunction with the hydrogel system, or that the hydrogel system without LIPUS treatment would not be capable of fully regenerating tissue on its own.

Histology staining for alizarin complexone indicative of new bone formation expressed a pattern similar to the DAPI staining (figure 56). The defect treated with LIPUS showed new bone formation after four weeks in continuity across the defect and its edges on both its periphery and interior surfaces. The interior of the tissue showed less bone formation with more inconsistent signal in various areas. The defect without LIPUS treatment also showed continuity in new bone formation across the defect area and its edges, however there was not a defined periphery and interior surface as the generated tissue exhibited reduced thickness in comparison to the defect treated with LIPUS. These results indicate an enhanced level of healing with combing LIPUS treatment as a remote mechanical stimulus for bony defect loading with an encapsulated cell hydrogel system. As this study was performed in smaller sample sizes, a more comprehensive study is warranted for further investigation.

# 6. FUTURE DIRECTIONS

Fracture repair continues to be a widely-researched field in medicine. Improved clinical strategies are continually investigated to address current treatment limitations. Researchers explore the cellular response to injury, cell fate at the fracture site, and signaling pathways and mechanisms involved including the role of growth factors and mechanotransduction in fracture repair.[269] The clinical need for fracture repair treatment methods is warranted as there are between five and six million fractures annually in the United States.[320] We have evaluated ultrasound as a means of producing a transdermal physical force that could stimulate osteoblasts encapsulated within collagen hydrogels and delivered to bony defects. As we showed that ultrasound does indeed produce a measurable physical force and when applied to hydrogels causes their deformation, the possibility to heal bony defects by controlling substrate stiffness and deformation by applied physical load may be a potential non-invasive therapy with increased efficacy and affordability. Cell therapy for bone repair has already been used clinically in the form of autogenous bone marrow aspirate that is collected and re-injected into a bony defect.[321] As the theme of regenerative engineering is translating into clinical treatments, the use of patient-specific cells and tissue healing potential not only in orthopedics but across all clinical specialties is emerging compared to more traditional approaches in medicine commonly leading to limitations of only the treatment of symptoms. As delivery vehicles in biomaterials are being optimized in biomedical research and translated to clinical therapies, our work here using patient-specific encapsulated cells within hydrogel matrices as a localized, injectable treatment for bony defects provides a likely viable option for enhanced bone regeneration applications.

## 7. REFERENCES


1. Giannoudis P V, Dinopoulos H, Tsiridis E. Bone substitutes: An update. *Injury*. 2005;36(3):S20-S27. doi:10.1016/j.injury.2005.07.029.

2. Gentleman E, Swain RJ, Evans ND, et al. Comparative materials differences revealed in engineered bone as a function of cell-specific differentiation. *Nat Mater*. 2009;8(9):763-770. doi:10.1038/nmat2505.

3. Mauffrey C, Madsen M, Bowles RJ, Seligson D. Bone graft harvest site options in orthopaedic trauma: A prospective in vivo quantification study. *Injury*. 2012;43(3):323-326. doi:10.1016/j.injury.2011.08.029.

4. Bansal MR, Bhagat SB, Shukla DD. Bovine cancellous xenograft in the treatment of tibial plateau fractures in elderly patients. *Int Orthop*. 2009;33(3):779-784. doi:10.1007/s00264-008-0526-y.

5. Bigham AS, Dehghani SN, Shafiei Z, Torabi Nezhad S. Xenogenic demineralized bone matrix and fresh autogenous cortical bone effects on experimental bone healing: Radiological, histopathological and biomechanical evaluation. *J Orthop Traumatol*. 2008;9(2):73-80. doi:10.1007/s10195-008-0006-6.

6. Nandi SK, Roy S, Mukherjee P, Kundu B, De DK, Basu D. Orthopaedic applications of bone graft & graft substitutes: A review. *Indian J Med Res*. 2010;132(7):15-30. doi:10.1016/j.cuor.2005.12.001.

7. Scaglione M, Fabbri L, Dell'omo D, Gambini F, Guido G. Long bone nonunions treated with autologous concentrated bone marrow-derived cells combined with dried bone

allograft. *Musculoskelet Surg*. 2014;98(2):101-106. doi:10.1007/s12306-013-0271-2.

8. Lynch SE, Genco RJ, Marx RE. *Tissue Engineering : Applications in Maxillofacial Surgery and Periodontics*. Chicago: Quintessence Pub. Co; 1999.

9. Pneumaticos SG, Triantafyllopoulos GK, Basdra EK, Papavassiliou AG. Segmental bone defects: From cellular and molecular pathways to the development of novel biological treatments. *J Cell Mol Med*. 2010;14(11):2561-2569. doi:10.1111/j.1582-4934.2010.01062.x.

10. Colby BSL, Ortman JM. The Baby Boom Cohort in the United States: 2012 to 2060. *US Census Bereau*. 2014.

11. Grayson WL, Bunnell BA, Martin E, Frazier T, Hung BP, Gimble JM. Stromal cells and stem cells in clinical bone regeneration. *Nat Rev Endocrinol*. 2015;11(3):140-150. doi:10.1038/nrendo.2014.234.

12. Che C-T, Wong M-S. Ligustrum lucidum and its Constituents: A Mini-Review on the Anti-Osteoporosis Potential. *Nat Prod Commun*. 2015;10(12):2189-2194. http://www.ncbi.nlm.nih.gov/pubmed/26882695. Accessed February 14, 2017.

13. Tanna N. Osteoporosis and fragility fractures: identifying those at risk and raising public awareness. *Nurs Times*. 105(38):28-31.

14. Li N, Luo D, Hu X, et al. RUNX2 and Osteosarcoma. *Anticancer Agents Med Chem*. 2015;15(7):881-887. http://www.ncbi.nlm.nih.gov/pubmed/25738872. Accessed February 14, 2017.

15. Delloye C, Cornu O, Druez V, Barbier O, Druez S V, Surgeon O. Bone allografts: What

they can offer and what they cannot. *J Bone Jt Surg [Br]*. 2007;89:574-579. doi:10.1302/0301-620X.89B5.

16. Kurtz SM, Lau E, Ong K, Zhao K, Kelly M, Bozic KJ. Future Young Patient Demand for Primary and Revision Joint Replacement: National Projections from 2010 to 2030. *Clin Orthop Relat Res*. 2009;467(10):2606-2612. doi:10.1007/s11999-009-0834-6.

17. Schäffler A, Büchler C. Concise Review: Adipose Tissue-Derived Stromal Cells-Basic and Clinical Implications for Novel Cell-Based Therapies. *Stem Cells*. 2007;25(4):818-827. doi:10.1634/stemcells.2006-0589.

18. Gazdag A, Lane J, Glaser D, Forster R. Alternatives to Autogenous Bone Graft: Efficacy and Indications. *J Am Acad Orthop Surg*. 1995;3(1):1-8. http://www.ncbi.nlm.nih.gov/pubmed/10790647.

19. Banwart JC, Asher MA, Hassanein RS. Iliac crest bone graft harvest donor site morbidity. A statistical evaluation. *Spine (Phila Pa 1976)*. 1995;20(9):1055-1060. http://www.ncbi.nlm.nih.gov/pubmed/7631235. Accessed February 14, 2017.

20. Lord CF, Gebhardt MC, Tomford WW, Mankin HJ. Infection in bone allografts. Incidence, nature, and treatment. *J Bone Joint Surg Am*. 1988;70(3):369-376. http://www.ncbi.nlm.nih.gov/pubmed/3279038. Accessed February 14, 2017.

21. Tomford WW, Starkweather RJ, Goldman MH. A study of the clinical incidence of infection in the use of banked allograft bone. *J Bone Joint Surg Am*. 1981;63(2):244-248. http://www.ncbi.nlm.nih.gov/pubmed/7007391. Accessed February 14, 2017.

22. Bhatt RA, Rozental TD. Bone Graft Substitutes. *Hand Clin*. 2012;28(4):457-468.

doi:10.1016/j.hcl.2012.08.001.

23. Perry C. Bone repair techniques, bone graft, and bone graft substitutes. *Clin Orthop Relat Res*. 1999.

24. Laurencin CT, Ambrosio a M, Borden MD, Cooper J a. Tissue engineering: orthopedic applications. *Annu Rev Biomed Eng*. 1999;1:19-46. doi:10.1146/annurev.bioeng.1.1.19.

25. Reichert W, Ratner BD, Anderson J, et al. 2010 Panel on the Biomaterials Grand Challenges. *J Biomed Mater Res - Part A*. 2011;96 A(2):275-287. doi:10.1002/jbm.a.32969.

26. Petite H, Viateau V, Bensaïd W, et al. Tissue-engineered bone regeneration. *Nat Biotechnol*. 2000;18(9):959-963. doi:10.1038/79449.

27. Burg KJ, Porter S, Kellam JF. Biomaterial developments for bone tissue engineering. *Biomaterials*. 2000;21(23):2347-2359. doi:10.1016/S0142-9612(00)00102-2.

28. Mouw JK, Ou G, Weaver VM. Extracellular matrix assembly: a multiscale deconstruction. *Nat Rev Mol Cell Biol*. 2014;15(12):771-785. doi:10.1038/nrm3902.

29. Logeart-Avramoglou D, Anagnostou F, Bizios R, Petite H. Engineering bone: challenges and obstacles. *J Cell Mol Med*. 2005;9(1):72-84. doi:009.001.08 [pii].

30. Karageorgiou V, Kaplan D. Porosity of 3D biomaterial scaffolds and osteogenesis. *Biomaterials*. 2005;26(27):5474-5491. doi:10.1016/j.biomaterials.2005.02.002.

31. Frost HM. A 2003 update of bone physiology and Wolff's Law for clinicians. *Angle Orthod*. 2004;74(1):3-15. doi:10.1043/0003-3219(2004)074<0003:AUOBPA>2.0.CO;2.

32. Alberts B, Johnson A, Lewis J, et al. *Molecular Biology of the Cell*. Sixth Edit. Garland

Science; 2014.

33. Bilezikian JP, Raisz LG, Martin TJ. *Principles of Bone Biology*. London: Elsevier, Amsterdam; 2008.

34. Saladin K. *Anatomy & Physiology: The Unity of Form and Function*. 4th ed. New York, NY: McGraw-Hill; 2007.

35. Einhorn TA, Buckwalter JA, O'Keefe RJ. *Orthopaedic Basic Science: Foundations of Clinical Practice*. Amer Academy of Orthopaedic; 2007.

36. MCAT Anatomy - Bones. http://www.aboutthemcat.org/anatomy/bones.php. Accessed April 1, 2017.

37. Harmata AJ, Uppuganti S, Granke M, Guelcher SA, Nyman JS. Compressive fatigue and fracture toughness behavior of injectable, settable bone cements. *J Mech Behav Biomed Mater*. 2015;51:345-355. doi:10.1016/j.jmbbm.2015.07.027.

38. Cushnie EK, Ulery BD, Nelson SJ, et al. Simple signaling molecules for inductive bone regenerative engineering. *PLoS One*. 2014;9(7):1-11. doi:10.1371/journal.pone.0101627.

39. Marieb E, Hoehn K. *Human Anatomy & Physiology*. 7th ed. San Francisco, CA: Pearson Benjamin Cummings; 2007.

40. Seibel MJ, Robins SP, Bilezikian JP. *Dynamics of Bone and Cartilage Metabolism*. Academic Press; 2006.

41. Gottfried ON, Dailey AT. Mesenchymal stem cell and gene therapies for spinal fusion. *Neurosurgery*. 2008;63(3):380-392. doi:10.1227/01.NEU.0000324990.04818.13.

42. Lauzon M-A, Drevelle O, Daviau A, Faucheux N. Effects of BMP-9 and BMP-2 on the

PI3K/Akt Pathway in MC3T3-E1 Preosteoblasts. *Tissue Eng Part A*. 2016;22(17-18):1075-1085. doi:10.1089/ten.TEA.2016.0151.

43. Tortora GJ, Derrickson B. *Principles of Anatomy and Physiology*. John Wiley & Sons; 2010.

44. Clarke B. Normal Bone Anatomy and Physiology. *Clin J Am Soc Nephrol*. 2008;3(Supplement 3):S131-S139. doi:10.2215/CJN.04151206.

45. Aarden EM, Nijweide PJ, Burger EH. Function of osteocytes in bone. *J Cell Biochem*. 1994;55(3):287-299. doi:10.1002/jcb.240550304.

46. Maycas M, Esbrit P, Gortázar AR. Molecular mechanisms in bone mechanotransduction. *Histol Histopathol*. December 2016:11858. doi:10.14670/HH-11-858.

47. Wu X-T, Sun L-W, Yang X, Ding D, Han D, Fan Y-B. The potential role of spectrin network in the mechanotransduction of MLO-Y4 osteocytes. *Sci Rep*. 2017;7:40940. doi:10.1038/srep40940.

48. Yavropoulou MP, Yovos JG. The molecular basis of bone mechanotransduction. *J Musculoskelet Neuronal Interact*. 2016;16(3):221-236.

49. Teitelbaum SL. Bone Resorption by Osteoclasts. *Science (80- )*. 2000;289(5484).

50. Datta HK, Ng WF, Walker JA, Tuck SP, Varanasi SS. The cell biology of bone metabolism. *J Clin Pathol*. 2008;61(5):577-587. doi:10.1136/jcp.2007.048868.

51. John Martin T, Kong Wah Ng, Nicholson GC. Cell biology of bone. *Baillieres Clin Endocrinol Metab*. 1988;2(1):1-29. doi:10.1016/S0950-351X(88)80006-5.

52. Marieb E, Hoehn K. *Human Anatomy & Physiology*. 8th ed. San Francisco, CA: Benjamin

Cummings; 2010.

53. Ortega N, Behonick DJ, Werb Z. Matrix remodeling during endochondral ossification. *Trends Cell Biol*. 2004;14(2):86-93. doi:10.1016/j.tcb.2003.12.003.

54. Cohen MM. Merging the old skeletal biology with the new. Intramembranous ossification, endochondral ossification, ectopic bone, secondary cartilage, and pathologic considerations. *J Craniofac Genet Dev Biol*. 2000;20(2):84-93.

55. Mackie EJ, Ahmed YA, Tatarczuch L, Chen K-S, Mirams M. Endochondral ossification: How cartilage is converted into bone in the developing skeleton. *Int J Biochem Cell Biol*. 2008;40(1):46-62. doi:10.1016/j.biocel.2007.06.009.

56. Schultz R. *The Language of Fractures*. William & Wilkins Company; 1972.

57. Schindeler A, McDonald MM, Bokko P, Little DG. Bone remodeling during fracture repair: The cellular picture. *Semin Cell Dev Biol*. 2008;19(5):459-466. doi:10.1016/j.semcdb.2008.07.004.

58. Einhorn T. The cell and molecular biology of fracture healing. *Clin Orthop Relat Res*. 1998.

59. McKibbin B. The biology of fracture healing in long bones. *J Bone Jt Surg*. 1978.

60. Parfitt A. Osteonal and hemi-osteonal remodeling: the spatial and temporal framework for signal traffic in adult human bone. *J Cell Biochem*. 1994.

61. Parfitt AM. Bone age, mineral density, and fatigue damage. *Calcif Tissue Int*. 1993;53 Suppl 1:S82-5-6.

62. Bolander M. Regulation of fracture repair by growth factors. *Exp Biol Med*. 1992.

63. Lieberman J, Daluiski A. The role of growth factors in the repair of bone. *J Bone Jt*. 2002.

64. Vo TN, Kasper FK, Mikos AG. Strategies for controlled delivery of growth factors and cells for bone regeneration. *Adv Drug Deliv Rev*. 2012;64(12):1292-1309. doi:10.1016/j.addr.2012.01.016.

65. Rodan G, Raisz L, Bilezikian J. *Principles of Bone Biology*. Academic Press; 1996.

66. Farley J, Hall S, Tanner M. Specific activity of skeletal alkaline phosphatase in human osteoblast-line cells regulated by phosphate, phosphate esters, and phosphate analogs and release of alkaline phosphatase activity inversely regulated by calcium. *J Bone*. 1994;9(4):497-508.

67. Whyte M. Physiological role of alkaline phosphatase explored in hypophosphatasia. *Ann N Y Acad Sci*. 2010;1192(1):190-200.

68. Harris H. The human alkaline phosphatases: what we know and what we don't know. *Clin Chim Acta*. 1990;186(2):133-150.

69. Heinegard D, Oldberg A. Structure and biology of cartilage and bone matrix noncollagenous macromolecules. *FASEB J*. 1989;3(9):2042-2051.

70. Watts N. Clinical utility of biochemical markers of bone remodeling. *Clin Chem*. 1999;45(8):1359-1368.

71. Garnero P, Hausherr E, Chapuy M. Markers of bone resorption predict hip fracture in elderly women: the EPIDOS Prospective Study. *J bone Miner Res*. 1996;11(10):1531-1538.

72. Vasikaren S, Eastell R, Bruyere O, Foldes A. Markers of bone turnover for the prediction

of fracture risk and monitoring of osteoporosis treatment: a need for international reference standards. *Osteoporosis*. 2011;22(2):391-420.

73. Price P. Role of vitamin-K-dependent proteins in bone metabolism. *Annu Rev Nutr*. 1988;8(1):565-583.

74. Kasai T, Bandow K, Suzuki H, Chiba N. Osteoblast differentiation is functionally associated with decreased AMP kinase activity. *J Cell Physiol*. 2009;221(3):740-749.

75. Kaartinen M, Pirhonen A, Linnala-Kankkunen A. Cross-linking of osteopontin by tissue transglutaminase increases its collagen binding properties. *J Biol Chem*. 1999;274(3):1729-1735.

76. Flores M, Norgård M, Heinegård D, Reinholt F. RGD-directed attachment of isolated rat osteoclasts to osteopontin, bone sialoprotein, and fibronectin. *Exp Cell Res*. 1992;201(2):526-530.

77. Horton M, Taylor M, Arnett T, Helfrich M. Arg-Gly-Asp (RGD) peptides and the anti-vitronectin receptor antibody 23C6 inhibit dentine resorption and cell spreading by osteoclasts. *Exp Cell Res*. 1991;195(2):368-375.

78. Tomoaia G, Pasca R. On the collagen mineralization. A review. *Clujul Med*. 2015;88(1):15.

79. Rich A, Crick F. The molecular structure of collagen. *J Mol Biol*. 1961;3(5):483-506.

80. Ramachandran G. Molecular structure of collagen. *Int Rev Connect Tissue Res*. 1963;1:127-182.

81. Mizuno M, Kuboki Y. Osteoblast-related gene expression of bone marrow cells during the

osteoblastic differentiation induced by type I collagen. *J Biochem*. 2001;129(1):133-138.

82. Mizuno M, Fujisawa R, Kuboki Y. Type I collagen-induced osteoblastic differentiation of bone-marrow cells mediated by collagen-α2β1 integrin interaction. *J Cell Physiol*. 2000;184(2):207-213.

83. Banerjee C, Hiebert S, Stein J. An AML-1 consensus sequence binds an osteoblast-specific complex and transcriptionally activates the osteocalcin gene. *Proc Natl Acad Sci*. 1996;93(10):4968-4973.

84. Merriman H, Wijnen A Van, Hiebert S, Bidwell J. The tissue-specific nuclear matrix protein, NMP-2, is a member of the AML/CBF/PEBP2/runt domain transcription factor family: interactions with the osteocalcin gene. *Biochemistry*. 1995;34(40):13125-13132.

85. Mundlos S, Otto F, Mundlos C, Mulliken J. Mutations involving the transcription factor CBFA1 cause cleidocranial dysplasia. *Cell*. 1997;89(5):773-779.

86. Viereck V, Siggelkow H, Tauber S. Differential regulation of Cbfa1/Runx2 and osteocalcin gene expression by vitamin-D3, dexamethasone, and local growth factors in primary human osteoblasts. *J Cell Biochem*. 2002;86(2):348-356.

87. Komori T, Yagi H, Nomura S, Yamaguchi A, Sasaki K. Targeted disruption of Cbfa1results in a complete lack of bone formation owing to maturational arrest of osteoblasts. *Cell*. 1997;89(5):755-764.

88. Zimmermann G, Moghaddam A. Allograft bone matrix versus synthetic bone graft substitutes. *Injury*. 2011.

89. Parikh S. Bone graft substitutes: past, present, future. *J Postgrad Med*. 2002.

90. Fleming J, Cornell C, Muschler G. Bone cells and matrices in orthopedic tissue engineering. *Orthop Clin North Am*. 2000.

91. Nandi S, Roy S, Mukherjee P, Kundu B, De D, Basu D. Orthopedic applications of bone graft & graft substitutes: a review. *Indian J Med Res*. 2010;132:15-30.

92. Laurencin CT, Jiang T, eds. *Bone Graft Substitutes and Bone Regenerative Engineering, 2nd Edition*. West Conshohocken, PA: ASTM International; 2014.

93. Kealey G. Disease transmission by means of allograft. *J Burn Care Res*. 1997.

94. Eastlund T. Infectious disease transmission through cell, tissue, and organ transplantation: reducing the risk through donor selection. *Cell Transplant*. 1995.

95. Tomford W. Transmission of disease through transplantation of musculoskeletal allografts. *JBJS*. 1995.

96. Boyce T, Edwards J, Scarborough N. Allograft bone: the influence of processing on safety and performance. *Orthop Clin North Am*. 1999;30(4):571-581.

97. Ricciardi B, Bostrom M. Bone graft substitutes: claims and credibility. *Semin Arthroplasty*. 2013;24(2):119-123.

98. Cutter C, Mehrara B. Bone grafts and substitutes. *J Long Term Eff Med Implants*. 2006;16(3).

99. Toolan B. Current concepts review: orthobiologics. *Foot ankle Int*. 2006;27(7):561-566.

100. De Long W, Einhorn T, Koval K, McKee M. Bone grafts and bone graft substitutes in orthopaedic trauma surgery: a critical analysis. *J bone Jt Surg*. 2007;89(3):649-658.

101. Feng Y, Wang S, Jin D, Sheng J, Chen S. Free vascularised fibular grafting with OsteoSet® 2 demineralised bone matrix versus autograft for large osteonecrotic lesions of the femoral head. *Int Orthop*. 2011;35(4):475-481.

102. Lo K, Ulery B, Ashe K, Laurencin C. Studies of bone morphogenetic protein-based surgical repair. *Adv Drug Deliv Rev*. 2012;64(12):1277-1291.

103. Lo KW, Ulery B, Deng M, Ashe K. Current patents on osteoinductive molecules for bone tissue engineering. *Recent Pat Biomed Eng*. 2011;4(3):153-167.

104. Lo K, Kan H, Ashe K. The small molecule PKA-specific cyclic AMP analogue as an inducer of osteoblast-like cells differentiation and mineralization. *J Tissue Eng Regen Med*. 2012;6(1):40-48.

105. Epstein N. Complications due to the use of BMP/INFUSE in spine surgery: the evidence continues to mount. *Surg Neurol Int*. 2013;4:343.

106. Carroll S. *Discovery and Nonclinical Development*. Springer US; 2007.

107. Egusa H, Saeki M, Doi M, Fukuyasu S. A small-molecule approach to bone regenerative medicine in dentistry. *J Oral Biosci*. 2010;52(2):107-118.

108. Lo K, Ashe K, Kan H. The role of small molecules in musculoskeletal regeneration. *Regen Med*. 2012;7(12):535-549.

109. Meijer G, Bruijn J de, Koole R, van Blitterswijk C. Cell-based bone tissue engineering. *PLoS Med*. 2007;4(2):e9.

110. Kimelman N, Pelled G, Helm G, Huard J. Review: Gene-and Stem Cell–Based Therapeutics for Bone Regeneration and Repair. *Tissue Eng*. 2007;13(6):1135-1150.

111. Fei Y, Xu R, Hurley M. Stem cell-based bone repair. *Am J Stem Cells*. 2012;1(2):106.

112. Tang M, Chen W, Liu J, Weir M. Human induced pluripotent stem cell-derived mesenchymal stem cell seeding on calcium phosphate scaffold for bone regeneration. *Eng Part A*. 2014;20:1295-1305.

113. Takahashi K, Yamanaka S. Induction of pluripotent stem cells from mouse embryonic and adult fibroblast cultures by defined factors. *Cell*. 2006;126(4):663.

114. Jaiswal N, Haynesworth S, Caplan A. Osteogenic differentiation of purified, culture-expanded human mesenchymal stem cells in vitro. *J Cell Biochem*. 1997;64(2):295-312.

115. Bianco P, Riminucci M, Gronthos S, Robey P. Bone marrow stromal stem cells: nature, biology, and potential applications. *Stem Cells*. 2001;19(3):180-192.

116. Kuznetsov S, Mankani M, Gronthos S. Circulating skeletal stem cells. *J Cell Biol*. 2001;153(5):1133-1140.

117. Rosada C, Justesen J, Melsvik D, Ebbesen P. The human umbilical cord blood: a potential source for osteoblast progenitor cells. *Calcif Tissue Int*. 2003;72(2):135-142.

118. Bari C De, Dell'Accio F, Tylzanowski P. Multipotent mesenchymal stem cells from adult human synovial membrane. *Arthritis Rheum*. 2001;44(8):1928-1942.

119. Zuk P, Zhu M, Ashjian P, De Ugarte D. Human adipose tissue is a source of multipotent stem cells. *Mol Biol Cell*. 2002;13(12):4279-4295.

120. Crisan M, Yap S, Casteilla L, Chen C, Corselli M. A perivascular origin for mesenchymal stem cells in multiple human organs. *Cell Stem Cell*. 2008;3(3):301-313.

121. Li M, Ikehara S. Bone-marrow-derived mesenchymal stem cells for organ repair. *Stem*

*Cells Int*. 2013.

122. Xiao C, Zhou H, Liu G, Zhang P, Fu Y, Gu P. Bone marrow stromal cells with a combined expression of BMP-2 and VEGF-165 enhanced bone regeneration. *Biomedical*. 2011;6(1).

123. Moore N, Lin N, Gallant N, Becker M. Synergistic enhancement of human bone marrow stromal cell proliferation and osteogenic differentiation on BMP-2-derived and RGD peptide concentration gradients. *Acta Biomater*. 2011;7(5):2091-2100.

124. Liu S, Yang R, Al-Shaikh R. Collagen in Tendon, Ligament, and Bone Healing: A Current Review. *Clin Orthop Relat Res*. 1995;318:265-278.

125. Jikko A, Harris S, Chen D. Collagen Integrin Receptors Regulate Early Osteoblast Differentiation Induced by BMP-2. *J bone Miner Res*. 1999;14(7):1075-1083.

126. Park S, Park S, Kim N, Chung C. BMP-2 induced early bone formation in spine fusion using rat ovariectomy osteoporosis model. *Spine J*. 2013;13(10):1273-1280.

127. Rush S. Bone Graft Substitutes: Osteobiologics. *Clin Podiatr Med Surg*. 2005;22(4):619-630. doi:10.1016/j.cpm.2005.07.004.

128. Ishihara A, Weisbrode S. Autologous implantation of BMP2-expressing dermal fibroblasts to improve bone mineral density and architecture in rabbit long bones. *J Orthop Res*. 2015;33(10):1455-1465.

129. Hong L, Mao J. Tissue-engineered rabbit cranial suture from autologous fibroblasts and BMP2. *J Dent Res*. 2004;83(10):751-756.

130. Duan Z, Zheng Q, Guo X, Li C, Wu B, Wu W. Repair of rabbit femoral defects with a

novel BMP2-derived oligopeptide P24. *J Huazhong Univ Sci Technol Med Sci*. 2008;28(4):426-430.

131. Kagami H, Agata H, Tojo A. Bone marrow stromal cells (bone marrow-derived multipotent mesenchymal stromal cells) for bone tissue engineering: basic science to clinical translation. *Int J Biochem Cell Biol*. 2011;43(3):286-289.

132. Arvidson K, Abdallah B, Applegate L. Bone regeneration and stem cells. *J Cell Mol Med*. 2011;15(4):718-746.

133. Liao H, Chen C. Osteogenic potential: Comparison between bone marrow and adipose-derived mesenchymal stem cells. *World J Stem Cells*. 2014;6(3):288-295.

134. Cowan C, Shi Y, Aalami O, Chou Y, Mari C. Adipose-derived adult stromal cells heal critical-size mouse calvarial defects. *Nat Biotechnol*. 2004;22(5):560-567.

135. Liu G, Zhang Y, Liu B, Sun J, Li W, Cui L. Bone regeneration in a canine cranial model using allogeneic adipose derived stem cells and coral scaffold. *Biomaterials*. 2013;34(11):2655-2664.

136. Tang Z, Cao J, Wen N, Wang H. Posterolateral spinal fusion with nano-hydroxyapatite–collagen/PLA composite and autologous adipose-derived mesenchymal stem cells in a rabbit model. *J Tissue Eng Regen Med*. 2012;6(4):325-336.

137. Colnot C. Cell sources for bone tissue engineering: insights from basic science. *Tissue Eng Part B Rev*. 2011;17(6):449-457.

138. Robey P. Cell sources for bone regeneration: the good, the bad, and the ugly (but promising). *Tissue Eng Part B Rev*. 2011;17(6):423-430.

139. Prgeeth Pandula P. Human umbilical vein endothelial cells synergize osteo/odontogenic differentiation of periodontal ligament stem cells in 3D cell sheets. *J Periodontal Res*. 2014;49(3):299-306.

140. Wu X, Wang S, Chen B, An X. Muscle-derived stem cells: isolation, characterization, differentiation, and application in cell and gene therapy. *Cell Tissue Res*. 2010;340(3):549-567.

141. Buttery L, Bourne S, Xynos J, Wood H. Differentiation of osteoblasts and in vitro bone formation from murine embryonic stem cells. *Tissue Eng*. 2001;7(1):89-99.

142. Asahara T, Kawamoto A. Endothelial progenitor cells for postnatal vasculogenesis. *Am J Physiol Physiol*. 2004;287(3):C572-C579.

143. Ripamonti U. Osteoinduction in porous hydroxyapatite implanted in heterotopic sites of different animal models. *Biomaterials*. 1996;17(1):31-35.

144. Epinette J, Manley M. *Fifteen Years of Clinical Experience with Hydroxyapatite Coatings in Joint Arthroplasty*. Springer; 2013.

145. Ohgushi H, Caplan AI. Stem cell technology and bioceramics: From cell to gene engineering. *J Biomed Mater Res*. 1999;48(6):913-927. doi:10.1002/(SICI)1097-4636(1999)48:6<913::AID-JBM22>3.0.CO;2-0.

146. Grüninger A, Hugo B, Stassinakis A. The Celay System. Preparation and use of ceramic in-and onlays produced by the copy milling method. *Schweiz Monatsschr Zahnmed*. 1995;106(2):126-140.

147. Brown W. A new calcium phosphate, water-setting cement. *Cem Res Prog*. 1987:351-379.

148. Qu S, Fan H, Chen J, Feng J, Fu R, Wei D. Effect of the crystallinity of calcium phosphate ceramics on osteoblast proliferation in vitro. *J Mater Sci Lett*. 2001;20(4):331-332.

149. Posner A, Betts F. Synthetic amorphous calcium phosphate and its relation to bone mineral structure. *Acc Chem Res*. 1975;8(8):273-281.

150. Bigi A, Cojazzi G, Panzavolta S, Ripamonti A. Chemical and structural characterization of the mineral phase from cortical and trabecular bone. *J Inorg Biochem*. 1997;68(1):45-51.

151. Hamadouche M, Sedel L. Ceramics in orthopaedics. *J Bone Jt Surg - Br Vol*. 2000;82(8):1095-1099.

152. Ducheyne P, Qiu Q. Bioactive ceramics: the effect of surface reactivity on bone formation and bone cell function. *Biomaterials*. 1999;20(23):2287-2303.

153. Matsuoka H, Akiyama H, Okada Y, Ito H. In vitro analysis of the stimulation of bone formation by highly bioactive apatite-and wollastonite-containing glass-ceramic: released calcium ions promote osteogenic. *J Biomed Res Part A*. 1999;47(2):176-188.

154. LeGeros R. Properties of osteoconductive biomaterials: calcium phosphates. *Clin Orthop Relat Res*. 2002;395:81-98.

155. Dang J, Leong K. Natural polymers for gene delivery and tissue engineering. *Adv Drug Deliv Rev*. 2006;58(4):487-499.

156. McKay W, Peckham S, Badura J. A comprehensive clinical review of recombinant human bone morphogenetic protein-2 (INFUSE® Bone Graft). *Int Orthop*. 2007;31(6):729-734.

157. Laurencin C, Khan Y, El-Amin SF. Bone graft substitutes. *Expert Rev Med Devices*.

2006;3(1):49-57. doi:10.1586/17434440.3.1.49.

158. Kraiwattanapong C, Boden S, Louis-Ugbo J. Comparison of Healos/bone marrow to INFUSE (rhBMP-2/ACS) with a collagen-ceramic sponge bulking agent as graft substitutes for lumbar spine fusion. *Spine (Phila Pa 1976).* 2005;30(9):1001-1007.

159. Boden S. Biology of lumbar spine fusion and use of bone graft substitutes: present, future, and next generation. *Tissue Eng*. 2000;6(4):383-399.

160. Geiger M, Li R, Friess W. Collagen sponges for bone regeneration with rhBMP-2. *Adv Drug Deliv Rev*. 2003;55(12):1613-1629.

161. Landsman A, Taft D, Riemer K. The role of collagen bioscaffolds, foamed collagen, and living skin equivalents in wound healing. *Clin Podiatr Med Surg*. 2009;26(4):525-533.

162. Hak D. The use of osteoconductive bone graft substitutes in orthopaedic trauma. *J Am Acad Orthop Surg*. 2007;15(9):525-536.

163. Barbanti S, Santos A, Zavaglia C. Poly (ε-caprolactone) and poly (d, l-lactic acid-co-glycolic acid) scaffolds used in bone tissue engineering prepared by melt compression–particulate leaching method. *J Mater*. 2011;22(10):2377.

164. Andreas K, Zehbe R, Kazubek M, Grzeschik K. Biodegradable insulin-loaded PLGA microspheres fabricated by three different emulsification techniques: investigation for cartilage tissue engineering. *Acta Biomater*. 2011;7(4):1485-1495.

165. Sahoo S, Toh S, Goh J. A bFGF-releasing silk/PLGA-based biohybrid scaffold for ligament/tendon tissue engineering using mesenchymal progenitor cells. *Biomaterials*. 2010;31(11):2990-2998.

166. Hidayah N, Fadzli A, Ng M, Ruszymah B, Naicker A. Porous PLGA sheet and acellularized muscle stuffed vein seeded with neural-differentiated MSCs are potential scaffolds for nerve regeneration. *Regen*. 2012;1:1-7.

167. Wang P, Wu T, Tsai W, Kuo W. Grooved PLGA films incorporated with RGD/YIGSR peptides for potential application on skeletal muscle tissue engineering. *Colloids Surfaces B Biointerfaces*. 2013;110(88-95).

168. Lavik E, Langer R. Tissue engineering: current state and perspectives. *Appl Microbiol Biotechnol*. 2004;65(1):1-8.

169. Tong W, Li X, Feng J, Chen J. Phase transitions of hydroxyapatite coatings during post-heat treatment and their performances under ultrasonic tests. *J Biomed Mater Res*. 2001;56(1):49-55.

170. Drury J, Mooney D. Hydrogels for tissue engineering: scaffold design variables and applications. *Biomaterials*. 2003;24(24):4337-4351.

171. Gilbert P, Havenstrite K, Magnusson K. Substrate elasticity regulates skeletal muscle stem cell self-renewal in culture. *Science (80- ).* 2010;329(5995):1078-1081.

172. Lutolf M. Biomaterials: Spotlight on hydrogels. *Nat Mater*. 2009;8(6):451-453.

173. Xie J, Baumann M, McCabe L. Osteoblasts respond to hydroxyapatite surfaces with immediate changes in gene expression. *J Biomed Mater Res Part A*. 2004;71(1):108-117.

174. Serre C, Papillard M, Chavassieux P, Boivin G. In vitro induction of a calcifying matrix by biomaterials constituted of collagen and/or hydroxyapatite: an ultrastructural comparison of three types of biomaterials. *Biomaterials*. 1993;14(2):97-106.

175. Viguet-Carrin S, Garnero P, Delmas P. The role of collagen in bone strength. *Osteoporos Int*. 2006;17(3):319-336.

176. Ye Q, Harmsen M, Luyn M van, Bank R. The relationship between collagen scaffold cross-linking agents and neutrophils in the foreign body reaction. *Biomaterials*. 2010;31(35):9192-9201.

177. Mi S, Khutoryanskiy V, Jones R. Photochemical cross-linking of plastically compressed collagen gel produces an optimal scaffold for corneal tissue engineering. *Res Part A*. 2011;99(1):1-8.

178. Zeugolis D, Paul G. Cross-linking of extruded collagen fibers—A biomimetic three-dimensional scaffold for tissue engineering applications. *J Biomed Mater Res Part A*. 2009;89(4):895-908.

179. Khan Y, Saadiq F. In vitro and in vivo evaluation of a novel polymer-ceramic composite scaffold for bone tissue engineering. *Eng Med Biol Scoiety, 2006*. 2006.

180. Sharmin F, McDermott C, Khan Y. *Regenerative Engineering: Role of Scaffolds, Cells, and Growth Factors*. (Lakshmi S Nair, ed.). Imperial College Press; 2015.

181. Engh C, Bobyn J, Glassman A. Porous-coated hip replacement. The factors governing bone ingrowth, stress shielding, and clinical results. *Bone Joint J*. 1987;69(1):45-55.

182. Sumner D, Galante J. Determinants of stress shielding: design versus materials versus interface. *Clin Orthop Relat Res*. 1992;274:202-212.

183. Kanayama M, Cunningham B, Haggerty C. In vitro biomechanical investigation of the stability and stress-shielding effect of lumbar interbody fusion devices. *Neurosurg Spine*.

2000;93(2):259-265.

184. Mouw JK, Ou G, Weaver VM. Extracellular matrix assembly: a multiscale deconstruction. *Nat Rev Mol Cell Biol*. 2014;15(12):771-785. doi:10.1038/nrm3902.

185. Yang J, McNamara LE, Gadegaard N, et al. Nanotopographical Induction of Osteogenesis through Adhesion, Bone Morphogenic Protein Cosignaling, and Regulation of MicroRNAs. *ACS Nano*. 2014;8(10):9941-9953. doi:10.1021/nn504767g.

186. Tsimbouri P, Gadegaard N, Burgess K, et al. Nanotopographical Effects on Mesenchymal Stem Cell Morphology and Phenotype. *J Cell Biochem*. 2014;115(2):380-390. doi:10.1002/jcb.24673.

187. Bettinger C, Langer R, Borenstein J. Engineering substrate topography at the micro-and nanoscale to control cell function. *Angew Chemie Int Ed*. 2009;48(30):5406-5415.

188. Kato RB, Roy B, De Oliveira FS, et al. Nanotopography Directs Mesenchymal Stem Cells to Osteoblast Lineage Through Regulation of microRNA-SMAD-BMP-2 Circuit. *J Cell Physiol*. 2014;229(11):1690-1696. doi:10.1002/jcp.24614.

189. Jang S, Kim J, Cha S. Platelet-rich plasma (PRP) injections as an effective treatment for early osteoarthritis. *Eur J Orthop Surg Traumatol*. 2013;23(5):573-580.

190. Patel S, Dhillon M, Aggarwal S. Treatment with platelet-rich plasma is more effective than placebo for knee osteoarthritis a prospective, double-blind, randomized trial. *Am J Sports Med*. 2013;41(2):356-364.

191. Filardo G, Kon E, Buda R, Timoncini A. Platelet-rich plasma intra-articular knee injections for the treatment of degenerative cartilage lesions and osteoarthritis. *Knee*

*Surgery, Sport Traumatol Arthrosc*. 2011;19(4):528-535.

192. Halpern B, Chaudhury S, Rodeo S. Clinical and MRI outcomes after platelet-rich plasma treatment for knee osteoarthritis. *Clin J Sport Med*. 2013;23(3):238-239.

193. Mishra A, Woodall J, Vieira A. Treatment of tendon and muscle using platelet-rich plasma. *Clin Sports Med*. 2009;28(1):113-125.

194. Øiestad B, Engebretsen L, Storheim K. Knee osteoarthritis after anterior cruciate ligament injury a systematic review. *Am J Sports Med*. 2009;37(7):1434-1443.

195. Shin YM, Hohman MM, Brenner MP, Rutledge GC. Electrospinning: A whipping fluid jet generates submicron polymer fibers. *Appl Phys Lett*. 2001;78(8):1149-1151. doi:10.1063/1.1345798.

196. Shin YM, Hohman MM, Brenner MP, Rutledge GC. Experimental characterization of electrospinning: the electrically forced jet and instabilities. *Polymer (Guildf)*. 2001;42(25):09955-09967. doi:10.1016/S0032-3861(01)00540-7.

197. Ki CS, Baek DH, Gang KD, Lee KH, Um IC, Park YH. Characterization of gelatin nanofiber prepared from gelatin–formic acid solution. doi:10.1016/j.polymer.2005.04.040.

198. Luu YK, Kim K, Hsiao BS, Chu B, Hadjiargyrou M. Development of a nanostructured DNA delivery scaffold via electrospinning of PLGA and PLA–PEG block copolymers. *J Control Release*. 2003;89(2):341-353. doi:10.1016/S0168-3659(03)00097-X.

199. James EN, Delany AM, Nair LS. Post-transcriptional regulation in osteoblasts using localized delivery of miR-29a inhibitor from nanofibers to enhance extracellular matrix deposition. *Acta Biomater*. 2014;10(8):3571-3580. doi:10.1016/j.actbio.2014.04.026.

200. Huang Z-M, Zhang Y-Z, Kotaki M, Ramakrishna S. A review on polymer nanofibers by electrospinning and their applications in nanocomposites. *Compos Sci Technol*. 2003;63(15):2223-2253. doi:10.1016/S0266-3538(03)00178-7.

201. Monteiro N, Martins M, Martins A, et al. Antibacterial activity of chitosan nanofiber meshes with liposomes immobilized releasing gentamicin. *Acta Biomater*. 2015;18:196-205. doi:10.1016/j.actbio.2015.02.018.

202. Fiorani A, Gualandi C, Panseri S, et al. Comparative performance of collagen nanofibers electrospun from different solvents and stabilized by different crosslinkers. *J Mater Sci Mater Med*. 2014;25(10):2313-2321. doi:10.1007/s10856-014-5196-2.

203. James EN, Nair LS. Development and characterization of lactoferrin loaded poly(epsilon-caprolactone) nanofibers. *J Biomed Nanotechnol*. 2014;10(3):500-507. http://www.ncbi.nlm.nih.gov/pubmed/24730245. Accessed April 5, 2017.

204. Ebrahimi-Barough S, Norouzi Javidan A, Saberi H, et al. Evaluation of Motor Neuron-Like Cell Differentiation of hEnSCs on Biodegradable PLGA Nanofiber Scaffolds. *Mol Neurobiol*. 2015;52(3):1704-1713. doi:10.1007/s12035-014-8931-2.

205. Marei NH, El-Sherbiny IM, Lotfy A, El-Badawy A, El-Badri N. Mesenchymal stem cells growth and proliferation enhancement using PLA vs PCL based nanofibrous scaffolds. *Int J Biol Macromol*. 2016;93(Pt A):9-19. doi:10.1016/j.ijbiomac.2016.08.053.

206. Borden M, Attawia M, Khan Y, El-Amin S. Tissue-engineered bone formation in vivo using a novel sintered polymeric microsphere matrix. *Bone Joint J*. 2004;86(8):1200-1208.

207. Borden M, Attawia M. The sintered microsphere matrix for bone tissue engineering: in vitro osteoconductivity studies. *J Biomed Mater Res*. 2002;61(3):421-429.

208. Dhandayuthapani B, Yoshida Y, Maekawa T. Polymeric scaffolds in tissue engineering application: a review. *Int J Polym Sci*. 2011.

209. Borden M, El-Amin S, Attawia M, Laurencin C. Structural and human cellular assessment of a novel microsphere-based tissue engineered scaffold for bone repair. *Biomaterials*. 2003;24(4):597-609.

210. Dasan KP, Rekha C. Polymer blend microspheres for controlled drug release: The techniques for preparation and characterization: A review article. *Curr Drug Deliv*. 2012;9(6):588-595.

211. Ravivarapu H, Burton K, DeLuca P. Polymer and microsphere blending to alter the release of a peptide from PLGA microspheres. *Eur J Pharm Biopharm*. 2000;50(2):263-270.

212. Smith S, Morhenn V, Webster G. The characteristics and utility of solid phase porous microspheres: a review. *J drugs dermatology*. 2005;5(10):969-974.

213. Mercadé-Prieto R, Zhang Z. Mechanical characterization of microspheres–capsules, cells and beads: a review. *J Microencapsul*. 2012;29(3):277-285.

214. Soppimath K, Aminabhavi T, Kulkarni A. Biodegradable polymeric nanoparticles as drug delivery devices. *J Control release*. 2001;70(1):1-20.

215. Freiberg S, Zhu X. Polymer microspheres for controlled drug release. *Int J Pharm*. 2004;282(1):1-18.

216. Mathiowitz E, Jacob J, Jong Y, Carino G. Biologically erodable microspheres as potential oral drug delivery systems. *Nature*. 1997;386(6623):410.

217. Laurencin C, Ambrosio A. Tissue engineering: orthopedic applications. *Annu Rev Biomed Eng*. 1999;1(1):19-46.

218. Botchwey E, Pollack S, Levine E. Bone tissue engineering in a rotating bioreactor using a microcarrier matrix system. *J Biomed Mater Res Part A*. 2001;55(2):242-253.

219. Newton I. 1687, Philosophiae naturalis principia mathematica, London: J. *Streater R Soc (Imprimatur S Pepys, 5 July*. 1987.

220. Lord R. *The Theory of Sound*. Dover, NY; 1945.

221. Curie J, Curie P. Piezoelectric and allied phenomena in Rochelle salt. *Comput Rend Acad Sci Paris*. 1880.

222. Hunt J. Applications of microwave, ultrasound, and radiofrequency heating. *Natl Cancer Inst Monogr*. 1982.

223. Johns LD, Straub SJ, Howard SM. Analysis of Effective Radiating Area, Power, Intensity, and Field Characteristics of Ultrasound Transducers. *Arch Phys Med Rehabil*. 2007;88(1):124-129. doi:10.1016/j.apmr.2006.09.016.

224. Kossoff G. Basic physics and imaging characteristics of ultrasound. *World J Surg*. 2000.

225. Zeng F, Fu Q, Morse R. Human hearing enhanced by noise. *Brain Res*. 2000.

226. Blauert J. *Spatial Hearing: The Psychophysics of Human Sound Localization*.; 1997.

227. Cobbold R. *Foundations of Biomedical Ultrasound*. New York, NY: Oxford University

Press; 2006.

228. Nyborg WL, Miller DL. Biophysical implications of bubble dynamics. *Appl Sci Res*. 1982;38(1):17-24. doi:10.1007/BF00385933.

229. Torr G. The acoustic radiation force. *Am J Phys*. 1984.

230. Nightingale K, Soo M, Nightingale R. Acoustic radiation force impulse imaging: in vivo demonstration of clinical feasibility. *Ultrasound Med*. 2002.

231. Zieniuk J, Chivers R. Measurement of ultrasonic exposure with radiation force and thermal methods. *Ultrasonics*. 1976.

232. Harris R, Nishiyama S, Wray D. Ultrasound assessment of flow-mediated dilation. *Hypertension*. 2010.

233. Taira A, Sakai H, Ogido T. Ultrasound biomicroscopic findings and therapeutic modalities for traumatic angle recession. *J Eye*. 2003;20(6):825-830.

234. Nightingale K, McAleavey S, Trahey G. Shear-wave generation using acoustic radiation force: in vivo and ex vivo results. *Ultrasound Med Biol*. 2003.

235. Turner C, Pavalko F. Mechanotransduction and functional response of the skeleton to physical stress: the mechanisms and mechanics of bone adaptation. *J Orthop Sci*. 1998;3(6):346-355.

236. Turner C, Owan I, Takano Y. Mechanotransduction in bone: role of strain rate. *Am J Physiol Metab*. 1995;269(3):E438-E442.

237. Burger E, Klein-Nulend J. Mechanotransduction in bone—role of the lacuno-canalicular network. *FASEB J*. 1999;13(9001):S101-S112.

238. Huang C, Ogawa R. Mechanotransduction in bone repair and regeneration. *FASEB J*. 2010;24(10):3625-3623.

239. Sikavitsas V, Temenoff J, Mikos A. Biomaterials and bone mechanotransduction. *Biomaterials*. 2001;22(19):2581-2593.

240. Turner CH, Pavalko FM. Mechanotransduction and functional response of the skeleton to physical stress: The mechanisms and mechanics of bone adaptation*. *J Orthop Sci*. 1998;3(6):346-355.

241. Duncan RL, Turner CH. Mechanotransduction and the functional response of bone to mechanical strain. *Calcif Tissue Int*. 1995;57(5):344-358.

242. Huang H, Kamm RD, Lee RT. Cell mechanics and mechanotransduction: pathways, probes, and physiology. *Am J Physiol - Cell Physiol*. 2004;287(1):C1-C11.

243. Iqbal J, Zaidi M. Molecular regulation of mechanotransduction. *Biochem Biophys Res Commun*. 2004;328:751-755.

244. Hughes-Fulford M. Signal transduction and mechanical stress. *Sci STKE*. 2004;249:1-8.

245. Deschner J, Hofman C, Piesco N. Signal transduction by mechanical strain in chondrocytes. *Curr Opin Clin Nutr Metab Care*. 2003;6(3):289.

246. Ruwhof C, van der Laarse A. Mechanical stress-induced cardiac hypertrophy: mechanisms and signal transduction pathways. *Cardiovasc Res*. 2000;47(1):23-37.

247. Zerath E. Effects of microgravity on bone and calcium homeostasis. *Adv Sp Res*. 1998;21(8):1049-1058.

248. Semb H. Experimental limb disuse and bone blood flow. *Acta Orthop Scand*.

1969;40(5):552-562.

249. Morey E, Baylink D. Inhibition of bone formation during space flight. *Science (80- )*. 1978;201(4361):1138-1141.

250. Cann C, Adachi R. Bone resorption and mineral excretion in rats during spaceflight. *Am J Physiol Integr Comp Physiol*. 1983;244(3):R327-R331.

251. Patterson-Buckendahl P, Cann C, Grindeland R. Osteocalcin as an indicator of bone metabolism during spaceflight. *Physiologist*. 1985;28:S227-S228.

252. Gross D, Williams W. Streaming potential and the electromechanical response of physiologically-moist bone. *J Biomech*. 1982;15(4):277-298.

253. Qin Y, Lin W, Rubin C. The pathway of bone fluid flow as defined by in vivo intramedullary pressure and streaming potential measurements. *Ann Biomed Eng*. 2002;30(5):693-702.

254. Turner C, Forwood M, Otter M. Mechanotransduction in bone: do bone cells act as sensors of fluid flow? *FASEB J*. 1994;8(11):875-878.

255. Liedert A, Kaspar D, Blakytny R, Claes L. Signal transduction pathways involved in mechanotransduction in bone cells. *Biochem Biophys Res Commun*. 2006;349(1):1-5.

256. Czech M. Signal transmission by the insulin-like growth factors. *Cell*. 1989;59(2):235-238.

257. Judex S, Lei X, Han D, Rubin C. Low-magnitude mechanical signals that stimulate bone formation in the ovariectomized rat are dependent on the applied frequency but not on the strain magnitude. *J Biomech*. 2007;40(6):1333-1339.

258. Roux W. *Die Entwickelungsmechanik; Ein Neuer Zweig Der Biologischen Wissenschaft: Eine Ergänzung Zu Den Lehrbüchern Der Entwickelungsgeschichte Und*. Leipzig: Wilhelm Engelmann; 1905.

259. Meyer G. Die architektur der spongiosa, archief fur den anatomischen und physiologischen. *Wissenschaften im Med*. 1867;27(4):1389-1394.

260. Wolff J. Das gesetz der transformation der knochen. *A Hirshwald*. 1892;1:1-152.

261. Dibbets J. One century of Wolff's law. *Bone Dyn Orthod Orthop Treat*. 1992:1-13.

262. Frost H. *The Laws of Bone Structure*. Springfield, IL: Charles C. Thomas; 1964.

263. Thompson D. *On Growth and Form*. London: Cambridge University Press; 1917.

264. Frost H. A Determinant of Bone Architecture: The Minimum Effective Strain. *Clin Orthop Relat Res*. 1983;175:286-292.

265. Frost H. Bone "mass" and the "mechanostat": a proposal. *Anat Rec*. 1987;219(1):1-9.

266. Frost H. Skeletal structural adaptations to mechanical usage (SATMU): 1. Redefining Wolff's law: the bone modeling problem. *Anat Rec*. 1990;226(4):403-413.

267. Frost H. Skeletal structural adaptations to mechanical usage (SATMU): 2. Redefining Wolff's law: the remodeling problem. *Anat Rec*. 1990;226(4):414-422.

268. Burr D, Martin R. Mechanisms of bone adaptation to the mechanical environment. *Triangle*. 1992;31(2):3.

269. Khan Y, Laurencin C. Fracture repair with ultrasound: clinical and cell-based evaluation. *J Bone Jt Surg Am*. 2008.

270. Baker K, Robertson V, Duck F. A review of therapeutic ultrasound: biophysical effects. *Phys Ther*. 2001;81(7):1351.

271. Kremkau F. *Diagnostic Ultrasound: Principles and Instruments*. WB Saunders Company; 2001.

272. Heckman J, Ryaby J. Acceleration of tibial fracture-healing by non-invasive, low-intensity pulsed ultrasound. *J Bone Jt Surg*. 1994;76(1):26-34.

273. ter Haar G, Coussios C. High intensity focused ultrasound: Physical principles and devices. *Int J Hyperth*. 2007;23(2):89-104. doi:10.1080/02656730601186138.

274. Hariharan P, Myers MR, Robinson RA, Maruvada SH, Sliwa J, Banerjee RK. Characterization of high intensity focused ultrasound transducers using acoustic streaming. *J Acoust Soc Am*. 2008;123(3):1706-1719. doi:10.1121/1.2835662.

275. Canney MS, Bailey MR, Crum LA, Khokhlova VA, Sapozhnikov OA. Acoustic characterization of high intensity focused ultrasound fields: A combined measurement and modeling approach. *J Acoust Soc Am*. 2008;124(4):2406-2420. doi:10.1121/1.2967836.

276. Coussios CC, Farny CH, Ter Haar G, Roy RA. Role of acoustic cavitation in the delivery and monitoring of cancer treatment by high-intensity focused ultrasound (HIFU). *Int J Hyperth*. 2007;23(2):105-120. doi:10.1080/02656730701194131.

277. Long T, Amin V, McClure S, et al. Ultrasound imaging for cavitation detection during HIFU ablation in brain. *Int Soc Opt Photonics*. 2007;6513. doi:10.1117/12.710843.

278. Heckman M, Whitesides T. Compartment pressure in association with closed tibial fractures. The relationship between tissue pressure, compartment, and the distance from

the site of the fracture. *J Bone Jt Surg AM*. 1994;76(9):1285-1292.

279. Gebauer D, Mayr E, Orthner E, Ryaby JP. Low-intensity pulsed ultrasound: Effects on nonunions. *Ultrasound Med Biol*. 2005;31(10):1391-1402. doi:10.1016/j.ultrasmedbio.2005.06.002.

280. Della Rocca G. The science of ultrasound therapy for fracture healing. *Indian J Orthop*. 2009;43(2):121-126. doi:10.4103/0019-5413.50845.

281. Helfrick A, Cooper W. *Modern Electronic Instrumentation and Measurement Techniques*. Prentice Hall; 1990.

282. Carr J. *Elements of Electronic Instrumentation and Measurement*. Pearson College Division; 1996.

283. Bakshi UA, Bakshi A V. *Electronic Measurements Instrumentation*. Pune, India: Technical Publications; 2008.

284. Reher P, Elbeshir E, Harvey W, Meghji S, Harris M. The stimulation of bone formation in vitro by therapeutic ultrasound. *Ultrasound Med Biol*. 1997;23(8):1251-1258.

285. Parvizi J, Parpura V, Greenleaf JF, Bolander ME. Calcium signaling is required for ultrasound-stimulated aggrecan synthesis by rat chondrocytes. *J Orthop Res*. 2002;20(1):51-57.

286. Yang R-S, Lin W-L, Chen Y-Z, et al. Regulation by ultrasound treatment on the integrin expression and differentiation of osteoblasts. *Bone*. 2005;36(2):276-283.

287. Tang C-H, Yang R-S, Fu W-M. Prostaglandin E2 stimulates fibronectin expression through EP1 receptor, phospholipase C, protein kinase Calpha, and c-Src pathway in

primary cultured rat osteoblasts. *J Biol Chem*. 2005;280(24):22907-22316.

288. Sant'Anna E, Leven R, Virdi A, Sumner D. Effect of low intensity pulsed ultrasound and BMP-2 on rat bone marrow stromal cell gene expression. *J Orthop Res*. 2005;23(3):646-652.

289. Walker W, Fernandez F. A method of imaging viscoelastic parameters with acoustic radiation force. *Phys Med Biol*. 2000;45(6):1437.

290. Claes L, Willie B. The enhancement of bone regeneration by ultrasound. *Prog Biophys Mol Biol*. 2007;93(1):384-398.

291. Ferrari C, Andrade M, Adamowski J, Guirro R. Evaluation of therapeutic ultrasound equipments performance. *Ultrasonics*. 2010;50(7):704-709.

292. Pal K, Banthia A, Majumdar D. Polymeric hydrogels: characterization and biomedical applications. *Des monomers Polym*. 2009;12(3):197-220.

293. Veronick J, Assanah F, Nair LS, Vyas V, Huey B, Khan Y. The effect of acoustic radiation force on osteoblasts in cell/hydrogel constructs for bone repair. *Exp Biol Med*. 2016;241(10):1149-1156.

294. Toprak E, Balci H, Blehm B, Selvin P. Three-dimensional particle tracking via bifocal imaging. *Nano Lett*. 2007;7(7):2043-2045.

295. Nightingale K, Palmeri M. On the feasibility of remote palpation using acoustic radiation force. *J Acoust Soc Am*. 2001;110(1):625-634.

296. Brandenburg J, Eby S, Song P, Zhao H. Ultrasound elastography: the new frontier in direct measurement of muscle stiffness. *Arch Phys Med Rehabil*. 2014;95(11):2207-2219.

297. Viola F, Walker W. A spline-based algorithm for continuous time-delay estimation using sampled data. *IEEE Trans Ultrason Ferroelectr Freq Control*. 2005;52(1):80-93.

298. Montgomery L, Elliott S, Adair H. Muscle and tendon heating rates with therapeutic ultrasound in horses. *Vet Surg*. 2013;42(3):243-249.

299. Chang W, Sun J, Chang S, Lin J. Study of thermal effects of ultrasound stimulation on fracture healing. *Bioelectromagnetics*. 2002;23(4):256-263.

300. Salem K, Schmelz A. Low-intensity pulsed ultrasound shortens the treatment time in tibial distraction osteogenesis. *Int Orthop*. 2014;38(7):1477-1482.

301. Weinbaum S, Cowin S, Zeng Y. A model for the excitation of osteocytes by mechanical loading-induced bone fluid shear stresses. *J Biomech*. 1994;27(3):339-360.

302. Klein-Nulend J, Van der Plas A, Semeins C. Sensitivity of osteocytes to biomechanical stress in vitro. *FASEB J*. 1995;9(5):441-445.

303. Kodama H, Amagai Y, Sudo H, Kasai S. Establishment of a clonal osteogenic cell line from newborn mouse calvaria. *Japan J Oral Biol*. 1981;23(4):899-901.

304. Wang D, Christensen K, Chawla K. Isolation and characterization of MC3T3-E1 preosteoblast subclones with distinct in vitro and in vivo differentiation/mineralization potential. *J Bone Miner Res*. 1999;14(6):893-903.

305. Quarles L, Yohay D, Lever L. Distinct proliferative and differentiated stages of murine MC3T3-E1 cells in culture: an in vitro model of osteoblast development. *J Bone Miner Res*. 1992;7(6):683-692.

306. Choi J, Lee B, Song K, Park R. Expression patterns of bone-related proteins during

osteoblastic differentiation in MC3T3-E1 cells. *J Cell Biochem*. 1996;61(4):609-618.

307. Wadhwa S, Godwin S, Peterson D. Fluid Flow Induction of Cyclo-Oxygenase 2 Gene Expression in Osteoblasts Is Dependent on an Extracellular Signal-Regulated Kinase Signaling Pathway. *J Bone Miner Res*. 2002;17(2):266-274.

308. Wadhwa S, Choudhary S, Voznesensky M. Fluid flow induces COX-2 expression in MC3T3-E1 osteoblasts via a PKA signaling pathway. *Biochem Biophys Res Commun*. 2002;297(1):46-51.

309. Forwood M. Inducible cyclo-oxygenase (COX-2) mediates the induction of bone formation by mechanical loading in vivo. *J Bone Miner Res*. 1996;11(11):1688-1693.

310. Ponik S, Pavalko F. Formation of focal adhesions on fibronectin promotes fluid shear stress induction of COX-2 and PGE2 release in MC3T3-E1 osteoblasts. *J Appl Physiol*. 2004;97(1):135-142.

311. Park J, Pillinger M, Abramson S. Prostaglandin E 2 synthesis and secretion: the role of PGE 2 synthases. *Clin Immunol*. 2006;119(3):229-240.

312. Goessling W, North T, Loewer S, et al. Genetic interaction of PGE2 and Wnt signaling regulates developmental specification of stem cells and regeneration. *Cell*. 2009;136(6):1136-1147.

313. Kabsch W, Mannherz H, Suck D, Pai E. Atomic structure of the actin: DNase I complex. *Nature*. 1990;347(6288):37.

314. Yeung T, Georges P, Flanagan L. Effects of substrate stiffness on cell morphology, cytoskeletal structure, and adhesion. *Cell Motil Cytoskeleton*. 2005;60(1):24-34.

315. Wang N, Butler J, Ingber D. Mechanotransduction across the cell surface and through the cytoskeleton. *Science (80- ).* 1993;260(5111):1124-1127.

316. Discher D, Janmey P, Wang Y. Tissue cells feel and respond to the stiffness of their substrate. *Science (80- ).* 2005;310(5751):1139-1143.

317. Shimomura S, Matsuno H, Tanaka K. Effect of mechanical instability of polymer scaffolds on cell adhesion. *Langmuir*. 2013;29(35):11087-11092.

318. Escoffre J, Bouakaz A. *Therapeutic Ultrasound*. New York, NY: Springer; 2015.

319. Rawool N, Goldberg B. Power Doppler assessment of vascular changes during fracture treatment with low-intensity ultrasound. *J Ultrasound Med*. 2003;22(2):143-153.

320. Praemer A, Furner S, Rice D, Kelsey J. *Musculoskeletal Conditions in the United States*. Rosemont, IL; 1992.

321. Gómez-Barrena E, Rosset P, Lozano D, Stanovici J. Bone fracture healing: cell therapy in delayed unions and nonunions. *Bone*. 2015;70:93-101.